The University of Nottingham

UNITED KINGDOM · CHINA · MALAYSIA

Faculty of Engineering

Department of Mechanical, Materials and Manufacturing Engineering

Development of an improved structural integrity assessment methodology for pressurised pipes containing defects

Sultan Salim Al Owaisi, BSc, MPhil, CEng

Thesis submitted to the University of Nottingham

for the degree of Doctor of Philosophy

August 2016

ABSTRACT

Metal loss due to corrosion is a serious threat to the integrity of pressurised oil and gas transmission pipes. Pipe metal loss defects are found in either single form or in groups (clusters). One of the critical situations arises when two or more defects are spaced close enough to act as a single lengthier defect, causing major impact on the pressure containing capacity of a pipe and leading to rupture rather than localised leak at the centre of defects. There have been many studies conducted to determine the distance needed for defects to interact leading to a failure pressure lower than that when the defects are treated as single and not interacting. Despite such efforts, there is no universally agreed defect interaction rule and pipe operators around the world have various rules to pick and choose from. In this work, the effects of defect shapes and orientations on closely spaced defects are tested experimentally and further analysed using finite element analysis. Burst pressures of commonly used ductile steel pipes in the oil and gas industries, namely X52 and X60, are measured under internal pressure loading. The pipes were machined with circular and curved boxed defects at different orientations to simulate actual metal loss defects. The burst pressure results were compared with those obtained using existing analytical methods. Comparison of the results showed conservatism in the existing analytical methods which may potentially lead to unnecessary plant shutdowns and pipe repairs. A failure criterion for both single and interacting defects was proposed and validated numerically using the experimental data obtained in this research work. The numerical results when using the proposed failure criterion showed that defect shapes and orientations have a great influence on the failure pressure of pipes containing interacting defects. A simplified

mathematical model based on the parametric results and relevant to the cases studied is proposed with the objective of reducing the known conservatism in the existing pipe standards when it comes to the assessment of defect interaction.

LIST OF PUBLICATIONS

1- Al-Owaisi S., Becker A. A., Sun W., *A review of the role and effect of residual stress on pipeline-flaw assessment.* Journal of Pipeline Engineering, 2014. **13** (4): p. 265-274.

2- Al-Owaisi S., Becker A. A., Sun W., *Numerical analysis of interacting metal loss defects – effects of shapes & orientations*, 5th Global Pipeline Integrity & Technology Summit 2015. 20-21 April 2015, Abu Dhabi, United Arab Emirates.

3- Al-Owaisi S., Becker A. A., Sun W., *Analysis of shape and location effects of closely spaced metal loss defects in pressurised pipes*. Engineering Failure Analysis, 2016. 68: P.172-186.

ACKNOWLEDGEMENTS

I would like to express my deepest and utmost appreciation to my research work supervisors, Prof Adib Becker and Prof Wei Sun. Their well-known expertise in finite element modelling and solid mechanics has helped tremendously in the theoretical understanding of the relevant theories and in completing this thesis.

I would like to express my gratitude to Petroleum Development Oman (PDO) for their financial support of the experimental part of the research and to Mr. Nasser Al-Behlani and Mr. Hussain Al-Salmi for liaising between PDO and Sultan Qaboos University (SQU) who helped in performing the experimental work. Likewise, I want to thank Prof Tanseem Pervez, Dr. Abdullah Al-Shabibi and Dr. Majid Al-Moharbi for their flexibility and unlimited technical support during the execution of the experimental work.

Deepest appreciation to Dr. Rupesh Patel for his support on Abaqus and Matlab, likewise my thanks go to Dr. Si Thu Kywa, Dr. Francesco Cortellino, Dr. James Rouse, Dr. Simon Woolhead and Dr. Balhassan Ali. Thanks to all of my colleagues in the SID office who were always helpful and who provided a comfortable and stimulating research environment.

Unlimited gratitude to my family members; my beloved mother, Bashair, Saja and Faisal who supported me and showed understanding and patience throughout the duration of the research work.

NOMENCLATURE

A	Local area of metal loss in the longitudinal plane
A_o	Original local area of metal loss
D	Specified outside diameter of the pipeline
D	Depth of defect
E	Modulus of elasticity
L	Length of defect
M	Folias factor (bulging factor)
P_f	Failure pressure
Pn	Normalised pressure
P_{Defect}	Failure pressure due to presence of single defects
P_{Multi}	Failure pressure due to presence of multiple defects
Q	Length correction factor
S	Space between defects
S_n	Normalised defect spacing (s/t)
T	Pipeline wall thickness
N	Poisson’s ratio
ε_1, ε_2, ε_3	Principal strains in the Cartesian axes
ε_{true}	True strain
ε_{eng}	Engineering strain
γ_m	Partial safety factor for longitudinal corrosion model prediction
γ_d	Partial safety factor for corrosion depth

$\sigma_{eq}/\ \sigma_e$	Equivalent von Mises stress
σ_{true}	True stress
$\sigma^{TrueUTS}$	True ultimate tensile stress
σ_{Eng}	Engineering stress
σ^{EngUTS}	Engineering ultimate tensile stress
σ_y	Specified minimum yield strength
σ_U	Ultimate tensile strength
σ_1, σ_2, σ_3	Principle stresses in the Cartesian axes

ABBREVIATIONS

AGA	American Gas Association
API	American Petroleum Institute
ASME	American Society of Mechanical Engineers
BC	Boundary condition
CB	Curved boxed defect
CNC	Computer numerical control
CR	Circular defect
DNV	Det Norske Veritas
EMAT	Electromagnetic acoustic emission
FE	Finite element
FEA	Finite element analysis
FEM	Finite element method
FFS	Fitness for service
GPa	Giga pascal
HFW	High frequency welded
HSAW	Helically submerged arced welded
ISO	International Organization for Standardization
J	Joules
LSAW	Longitudinally submerged arc welded
MFL	Magnetic flux leakage
MPa	Mega pascal

NLGEOM	Nonlinear geometry
NDT	Non-destructive testing
PHMSA	Pipeline and Hazardous Materials Safety Administration (USA)
POF	Pipeline Operator Forum
RP	Recommended practice
RSTRENG	Remaining strength
SMYS	Specified minimum yield strength
UT	Ultrasonic
UTS	Ultimate tensile strength

TABLE OF CONTENTS

TABLE OF FIGURES

LIST OF TABLES

CHAPTER 1: INTRODUCTION

1.1 Summary

The overall scope of this research project is to study the effect of shapes and orientations on closely spaced defects to further improve the assessment capability of these metal loss defects when they occur in internally pressurised pipes. Such an improved understanding will have a major impact on the decision making process of operators when it comes to the rehabilitation options which are normally taken to safeguard the integrity of these pipes. The objectives in this study are set to be achieved by obtaining the stress and strain data from tensile tests and gathering the failure burst pressure of short pipes from comprehensive experimental burst-pressure tests. The pipes materials, diameters and wall thicknesses used in the study represent the commonly used pipes in the oil and gas transmission sector. The metal loss defects machined in the pipes are in line with the detection and sizing accuracy of pipe inspection tools as stated in the Pipeline Operators Forum (POF) guidelines [1]. The objectives of this research work were achieved firstly by understanding the limitations of the existing defect assessment codes and then developing test pipe specimens which included various spaced and oriented defects. A schematic of the research methodology is shown in Figure 1-1.

A total of 31 pipe specimens with a length of 1.8 m were burst tested. The tested pipes were initially analysed using existing analytical methods. Finite Element (FE) models were then created to depict the exact pipe and defect dimensions in order to obtain the failure pressure. Once satisfied with the FE numerical results, a parametric study considering

defect spacing, shape, depth and length was carried out to achieve simplified defect interaction rules.

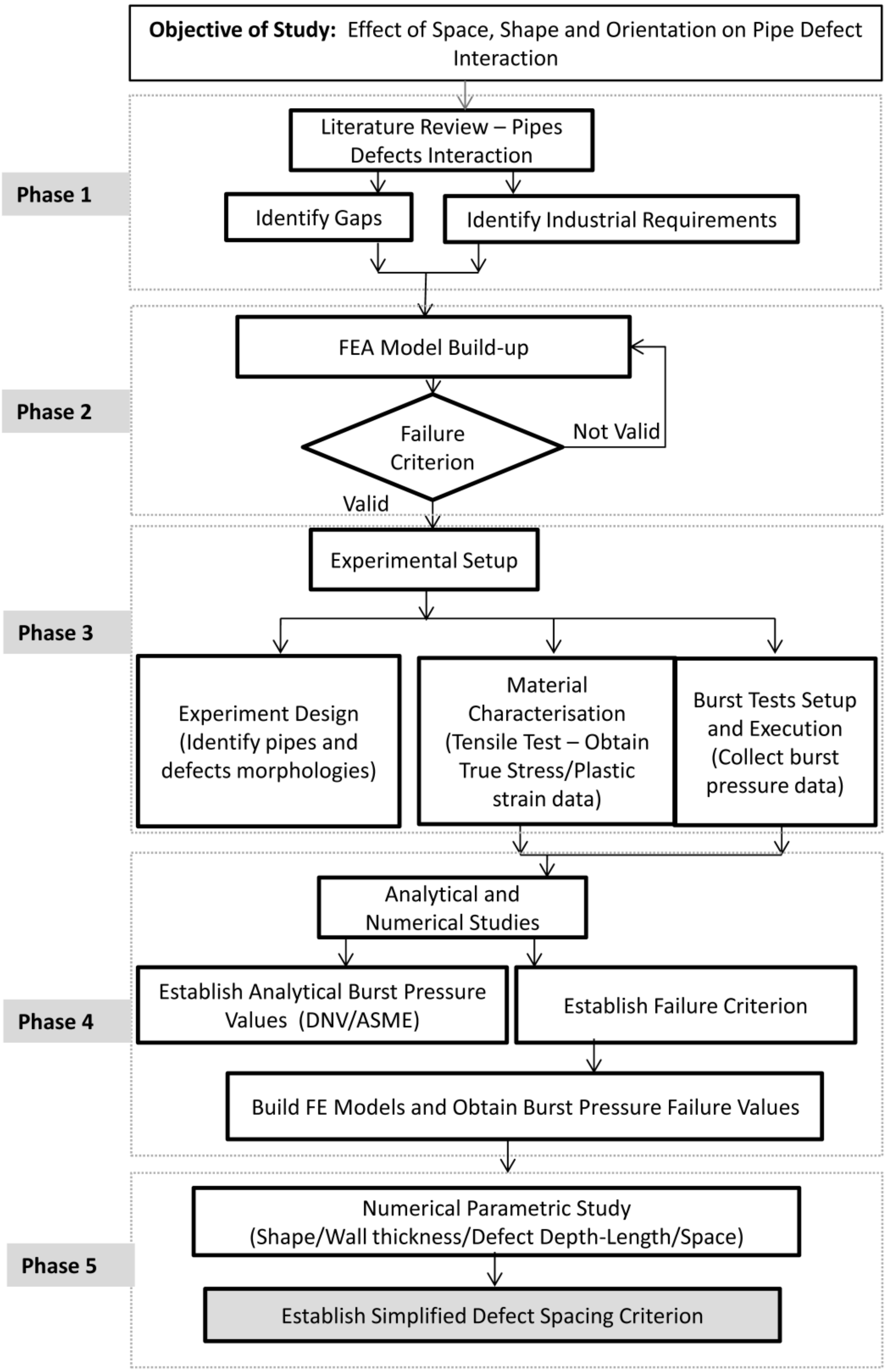

Figure 1-1: Research Methodology Flowchart

1.2 Background and Motivation

Metal loss defects as a result of corrosion, both internal and external, represent an insidious form of pipe damage that has the potential, when unrecognized, to result in pipe failure. Corrosion defects occur in the form of single and cluster defects with each having different consequences, either localised leak or rupture. Between 2010 and 2013, pipe failures due to corrosion and material degradations resulted in a financial loss of more than $466 million of estimated total costs to gas pipe network operators [2]. The ability to predict failure pressures of each of these forms of corrosion defects is extremely valuable to pipe operators to safeguard integrity, as such understanding paves the way to determining the remaining life of the pipes as well as future repair and maintenance related strategies.

Defect assessment has been researched since the 1970's right up to the present time. In chronological order, a number of examples, both experimental and numerical, are given in references [3-16]. The most widely used code for a single defect assessment is ASME B31G [17] which utilizes a semi-empirical method. However, this code provides no guidance for assessing defects that are closely spaced to each other. Interacting defects that are sufficiently spaced close to each other yield failure pressures lower than that for a single defect and tend to fail in a rupture manner. DNV RP F101 [18] recommended practice is widely used in industry for predicting the failure pressure of both single and interacting defects. Though both design codes are widely used in the oil and gas sectors, conservatism in predicting the safe working pressure has been cited in several research works [8, 11, 15, 16, 19-21]. A literature review [22-24] indicates that around 360 pipe burst tests were conducted since 1970 to date. The vast majority of these tests were mainly conducted on single defects. There are few experimental burst projects carried out on interacting defects starting with the ones conducted by Mok et al. [25], with the latest work being conducted by Freire José et al. [26]. Due to insufficient data available in the literature on exact defect dimensions, actual pipe wall thickness vs nominal thickness and material properties, it is difficult to replicate majority of the tests referred to in the published literature for further studies.

1.3 Research Aim and Objectives

One of the main issues related to defect interaction is the agreement of existing codes and standards on the critical spacing factor by which defect interaction is expected to take place. Oil and gas pipe operators are faced with inconsistencies with regards to the decision upon which closely-spaced defects can be assumed to be clustered in one defect. ASME B31G [17] states that defect interaction takes place when defects are spaced in the longitudinal direction by a distance equal to 3 wall thicknesses, while DNV-RP-F 101 [18] considers defect interaction to occur for pipes with a 20 inch external diameter with wall thickness of 9.5 mm and 10.5 mm when the defects are spaced by about 15 wall thicknesses and 14 wall thicknesses respectively. The Pipeline Operator Forum (POF) [1] which provides oil and gas operators with guidance on pipe inspection tools gives a different recommendation on defects interaction by stating that defects interact only when spaced by maximum of 6 wall thicknesses. Both ASME B31G and POF do not cover defect interaction in the circumferential direction, while DNV-RP-F1010 provides some directions.

In view of the above inconsistencies found in the widely used codes and standards for pipe integrity, it was decided to develop an improved method for determining the burst pressure of pipes by carrying out detailed experimental and numerical studies. This work investigates the effect of spacing, shape and orientation on metal loss defect interaction rules and the failure pressure of pipes. This primary research aim is supported by achieving the following research objectives which represent the key steps in providing simplified rules for defect interaction:

- Improve the understanding of the interaction rules for pipelines containing flaws.
- Develop a failure criterion for predicting failure pressure as a result of defect interaction.
- Use FE modelling to study the failure pressure of interacting defects in thin-wall pipes.
- Conduct parametric studies with the goal to cover a wider range of parameters those considered in the experimental work.

1.4 Thesis Layout

The literature review in Chapter 2 follows the research work introduction. The review in this chapter provides an overview of the pipe manufacturing process, paving the way to analysing the degradation mechanisms that these pipes are further exposed to during their lifetime. It includes the different types of corrosion defects and ends with an overview of the existing defect assessment methods. The last part of Chapter 2 highlights the areas which need to be further investigated and improved in the criteria of pipe defect interaction. Chapter 3 provides an overview of the FE modelling and procedures adopted in this study. It also contains the mesh sensitivity analysis carried out in order to facilitate the accurate modelling of the pipe flaws using the Abaqus FE code. Chapter 4 provides the single and interacting defect failure criteria and validation models. Chapter 5 presents the experimental work for burst pressure testing of pipes. This includes the tensile tests conducted, defect machining process, test setup and burst pressure values obtained from the 31 tested pipes. Chapter 6 is mainly dedicated to the numerical and analytical validations based on experimental results. This chapter provides a comparison between numerical and analytical results on the one hand and experimental results on the other. A parametric study examining the effects of defect spacing, pipe thickness, defect length and defect depth is included in Chapter 7. The same chapter also includes a framework for calculating the failure pressure of interacting defects. Chapter 8 which is the last chapter covers the main conclusions of the research work and provides recommendations for future studies.

CHAPTER 2: LITERATURE REVIEW

2.1 Introduction

In Chapter 1 it was observed that the use of carbon steel pipes for transportation of oil and gas commodities has led to the introduction of pipe defect assessment due to the inevitable presence of corrosion processes. This review therefore gives an overview of the pipe forming processes and corrosion mechanisms and provides details of the existing defects assessment methods. Conclusions on the literature review findings and identification of the knowledge gaps are covered in the last section of this chapter.

2.2 Pipeline Forming Routes

This section provides an introduction to pipeline manufacturing processes. Pipelines utilised by oil and gas operators are manufactured through two main principal processes; either seamed or seamless. The pipes used in the experimental work of this thesis are seamed pipes. The seamed pipeline category is further subcategorised into 3 main types; namely Longitudinally Submerged Arc Welded (LSAW), Helically Submerged Arced Welded (HSAW) and High Frequency Welded (HFW). Most of the pipelines used for the oil and gas sectors are either seamless or longitudinally welded (LSAW/HFW), although spirally welded pipes are being re-introduced into the oil and gas sectors.

2.2.1 Seamless Pipe Manufacturing Process

The raw material at the start of the process consists of steel billets, where the chemical properties are specified upfront prior to the arrival of these billets at the steel mills. The weight, length and diameters of these billets are also specified upfront in order to achieve the final required pipe dimensions. The first process, after identification, involves heating the billets to temperatures around 1250 °C in a rotary furnace. Once heated for the specified soaking time, the billet is pushed or pulled through a mandrill, called a piercer, in the centre producing a hollow pipe. This process could be repeated more than once in order to arrive to the final desired length and thickness. Once the pipeline is formed, it goes through various heat treatments and testing processes prior to final inspection and marking. The production size for oil and gas transmission pipelines normally ranges between external diameters of 4 and 16 inches. Figure 2-1 shows a typical overview of the whole process.

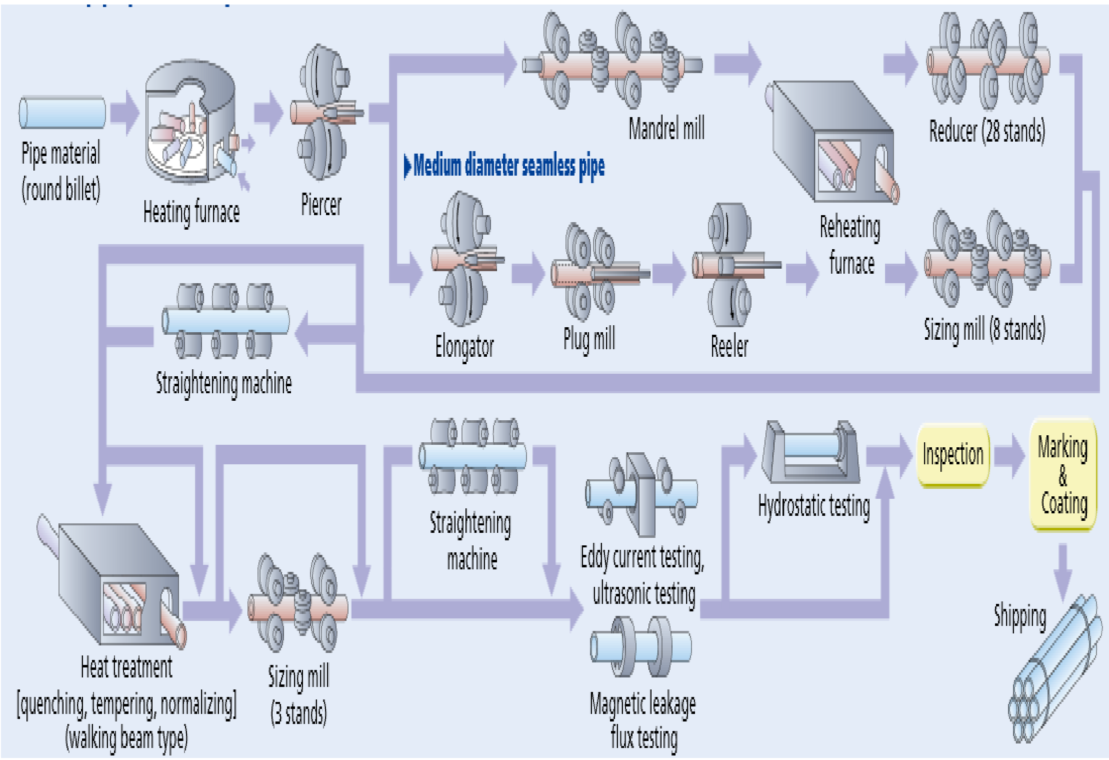

Figure 2-1: Seamless pipeline manufacturing process [27]

2.2.2 Welded (Seamed) Pipe Manufacturing Processes

2.2.2.1 High Frequency Welding Process

High Frequency Welded (HFW) pipelines are normally produced from rolls of steel. In the production of this type of pipeline, the pipe is cold formed into a cylindrical shape. A pressure is applied to force the two edges of the cylinder to come close to each other and an electric current is used to heat the edges of the strip for the fusion weld. As illustrated in Figure 2-2, the process of HFW in pipes, involves uncoiling of the steel coil, flattening, edge preparation, cylindrical forming, electrical welding, inspection and normalising of the weld made, expansion and straightening of the line pipe, hydro-testing, seam and full body inspection, finally weighing and marking as required by the client. The production sizes of HFW process normally range between external diameters of 2 and 24 inches.

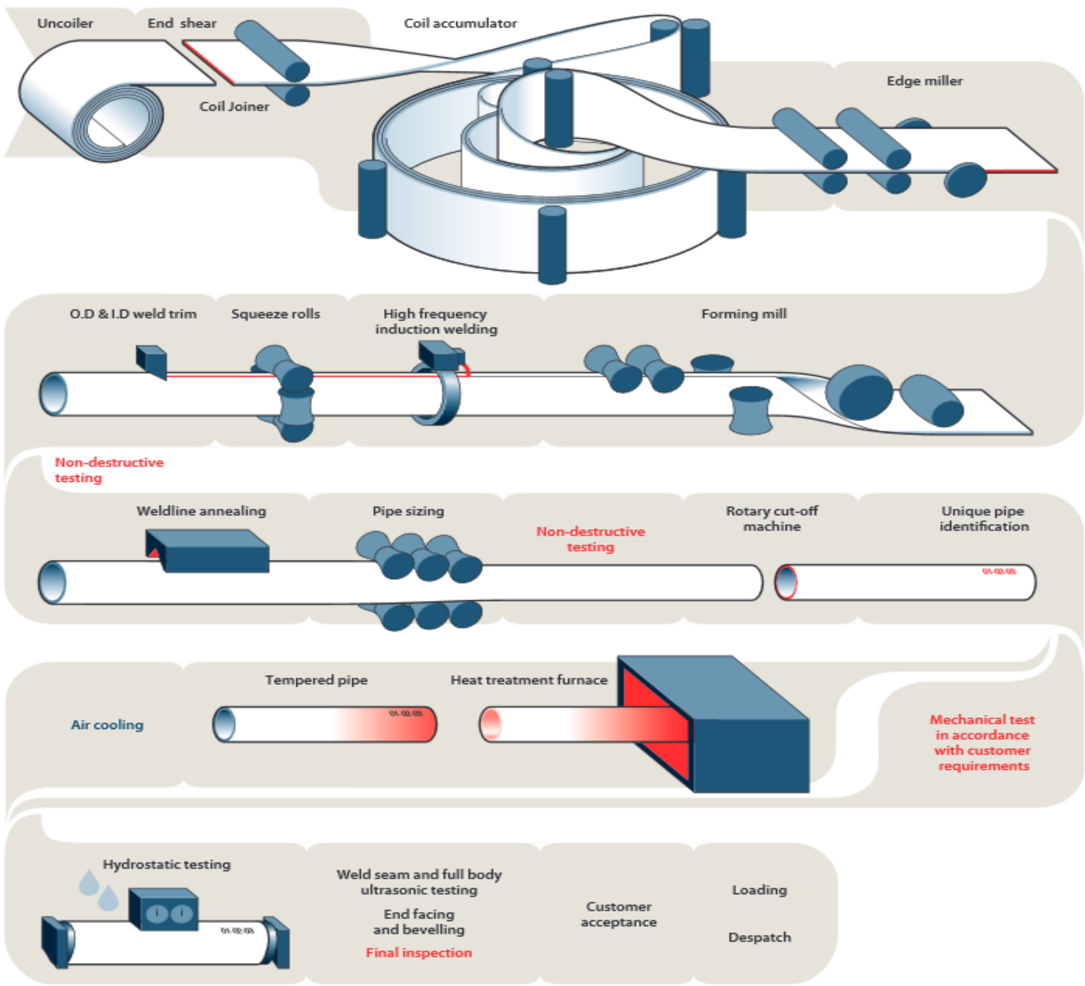

Figure 2-2: Typical HFW pipeline process [28]

2.2.2.2 Submerged Arc Welded (LSAW)

Longitudinal Submerged Arc Welded pipelines (LSAW) derive their name from the welding process as the welding arc is submerged in a flux while the welding takes place. A flat steel plate is used for this process. The butt joint of the pipe is welded in at least two phases, one of which is on the inside of the pipe. Filler metal for the welds is obtained from the electrodes and a flux is injected around the weld pool to protect the steel and weld area from any impurities in the air when heated to welding temperatures. There are two main forming processes, namely JCO and UOE. As the name implies for each of these processes, the linepipe is formed using press and roller machines to form the linepipe into “J” then

“C” to “O” shapes for the JCO process and for UOE method it uses a "U" press, and "O" press for forming and where the final stage uses and expander “E” for giving the desired ovality in the pipe. Depending on the size and thickness, steel mills select one of these two processes. The production sizes for oil and gas transmission pipelines normally range between external diameters of 18 and 72 inches. The UOE forming steps are depicted in Figure 2-3 while the whole process is illustrated in Figure 2-4.

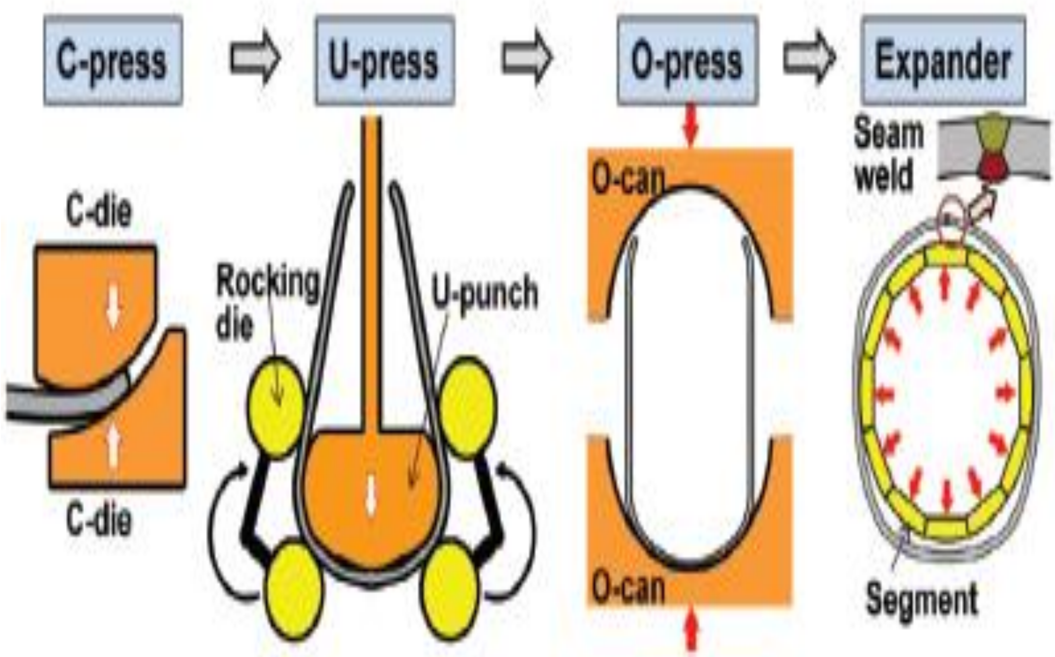

Figure 2-3: UOE forming steps [29]

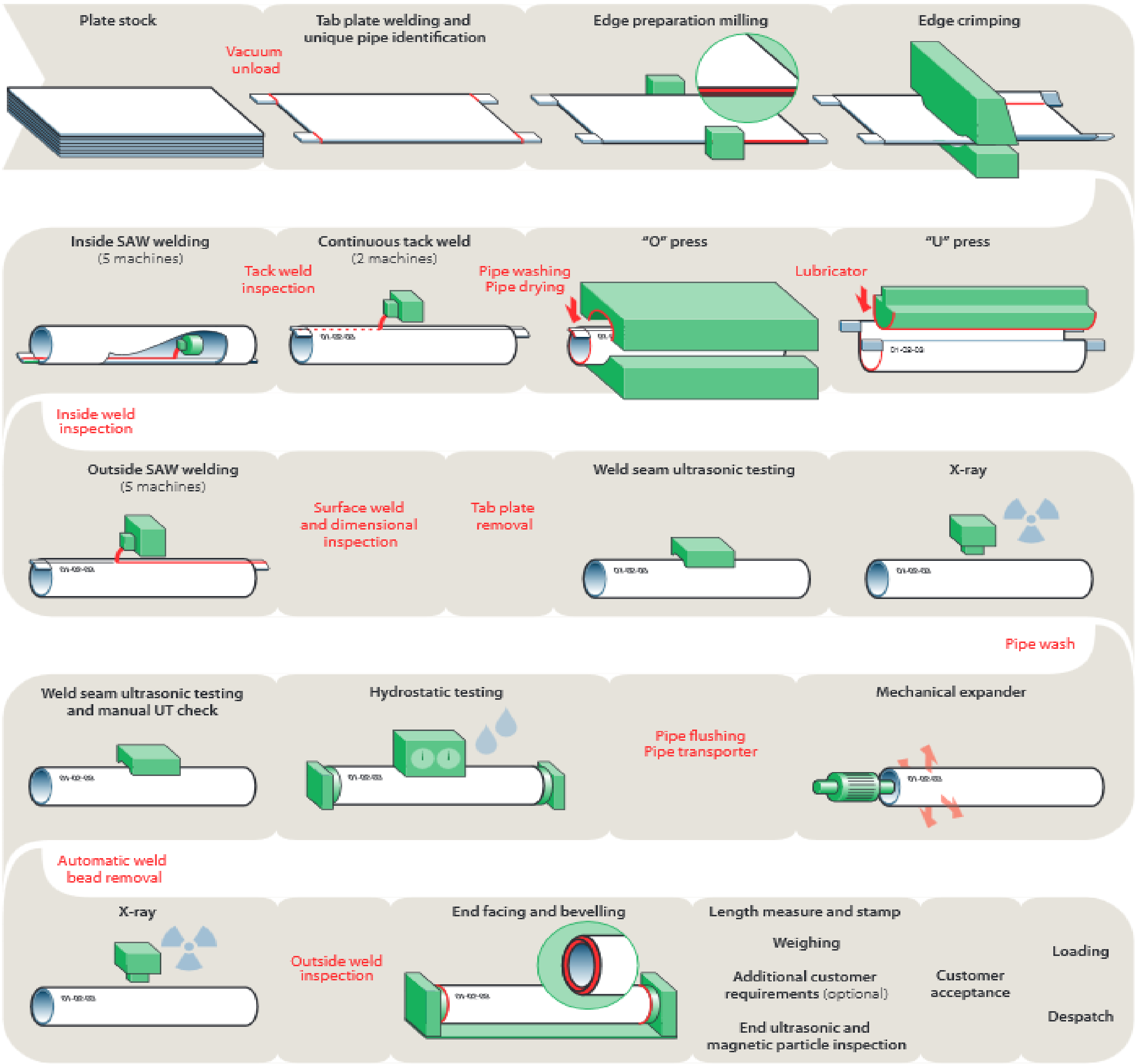

Figure 2-4: Typical LSAW (UOE) process [30]

2.2.2.3 Helically Submerged Arced Welded (HSAW)

As the name implies, this process of manufacturing pipes is made by uncoiling the steel coil and welding it in a helical/spiral manner by a submerged arc welding making it the most productive and cost effective among all the other steel manufacturing processes. During this process, the weld pool is protected against oxidation by a flux produced from the electrode fed separately onto the weld. Similar NDT checks to those made on the previous manufacturing processes are made on the final production, namely visual, ultrasonic inspection and hydrotesting. The benefit of this method is that it allows mass production and production of large size diameters up to 144 inch. Figure 2-5 gives an overview of this process.

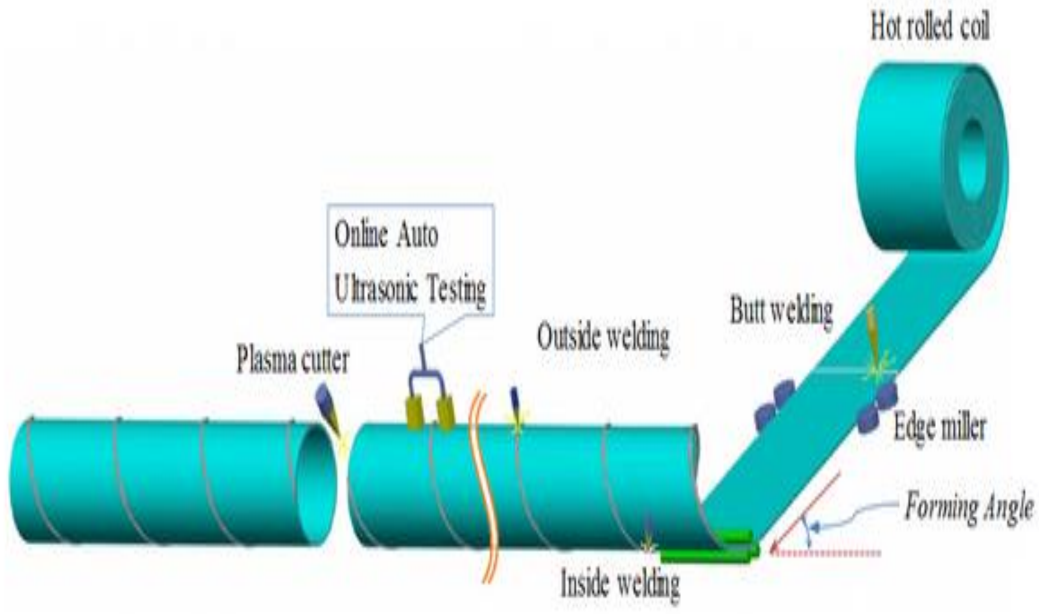

Figure 2-5: Typical HSAW Pipe Manufacturing Process [31]

2.2.3 Final Remarks on Pipe Forming Methods

Seamless pipelines do not have seam welds which aid in eliminating defects which are normally associated with seam welds. However, the cost of manufacturing SMLS pipelines is typically higher than that of seamed pipelines, and for this reason oil and gas operators have tended to overrule the choice of this type in long oil and gas transmission networks unless deemed technically necessary. It can be also noted that the seamed process used for producing pipes transform a steel plate to a cylindrical shape which implies plastic deformations. The use of HSAW pipes in the oil and gas sector is very limited and this is attributed to the potential subsequent failure, i.e. springback. Past experience has also shown that this type of pipe is susceptible to stress-oriented hydrogen induced cracking where H_2S is present [32].

It is worth noting that there are no studies in the literature conducted to look at the effects of different types of steel pipe manufacturing processes on the failure pressure of pipe defects.

2.3 Corrosion Mechanism – An Overview

Once carbon steel pipes are manufactured as per section 2.1 and installed for operation, they undergo a natural process of degradation if not protected by proper external coatings, cathodic protection and preselected inhibitors where needed. Corrosion is well-known to be one of the main contributors of oil and gas pipeline failures around the world. Figure 2-6 shows corrosion is among the top 3 contributors of all pipeline incident failures as reported by PHMSA [33].

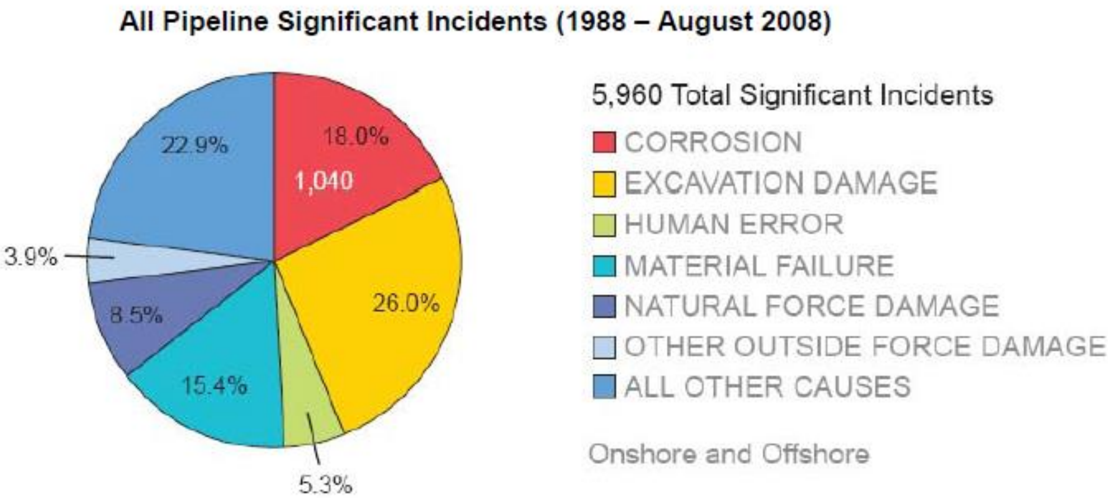

Figure 2-6: Causes of significant incidents in onshore and offshore pipelines [33]

In this section, a brief description of the corrosion process and the types of corrosion encountered in the oil and gas sector are explained. Furthermore, the available inline inspection techniques for detection of corrosion and cracks will be summarised. A thorough understanding of the corrosion process and the required inspection and maintenance tasks for each pipeline mode of corrosion failure will give operators the confidence to operate pipelines for years beyond their intended design life.

2.3.1 Mechanism

Corrosion is the natural degradation process of metals. Corrosion of engineering materials is an electrochemical process which occurs in the presence of four factors which are; the anode (Oxidation), the Cathode (Reduction), a metallic path which connects the anode and the cathode, and an electrolyte (soil and underground water for external pipe wall corrosion or untreated crude for internal pipe wall corrosion). The positive ions from anode called the cations are more reactive and react with the solution to form hydroxides and may then form oxides which precipitate. The circuit is completed when the negative ions called the anions flow to the cathode where water and oxygen reduction occurs. A typical corrosion process is shown below and depicted in Figure 2-7.

As iron dissolves due to the presence of corrosive elements, be it salty water containing other forms of sediments, it releases positively charged irons:

$$Fe \rightarrow Fe^{++} + 2e^{-} \qquad \textbf{(2-1)}$$

The electrons produced from the reaction in (2-1), move through the metal pipe to a location where these electrons are consumed in a chemical reaction that produces hydroxyl ions. The circuit is completed by movement of the ions through the electrolyte as shown in the chemical reactions below:-

$$O_2 + 2H_2O + 4e^{-} \rightarrow 4OH^{-} \qquad \textbf{(2-2)}$$

$$2H_2O + 2e^{-} \rightarrow H_2 + 2OH^{-} \qquad \textbf{(2-3)}$$

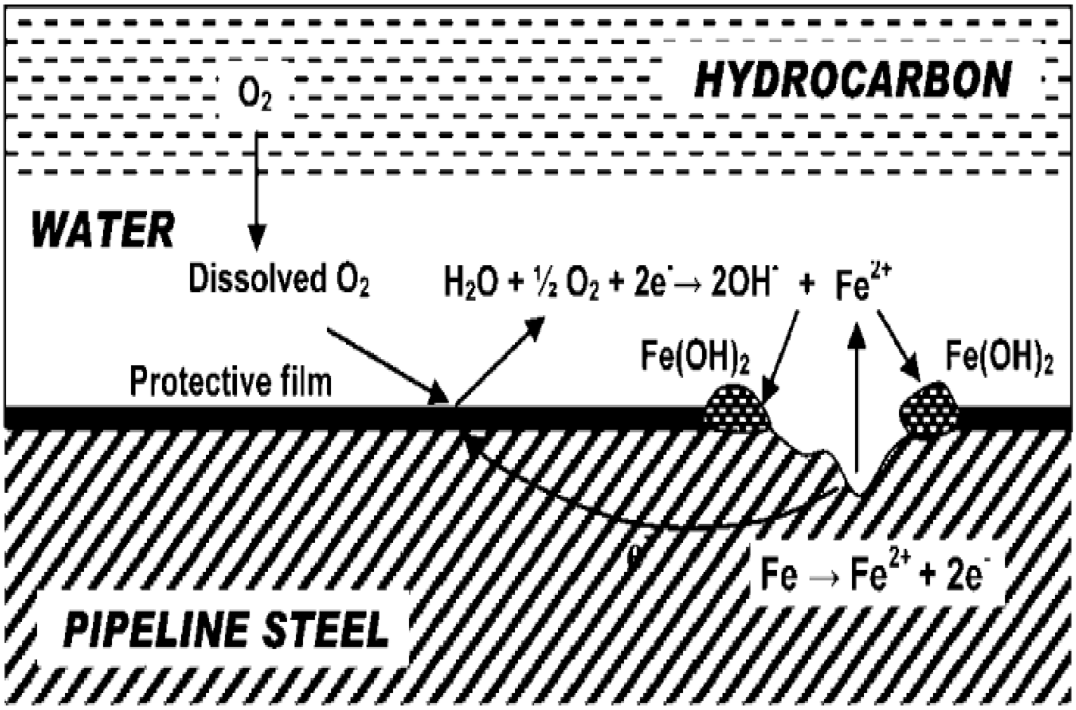

Figure 2-7: Process of corrosion in wet hydrocarbon pipe induced by low flow [34]

There are several factors affecting the initiation and speed of the corrosion process, and the list below is not exhaustive:

- Presence of water
- Presence of debris
- Presence of dissolved gases such as carbon dioxide, hydrogen sulphide, and oxygen.
- Temperature
- Fluid velocity
- pH which is equal to -log [H+]
- Pressure
- Metallurgical factors
- Dissimilar metals

2.3.2 Forms of Corrosion

There is no universally accepted list or number of types of corrosion; however, these types could be listed by the process in which they are initiated.

2.3.2.1 General Corrosion

This form of corrosion occurs through the entire body of the exposed structure. It can be seen clearly when a bare steel bar is left for a long period near the sea. It is widely seen in pipelines which carry wet crude oil where low velocity water settles at the bottom of the pipeline at the 6 O'clock position creating long grooves of corrosion area.

2.3.2.2 Pitting Corrosion

This type of corrosion occurs at selective parts of the pipeline which could be as a result of inhomogeneity at the grain level. The shape of the pit is normally circular and the radius is normally below 10 mm which is a value specified normally by the inline inspection companies for detection of metal loss defects. Presence of microbial activities has also been found to create this form of corrosion as well.

2.3.2.3 Galvanic Corrosion

Coupling of dissimilar materials and in the presence of water and oxygen normally leads to corrosion of the more reactive metal as defined in the galvanic series producing this type of corrosion.

2.3.2.4 Crevice Corrosion

This form of corrosion occurs locally where crevices are being formed. The presence of moisture/water in these crevices leads to selective and local corrosion and is normally seen at unprotected and poorly tightened flange faces.

2.3.2.5 Environmentally Induced Corrosion (EIC)

This form of corrosion is initiated as a result of presence of tensile stresses, susceptible material to cracks and a corrosive environment leading to brittle fracture of a normally ductile alloy. There are three general forms of EIC which are SCC, CFC and HIC.

a. Stress Corrosion Cracking (SCC)

SCC is normally initiated as a result of a conjoint action of static tensile stress and the presence of specific environmental conditions in the presence of a susceptible metal. Further details on the conditions triggering SCC can be found in ASME B31.8S [35].

b. Corrosion Fatigue Cracking (CFC)

This form of corrosion occurs as a result of the combined effects of cyclic stress and corrosion. Common occurrence in pipelines is at locations where compressors and pumps produce vibrations.

c. Hydrogen Induced Cracking (HIC)

Hydrogen induced cracking (HIC) occurs internally when hydrogen from H_2S gas is diffused in the metal causing crack initiation and subsequent propagation [36] while externally it could be as a result of cathodic reduction of water.

2.3.3 Inline Corrosion Inspection Techniques

Pipeline inspection is extremely important and it forms part of the pipeline integrity management system of any pipeline operating company. Periodical or risk based inspection intervals are also mandated by government regulations all over the world. The data gathered on locations, orientations and dimensions including (length, width, depth) of the corrosion defects are invaluable to determine the statuesque of the pipe system and whether it is safe to operate or otherwise. The defects morphology can be developed into 3 dimensional solid models and an FE simulation can also be performed following receipt of the inspection reports. Inline inspection data is also used to monitor the condition of the pipe and extract a trend on corrosion rates. There are several advanced in-line inspection technologies available nowadays ranging from the well-known manganic flux leakage (MFL) tools to the latest ones which combine both MFL as well ultrasonic measurement (compo tools) which are capable of providing good detection and sizing of cracks and flaw-like cracks in addition to the metal loss defects. The choice of which type of technology to use depends on the types of defects in the pipeline, and the pipeline operator must take into consideration this factor in addition to the financial implication of the choice made. As these inspection tools have built-in measurement uncertainties, upper limit accuracy values have to be included during any defect assessment work. The sections below give a summary of the two main inline non-destructive testing inspection technologies used in the oil and gas industries.

2.3.3.1 Magnetic Flux Leakage (MFL)

The source of this inspection technique lies in the benefit of utilising magnetic principles. The corrosion defect is detected by the distortion of a magnetic field induced on the pipe wall, as seen in Figure 2-8. The distortions, whether it is for internal or external defects, are sensed via multiple detectors mounted on the inspection device which generate signals. The data collected from these sensors is then transmitted to a strip chart. Special software, with the aid of specialists, interpret the data collected to produce defect details containing their location, orientation, depth, length and width. Built-in codes within the software also produce safe working pressures for each defect including those defects which are called clustered (interacting) defects. The interaction rule can be dictated by the pipeline operators. There are different types of MFL tools ranging from the standard high resolution tool to the more complex ones which combine axial and transverse magnetics and those combining MFL and other NDT techniques such as ultrasonic (UT) techniques within the same tool.

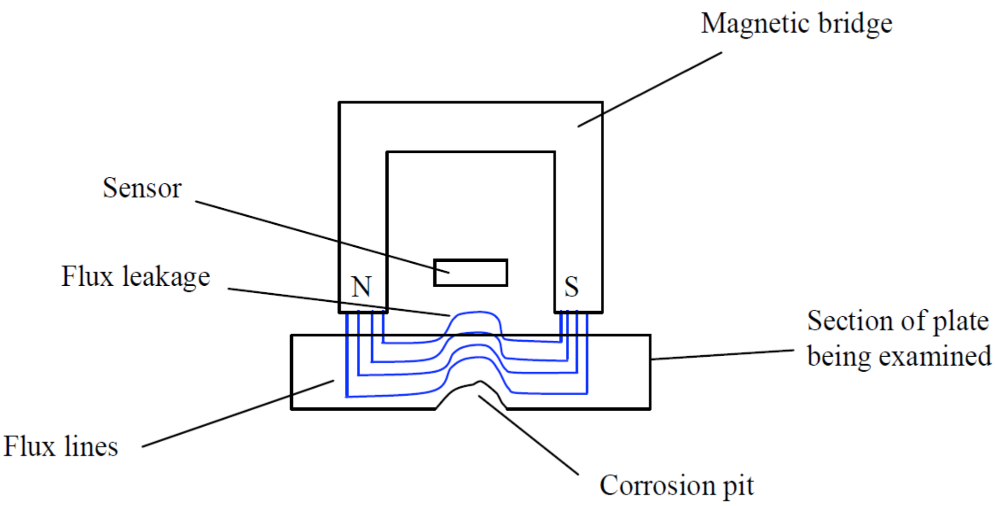

Figure 2-8: Principle of MFL showing the distortion of the MFL signals at the corrosion pit [37]

2.3.3.2 Ultrasonic (UT)

The principle of this technique is based on ultrasound waves transmitting signals circumferentially around the inside diameter wall and measuring the reflection time. The time elapsed between the interface and back wall echoes provide a direct measurement of the remaining wall thickness. Figure 2-9 depicts the UT principle. The standard ultrasonic inspection tool requires a liquid as a couplant for the UT waves to be transmitted to the wall of the pipeline. A new technology, however, has been recently released to the industry utilising the so called electromagnetic acoustic emission (EMAT), allowing the inspection of pipelines with no need for a couplant. EMAT allows metal loss to be determined quantitatively by measuring the time-of-flight of the back wall echo signal where the ultrasound signal is generated at the surface of the pipe wall rather than away from it [38].

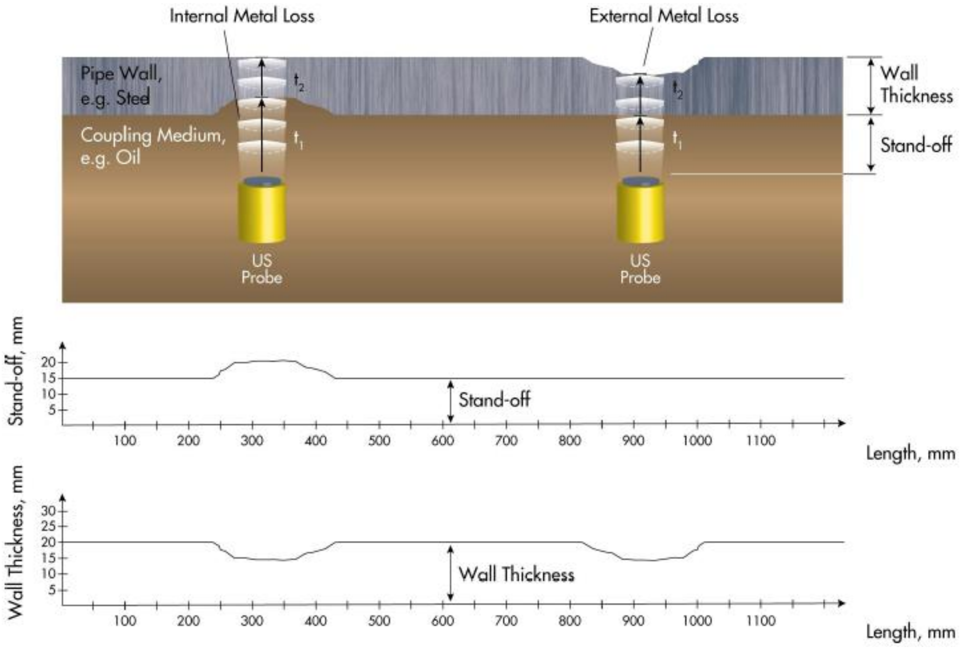

Figure 2-9: Principle of standard UT inspection technique showing the ultrasound waves transmitted and reflected back for internal and external metal loss defects [39].

2.4 Assessment of Corrosion

This section gives an overview of the flaw assessment methods used in assessing flaws which can be metal loss located at the internal or external surfaces of the pipelines or cracks. These types of assessments are crucial for determining the safe working pressure and thus allowing operators to operate within the safe operating windows of the pipeline. Assessment methodologies are generally used for determining the remaining strength of externally or internally corroded pipe subjected to internal pressure. Remaining strength is calculated based on the defects morphology as well as the pipe dimensions and material properties. Developments in defects assessment have also now taken into consideration the effects of neighbouring defects using interaction rules on the overall remaining strength of the pipeline. The interaction rules are usually expressed in terms of physical spacing between individual defects and classifying them as clusters [40]. There are few experimental burst projects carried out on interacting defects starting with the one conducted by Mok et al. [25] and ending with latest work conducted by Freire José et al. [26]. The sections below highlight the most widely used methods in industry for corrosion defect assessments.

2.4.1 Experimental Burst Tests on Pipes with Metal Loss Defects

Reliable and accurate predictions of failure pressure of pipes with metal loss defects is crucial in the integrity assessment of oil and gas pipes. This can be achieved by full scale pipe burst tests and investigated further by numerical modelling. Literature reviews [22-24] have indicated that around 360 burst tests of pipes with metal loss defects have been conducted since 1970 to date. The prime objectives of these burst tests were to achieve the followings:

- Produce empirical mathematical formulae that are able to predict the safe working pressure of pipes with metal loss defects (mainly corrosion defects away from welds).
- Investigate the effect of pipe material grades and dimensions (diameter and wall thicknesses) on the failure pressure.
- Determine the effect of defects morphology and orientation on the safe working pressure.
- Validate and improve both existing empirical formulae and numerical models.

The vast majority of these tests were mainly conducted on single metal loss defects, whether machined or actual metal losses due to corrosion. These tests have produced the existing failure methods in design codes such as ASME B31G. There are a few experimental burst projects carried out on interacting defects, starting with the ones conducted by Mok et al. [25] in 1986 which did not give a defined limit of when defect interact; rather it gave a general statement stating that the burst pressure of longitudinally aligned defects is independent of the separation distance for defects that are relatively far from each other. No further quantification of the spacing between the defects was given. The latest experimental work conducted by Freire José et al. [26] in 2013, provided guidance on the shape of failure experienced by interacting defects without further stating the critical spacing criterion.

Cosham et al. [22] stated that some of the experimental burst tests are not reliable due to the pipes being subjected to pressure reversals (varying number of pressure cycles). Additionally, due to insufficient published data available on defect dimensions, actual pipe wall thickness vs nominal thickness and material properties, it is difficult to replicate majority of the tests referred to in the literature for further studies.

2.4.2 Levels of Defects Assessment Techniques and Acceptance Criteria

2.4.2.1 Level 1 Assessment

Level 1 assessment is based on using semi-empirical formulae which are based on design calculations and observed data. The level of details required for this assessment is relatively shallow and does not involve the details of the situation being assessed. However, this assessment provides a good basis for allowing operators to make a good judgment on the fitness of the facilities/pipelines they are operating. In defects assessment, level 1 involves assessment of single defects based on their length and depth where ASME B31G code [41] and DNV RP-F101 [18] fit into this category. The main advantage of this assessment is that it allows the user to make an assessment in a very short time period.

2.4.2.2 Level 2 Assessment

Level 2 is based also on using semi-empirical formulae; however, the details required for this level of assessment are more detailed than those required in Level 1 where the user needs to input the defects depth profile as well as the width. In defect assessment, this involves gathering more details on the morphology of the defects where the depth profile plays a major role in the assessment. RSTRENG effective area [5] and DNV RP-F101 [18] methods fall under this category.

2.4.2.3 Level 3 Assessment

This assessment involves numerical techniques such as the FE method. A Level 3 assessment is primarily intended for use by engineering specialists experienced and knowledgeable in performing fitness for service (FFS) assessments. This analysis is carried out in situations where level 1 and level 2 assessments produce conservative failure pressure suggesting to the operator a system shutdown or immediate action in pressure de-rating, repair or section replacement. For offshore operations, carrying out such assessments on pipelines with interacting defects may prove to be a wise decision to take, as the costs associated with repairs are usually quite high taking into consideration the cost of barges, divers, associated repair facilities and possible operational shutdowns where the cost could be in the order of hundreds of thousands of dollars. Normally this analysis is carried out by consultancy firms; hence the cost is higher than level 1 or 2 analyses. Operators are advised to carry out cost comparisons between rehabilitation of the affected length of the pipeline and carrying out such detailed analysis especially for onshore pipes.

2.4.3 Flaw Assessment Methods and Techniques

Several assessment techniques for metal loss defects in pressurised pipes have been devised based on experimental observations. The most commonly used are the ASME and DNV codes which will be discussed in this section. All of these codes provide simplified acceptance criteria which are derived based upon a limit-load solution for a blunted axial crack-like flaw in a pressurized pipe [42]. A detailed review of the failure criterion used in FE analysis to predict failure pressure in pipes with metal loss defects will be further explored along with a review of numerical studies conducted for both single and interacting defects.

2.4.3.1 ASME B31G

The manual of corrosion defects assessment was initially published in 1984 by the American Society of Mechanical Engineers (ASME) following the extensive work done by the American Gas Association (AGA) in the early 1970's [6]. AGA carried out experiments on pipelines with various sizes of corrosion metal loss defects to develop methods for predicting the pressure strength. The ASME B31G committee further validated the methodology adopted by AGA through an experimental program of 47 full-scale tests of pipelines containing actual corrosion defects [22]. Unfortunately, specific details with regards to the defects morphology and steel mechanical properties used are not available. The tests done were limited to API 5L Grade X52 pipelines with a diameter of 762 mm and up to a wall thickness of 9.5 mm [44]. The defects in this code were idealised with a parabolic shape and the area of the metal loss area is assumed to be equal to (2/3)dL. Both 1984 and 1991 revisions of ASMEB31 are prescribed by several papers as overly conservative method with the following limitations:-

- Not valid for defects occurring in the weld or heat affected zones.
- Based on single defects with a parabolic shape.
- Gives conservative results for long defects as it considers any defect with $L > \sqrt{20Dt}$ as an infinite defect. In other words, the values for burst pressures predicted by the B31G equation are excessively low. The main reason for this behaviour is the hypothesis of infinite length mentioned above together with the expression adopted by this method to calculate the flow stress.

The failure pressure based on the original ASME B31G-1984 is calculated as follows:-

For short length defects, where L is defined by

$$\mathrm{L} \leq \sqrt{20\mathrm{D} \cdot \mathrm{t}} \qquad \textbf{(2-4)}$$

The failure pressure, P_f , is defined by the below formula, where the defect take a parabolic shape:

$$P_f = \frac{2(1.1\sigma_{y)}t}{D}\left[\frac{1-({}^2/_3\ \frac{d}{t})}{1-({}^2/_3\ )((\frac{d}{t})/M))}\right] \qquad \textbf{(2-5)}$$

For long length defects, where L is obtained by the following equation;

$$L > \sqrt{20Dt} \qquad \textbf{(2-6)}$$

the failure pressure, P_f, is calculated by the following equation where the defect takes a rectangular shape:

$$P_f = \frac{2(1.1\sigma_{y)}t}{D}\left[\frac{1-(\frac{d}{t})}{1-((\frac{d}{t})/M))}\right] \qquad \textbf{(2-7)}$$

The Folias factor, bulging factor, M for the above failure pressure cases, is calculated by the following formula:

$$M = \sqrt{1 + 0.6275(\frac{L}{D \cdot t})^2 - 0.00375\ (\frac{L^2}{D.t})^2} \qquad \textbf{(2-8)}$$

The bulging factor (Folias factor, M) is a geometric parameter developed to account for the stresses induced by the bulging which occurs at the corrosion defect of a pressurised pipelines [43].

Based on further experiments, AMSE B31G was modified in 1991, where the Folias factor was modified and the failure pressure for long defects was further refined as follows:

$$M = \sqrt{1 + 0.8(\frac{L^2}{Dt})^2} \qquad \textbf{(2-9)}$$

$$P_f = \frac{2(1.1\sigma_{y)}t}{D}\left[1 - \frac{d}{t}\right] \quad \textbf{(2-10)}$$

In 2009, ASME B31G was further refined to overcome the limitations built in the 1984 and 1991 revisions by modifying the Folias factor and the defect geometrical approximation factors, as follows:

$$P_f = \frac{2\sigma_y t}{D}\left[\frac{1 - 0.85(\frac{d}{t})}{1 - 0.85(\frac{d}{t})/M}\right] \quad \textbf{(2-11)}$$

where M is defined by:

$$M = \begin{cases} \sqrt{1 + 0.6275(\frac{L}{D \cdot t})^2 - 0.00375\,(\frac{L^2}{D.t})^2} & For \;\; L \leq \sqrt{50D \cdot t} \\ 0.032\left(\frac{L^2}{D \cdot t}\right) + \; 3.3 \; For \;\; L > \sqrt{50D \cdot t} & \end{cases} \quad \textbf{(2-12)}$$

However, this method gives a conservative failure pressure for cases where the pipeline contains interacting defects.

2.4.3.2 RSTRENG (0.85DL and Effective Area Method)

The RSTRENG method was an improvement extension to ASME B31G-1991 [44] as to simplify the excessive conservatism. The acronym of RSTRENG stands for remaining strength. The initial method of RSTRENG assumed a defect area of 0.85 DL, is given by the following equation, similar to that of the modified ASMEB31-2009 but with an additional 68.95 MPa to the yield stress.

$$P_f = \frac{2(\sigma_y + 68.95)\ t}{D}\left[\frac{1 - 0.85(\frac{d}{t})}{1 - 0.85(\frac{d}{t})/M}\right] \tag{2-13}$$

where M is defined by:

$$M = \begin{cases} \sqrt{1 + 0.6275(\frac{L}{D \cdot t})^2 - 0.00375\ (\frac{L^2}{D.t})^2} & For\ \ L \leq \sqrt{50D \cdot t} \\ 0.032\left(\frac{L^2}{D \cdot t}\right) + \ 3.3\ For\ \ L > \sqrt{50D \cdot t} \end{cases} \tag{2-14}$$

An iterative method based on the modified B31G that finds a minimum location within the defect profile was further developed. This method uses the measured profile of the defects (River Bottom Profile), as illustrated in Figure 2-10, and as such it requires accurate definition and measurement of the defects profile.

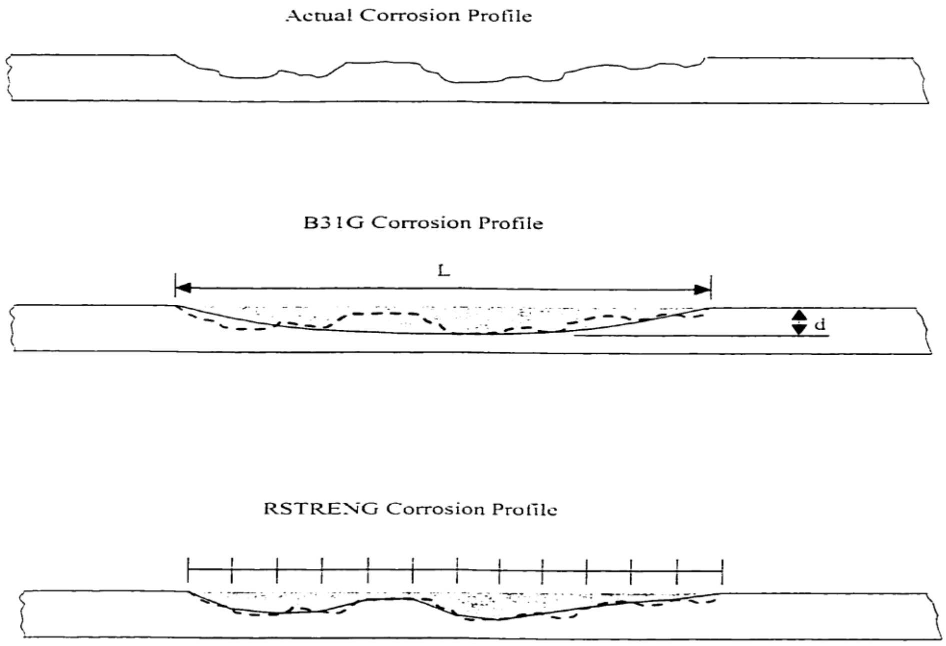

Figure 2-10: Corrosion Defect Profile According to RSTRENG Methodology [45]

Failure to measure the minimum location will lead to inaccurate failure pressure values, particularly for internal defects since the existing NDT techniques used for internal defect inspection, be it ultrasonic or magnetic flux, are prone to have inherent inaccuracy levels. Calculations are carried out to predict the failure pressure of various subsections of the total defect profile. The length of each subsection is taken as L and the area of metal loss, A, is calculated. The calculation process is iterative and as such executed in a computer software and repeated for all possible combinations of the various subsections. The minimum failure pressure is predicted in accordance with equations 2-15 to 2-21 below:-

$$P_f = P_O min\{R_{s,i}\} \quad i = 1,2,3, \dots n \tag{2-15}$$

$$P_O = \frac{2\sigma_f}{\left(\frac{\mathrm{D}}{t}\right)} \tag{2-16}$$

$$\sigma_f = \sigma_{SMYS} + 69\ (MPa) \tag{2-17}$$

$$R_s = \frac{1 - \left(\frac{A_i}{A_{O,i}}\right)}{1 - \left(\frac{A_i}{A_{O,i}}\right) \frac{1}{\sqrt{1 + 0.6275\left(\frac{L_i}{\sqrt{Dt}}\right)^2 - 0.003375\left(\frac{L_i}{\sqrt{Dt}}\right)^4}}} \tag{2-18}$$

$$for\ \left(\frac{d}{t}\right) \leq 0.8\ ;\ \left(\frac{L_i}{\sqrt{Dt}}\right) \leq 7.071 \tag{2-19}$$

$$R_s = \frac{1-\left(\frac{A_i}{A_{O,i}}\right)}{1-\left(\frac{A_i}{A_{O,i}}\right)\frac{1}{\left[3.3+0.032\left(\frac{L_i}{\sqrt{Dt}}\right)^2\right]}} \tag{2-20}$$

$$for\ \left(\frac{d}{t}\right) \leq 0.8\ ;\ \left(\frac{L_i}{\sqrt{Dt}}\right) > 7.071 \tag{2-21}$$

However, this method can give good results for external defects where the user can provide precise defect geometry, more accurate than the internal defects.

2.4.3.3 DNV RP F101

British Gas Technology along with DNV joined together in 1999 through a task force to come up with an assessment method which takes out the conservatism built in both ASME B31G code and RSTRENG and can be further used for high strength steels [9]. The outcome of this joint collaboration led to the release of an assessment code of practice which not only calculates the safe pressure for single defects subjected to internal pressure but it also calculates the safe working pressure (SWP) for complicated defects under the action of composite loads in multiple factors. The failure prediction was based on ultimate tensile strength of the pipe.

The failure pressure in the DNV code is based on ultimate tensile strength of the pipe and obtained via the following formula:

$$P_f = \gamma_m \frac{2(\sigma_U)t}{D-t}\left[\frac{1-\gamma_d\left(\frac{d}{t}\right)}{1-\gamma_d(\frac{d}{t})/Q)}\right] \quad \textbf{(2-22)}$$

The Folias factor has been substituted by the Q factor which is based on laboratory tests conducted by DNV [46] as follows:

$$Q = \sqrt{1+0.31(\frac{L}{\sqrt{Dt}})^2} \quad \textbf{(2-23)}$$

The validity of the Folias factor used by ASMEB31G and RSTRENG was investigated by Cronin and Pick [47] and found to be inconsistent with the corresponding FE results.

The DNV RP F101 manual considers both single and complex (interacting) shaped defects, the details of which can be further accessed in the manual itself. Based on the DVN code, there is no interaction between defects if the longitudinal and circumferential distances satisfy the following conditions:

$$Longitudinal\ limit\ (S_l) = 2.0\sqrt{D \cdot t} \tag{2-24}$$

$$Circumferential\ limit\ (S_c) = \pi\sqrt{D \cdot t} \tag{2-25}$$

2.4.3.4 Finite Element (FE) Method

2.4.3.4.1 Failure Criterion

In a ductile steel pipe failure, two possible scenarios of metal moss defects have been identified [22] as follows:-

First, as the pipe internal pressure rises, local thinning will occur in the remaining pipe wall ligament. As thinning progresses, necking of the ligament and failure will occur due to void nucleation, growth and coalescence, similar to that seen in a tensile test of a steel specimen.

Second, a crack could initiate at the defect as a result of micro-stress raisers (e.g. local surface irregularities caused by defective machining) through void nucleation and growth. Toughness of the pipe material governs what happens next in terms of crack behaviour and progress. Unstable crack propagation is quantitatively explained in terms of fracture mechanics theory. However, the first defect assessment equation [3] which is incorporated in all the existing defects methods incorporates a bulging factor that accounts for stress amplification at the defect ligament resulting in a flow stress, σ_f given by:

$$\frac{K_c^2\pi}{8c\sigma_f^2} = In\ sec\frac{\pi}{2}\frac{M_T\sigma_T}{\sigma_f} \quad \textbf{(2-26)}$$

The flow stress depends on the strain hardening characteristics of the metal and the assumed yield criterion, where experimental results show that the failure stress can be approximated by either the SMYS or UTS depending on the defect method as will be seen in the subsequent sections.

Through the use of FE analysis, two failure criteria are cited in the literature to predict the failure pressure of metal loss defects in pipes; strain-based and stress-based criteria. The first criterion is a strain-based criterion which has been refuted by an investigation by British Gas through the work of Kirkwood et al [7] who concluded that a strain-based approach overestimates the failure pressure. Earlier and through the work of Chouchaoui [48], it was concluded that a great deal of scatter existed when predicting the failure pressure of pipes with metal loss defects. A later work by Kim et. al [48] presented a comprehensive study that compared stress-based and strain-based failure criteria which were derived as a function of stress triaxilaity on metal loss assessments. Both experimental and numerical validations were carried out in the study. The authors concluded that the stress-based criterion predicted the failure pressure with higher accuracy than that predicted by the strain-based failure criterion. Figure 2-11 depicts the outcome of the study conducted by Kim et al [48]. This further confirms the fact that in metal loss defect assessment, the use of the stress-based criterion evaluated by the true ultimate tensile stress (UTS) would yield a reliable failure prediction value.

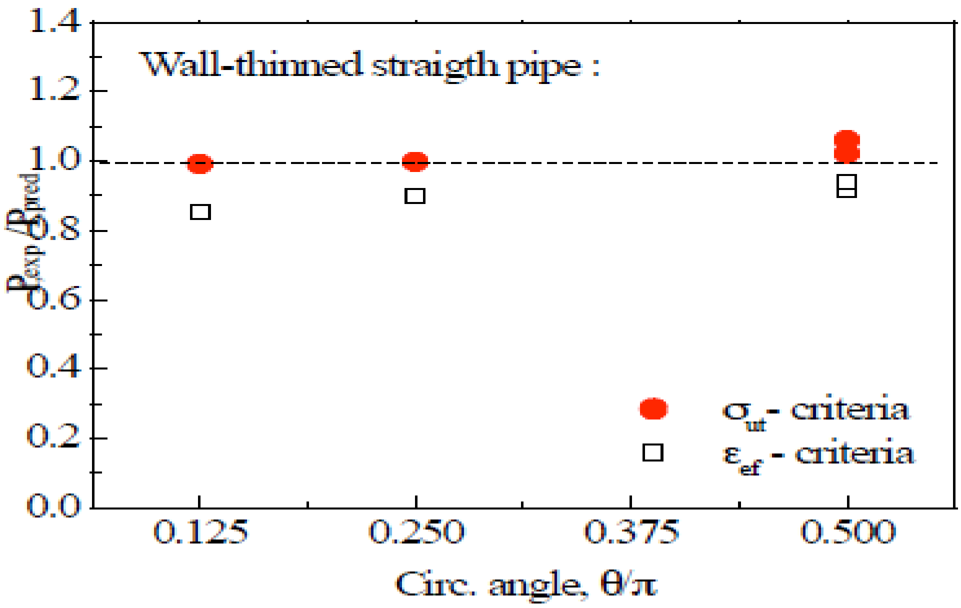

Figure 2-11: Comparison of experimental and estimated failure pressures of local wall-thinned straight pipe using stress and strain-based failure criteria [48]

2.4.3.4.2 Finite Element Analysis of Single Defects

Numerical assessment of corroded pipes with single axial defects was undertaken by Chiodo and Claudio [42]. The authors used a quarter-symmetric model with 8-node, 3-D elements arranged into several variable thickness layers over the pipe half-length. The study looked at the application of a stress-based criterion based upon plastic instability analysis to predict the failure pressure of pipes with axial metal loss defects. The aim of the study was to further obtain insight into effects of defect geometry and material properties on the attainment of a local limit load to support the use of stress-based burst strength criteria in defects assessment. Previous experimental burst testing carried out on pipe specimens with varying defect configurations made out of API X65 and X100 steels has revealed the effectiveness of a stress-based criterion in burst pressure predictions using the following equation:

$$\sigma_f = \eta\sigma_u \tag{2-27}$$

The adjustment factor, η, which takes values between 0.8 and 1.0 exhibits a potential dependence on defect geometry and possibly on the material's strain hardening capacity. The overall results from this study suggest that the use of stress-based criteria based upon plastic instability analysis of the defect ligament is a valid engineering tool for integrity assessments of pipelines with axial corroded defects.

Building on to what was proposed by Chiodo and Claudio [42], Chen-Liang et. al [49], carried further analysis on existing literature covering burst test data to verify the accuracy of a stress-based criterion on predicting failure pressure in defective pipes. The FE models constructed in this study were based on using 20-node, reduced integration brick elements (C3D20R). Taking advantage of symmetry, only one quarter of the pipe segment was modelled. The authors The failure criterion adopted in their study stipulates that failure takes place when the von Mises stress through the remaining wall thickness ligament within the defect exceeds that true ultimate tensile stress. The single defect schematic and corresponding stress contours through the ligament are further presented in Figure 2-12.

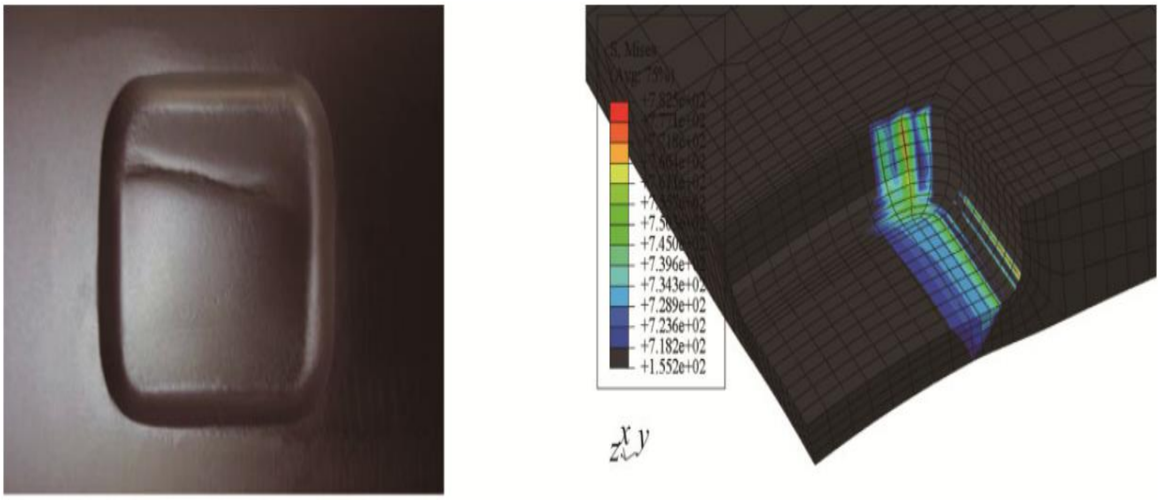

(a) Photograph of defect after failure (b) von Mises stress

Figure 2-12: Comparison of experimental with numerical results utilising the proposed failure criterion [49]

Bedairi et al [50] conducted a numerical analysis using implicit FE program Abaqus [51] to predict failure pressure of single metal loss defects based on average tensile test results. Following the previous works, symmetry was also utilised reduce the computational time whereby one quarter of the pipe containing the defect was modeled and 20 node reduced integration quadratic elements (C3D20R) were used. Plain strain conditions were simulated to restrain the pipe from expanding or contracting in the longitudinal direction Experimental burst tests of pipes with external diameter of 508 mm and wall thickness of 5.7 mm with varying metal loss depths in a rectangular shape were carried out. The failure criterion used by the authors postulates that initiation of failure occurs when the von Mises stress at the base of the defect reaches the true ultimate tensile stress. Comparison between experimental and FE results for these single metal loss defects shows an average difference of 3.2 % compared to that of 35.8 % when using RSTRENG which was discussed in section 2.4.2.2. An example from the study of the stress contour at a defect with 45% wall loss is shown in Figure 2-13. Similar numerical models and failure criteria were also used by

Fekete et. al [20] where the failure pressure of corroded pipes were established in the FE simulations when the von-Mises equivalent stress at the deepest point of the defect area reaches the ultimate tensile strength of the considered pipe material.

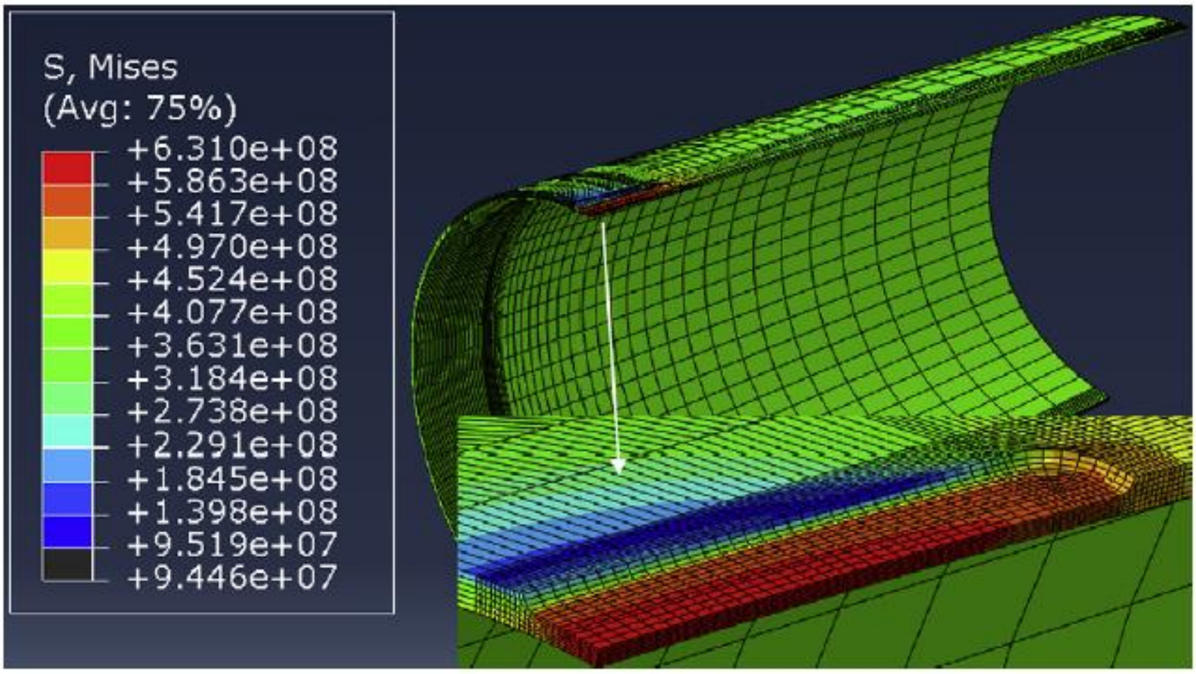

Figure 2-13: Effective stress contours of 45% metal wall loss defect model [50]

Bin et. al [23] carried out an extensive series of FE analyses on various elliptical single metal loss defects to derive a general solution for the assessment of defects in high strength steel pipes, i.e. API X80 and above. Three dimensional (3D) nonlinear FE models with quarter symmetry and C3D20R elements were used and implemented in the commercial software, ABAQUS. The main focus of the study was to investigate the effect of the length and depth of the corrosion defects to the failure pressure of pipes with metal loss defects. The failure criterion adopted in their study considers failure pressure to occur when the von Mises equivalent stress at the mid surface node of the ligament reaches the true ultimate tensile strength of the material as shown in Figure 2-14. The study produced a formula for calculating the failure pressure of defective pipes with single defects suitable for high grade strength steels as follows:

$$P_f = \frac{4\,t}{\sqrt{3D}}\sigma_u \left\{1 - \frac{d}{t}\left[1 - 0.7501\exp\left(\frac{-0.4174L}{\sqrt{Dt}}\right)\left(1 - \frac{d}{t}\right)^{-0.1151}\right]\right\} \quad (2\text{-}28)$$

Although the criterion used by Bin et. al [23] is different from the previous two studies, [42, 50] the location of the selected node does not make a major difference as the analysis was performed on thin wall pipes, D/T > 20, and with sufficient mesh refinement, the variation of stress around the highest stress region within the defect is minimal.

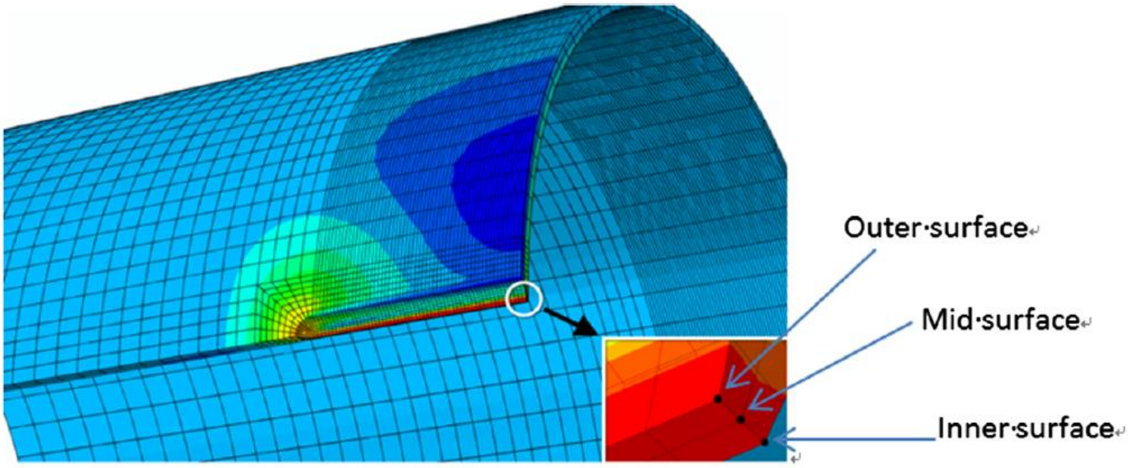

Figure 2-14: FE model of a pipe with metal loss defects showing the location showing the mid surface node location selected for the failure criterion [23]

2.4.3.4.3 Interacting defects Finite Element Analysis

Advantica group were among the first research centres to utilise FE analysis on interacting defects [52] where again symmetry of geometry was considered and quadratic reduced integration elements were used. The outcome of the research work was a new guidance for interaction of metal loss defects in pipelines. The failure criterion used in the study stipulates that failure of a pair of defects is deemed to occur when the maximum von Mises equivalent stress in either wall thickness ligament is equal to the true ultimate tensile strength of the material, see Figure 2-15.

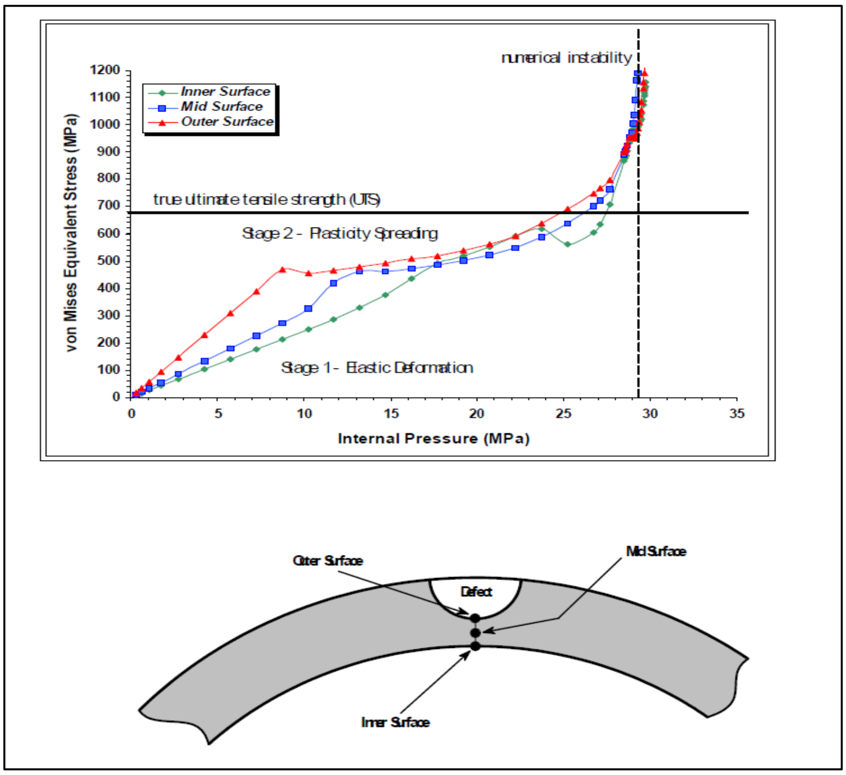

Figure 2-15: von Mises Equivalent Stress Variation with Increasing Pressure Through Minimum Ligament [52]

It is concluded from this work that the 6t criterion (defect clusters interact when they are spaced six wall thicknesses (6t) from each other) used at present can be over-conservative, particularly when assessing the interaction of small pit-like corrosion defects. Differences in failure pressures between defects of similar dimensions with varying spacing is than 10 %. Additionally, they also concluded that FE analysis can achieve failure prediction with high confidence in all cases of defect interaction.

The University of Waterloo in Canada through the work of Chouchaoui and Pick [8] were also among the first to use FE analysis to investigate the accuracy of the existing corrosion defects assessment methods such as ASME B31G and the behaviour of longitudinally aligned pipe metal loss defects. They demonstrated, through experimental burst tests on pipe material grade of API 5L X46 with outside diameter of 304.8 mm and wall thickness of 6.35 mm as well as FE analysis, that the failure pressures predicted by empirical methods are conservative. The pipes which were used in the experimental work failed in closed ended condition in a pipe length of 1.8 m where FE analysis showed that the radial end constraint does not influence the behaviour of the metal loss defects located at the centre of the pipe and away from the pipe seam weld. A failure criterion based on the von Mises equivalent stress was used to predict failure when the ligament between the two defects reaches the material true ultimate tensile strength. The study analysed mainly longitudinally spaced defects and considered only parabolic shaped defects. Figure 2-16 depicts the FE model used in the study.

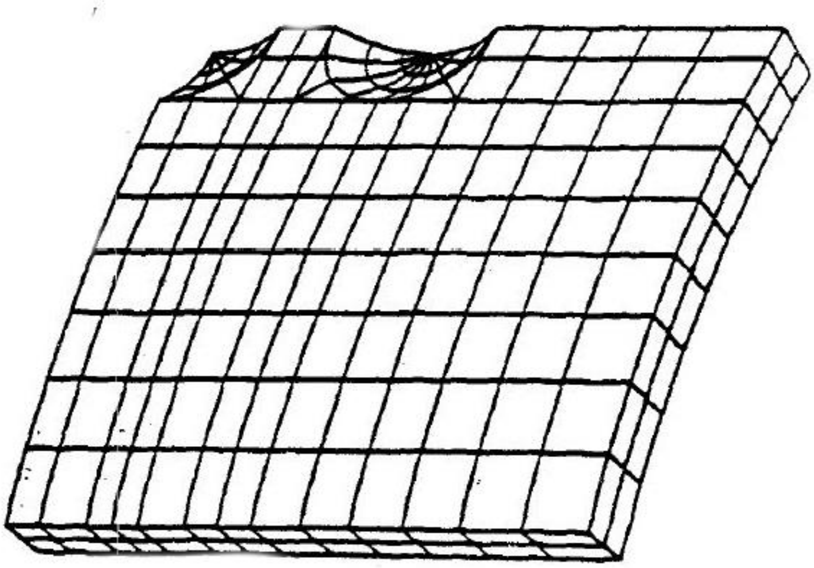

Figure 2-16: Finite element models with longitudinally aligned metal loss defects [8]

The failure criterion adopted in their study utilises the true ultimate tensile stress as an indicator for interaction to occur between the ligaments separating the defects. Comparison between von Mises and Tresca stresses revealed that the latter predicts failure pressure with conservatism. The study concluded that the criterion for interaction of longitudinally aligned defects is judged on the basis of the deepest individual defect, and for multiples of defects where there are more than two aligned defects, the central defect will have the tendency to fail first.

The flaw assessment work using FE analysis continues to be an interest within the University of Waterloo where lately they have published work on the interaction of cracks with single corrosion defects [50]. The assessment of the single corrosion metal loss defects follows the earlier discussed failure criterion where failure is judged by the highest node at the base of the defect reaching the true ultimate tensile strength. The published results [50] on crack assessment using FE analysis shows an error of more than 15% against the experimental work. The main contribution to this high error percentage was the slightly inaccurate modelling of the crack end shape as round corners rather than elliptical.

In Brazil and through the efforts of Petrobras R&D centre and a number of Brazilian Universities, a new interacting rule given the name of Critical Path Method (CPM) has evolved. The method has been validated by both experimental and FE methods. The FE models considered quarter symmetry, C3D20R elements and various through thickness elements. It basically suggests a set of rules allowing the drawing of failure lines that represent adjacent areas positioned along selected circumferential and longitudinal directions of pipeline that contain defects clusters [26]. Failure pressures are calculated for the individual drawn lines to provide the most critical one. The critical line which follows the failure criterion where the maximum true ultimate tensile stress is reached, is then considered as the most probable rupture path, and it corresponds to the minimum calculated internal pressure to take the pipeline to failure. Figure 2-17 shows the possible critical path (CP) lines for a group of three defects where the metal-loss depth of defect d_2 is smaller than the metal-loss depths of defects d_1 and d_3.

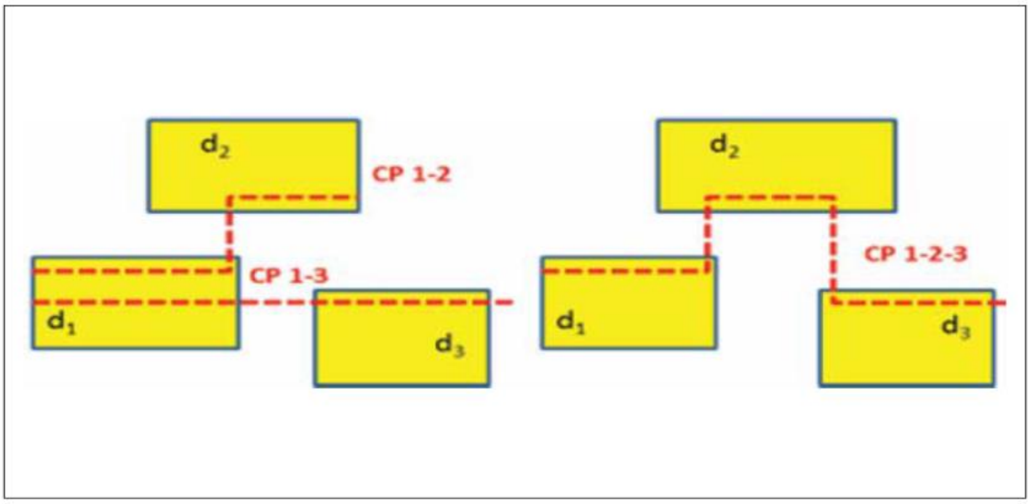

Figure 2-17: CPM method showing possible failure paths for a group of three defects where the metal loss depth of defect 2 is smaller than the metal loss depths of defects 1 and 3 [26]

The group has also produced graphical representations showing the CPM method in comparison with the corresponding experimental results and computed FE von Misses stress contours, as depicted in Figure 2-18. The most probable fracture critical path (smallest calculated burst pressure) indicated by the Critical Path Method is represented by the dashed lines. Finite Element solutions at the numerical burst pressure are represented by contour plots of the von Mises equivalent stresses.

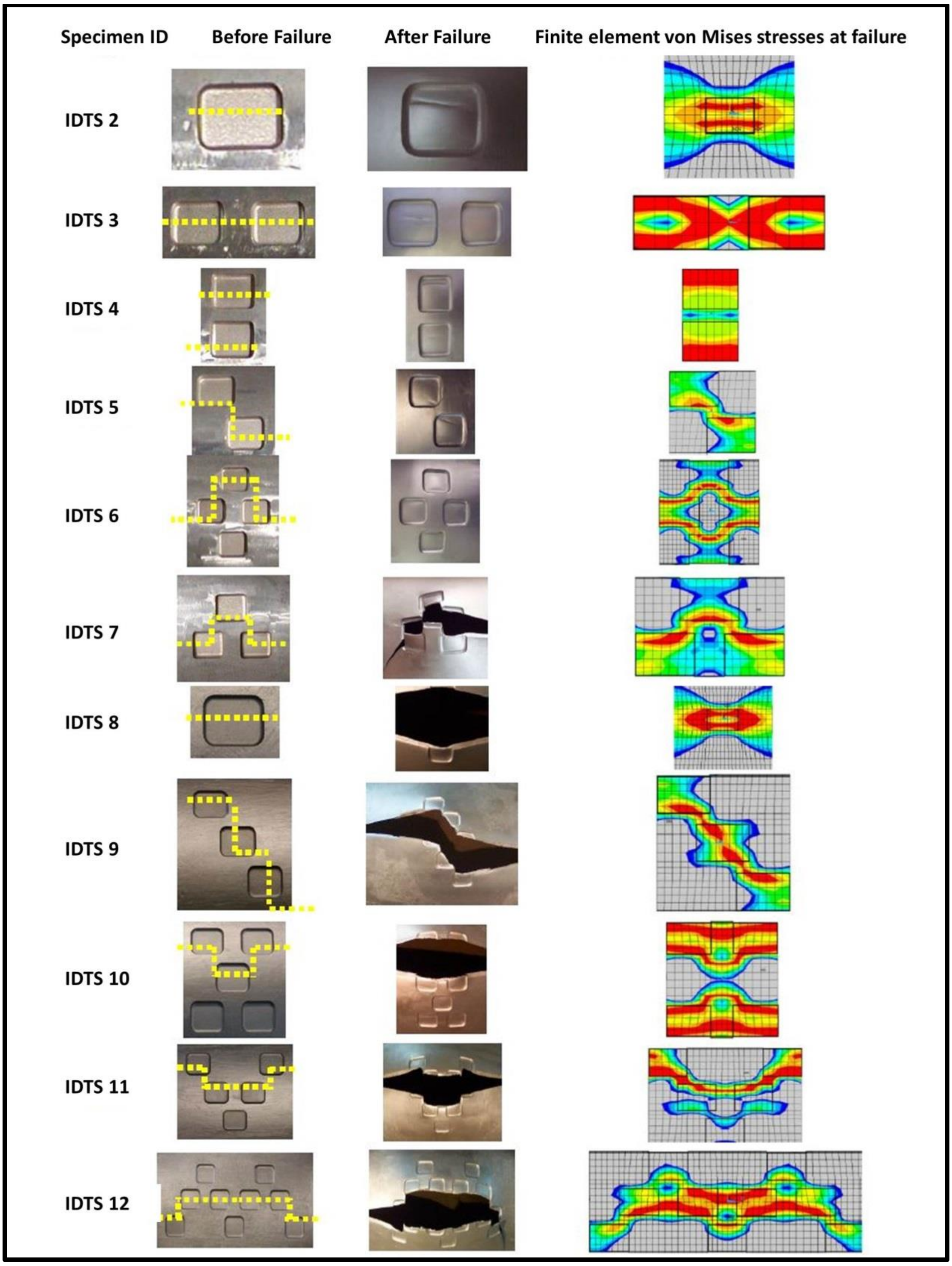

Figure 2-18: Actual geometric arrangements of defects before and after the burst test [26]

The group concluded from the study that the predicted failure pressure differences between the proposed method and the experimental values falls within 5%, which the authors claimed to be as a result of the scatter that exists in any experimental results. The authors also concluded that the CPM method predicts failure pressure which is more accurate than the existing defect assessment methods and is closer to the FE solutions and actual experimental results.

2.4.3.5 Final Remarks on Defects Assessment Methods

The empirical methods listed in this section allow operators to make quick decisions on the integrity status of their operating pipelines based on methods that rely on derived formulae based on experimental tests. However, these methods have proven to be conservative when it comes to defects spaced close to each other or on long grooving corrosion defects. Based on experimental measurement, the burst pressure percentage error for RSTRENG was found to be 20% conservative and 34% conservative for B31G [53]. It was highlighted earlier that the standard methods used in assessing corrosion defects have been based on experimental work utilising low and medium strength steels (lower than X70), although the standard practice developed by DNV takes into account high strength steel and its results are often less conservative for lower strength steel, typically X42 and below [54]. It is also concluded that there are no universally agreed failure criteria for use in numerical analysis for both single and interacting defects. Furthermore, there is no single agreed defect interaction rule, and pipeline operators around the world have various rules to pick and choose from.

2.5 Role and Effect of Residual Stress on Pipeline Flaws Assessment

2.5.1 Overview

Residual stress is defined as the locked stress that resides in a material when no external forces are being applied. The effect of residual stress has received little attention in the past and this could be attributed to the historical difficulties associated with obtaining accurate measurement and prediction results [55]. Concentrated efforts are being made through conferences such as the one dedicated to residual stress named "The European Conference on Residual Stress – ECRS" [56] to shed light on the knowledge and experience around the world on residual stress. Law et al [57] stated that there is little knowledge available on residual stress data of as-manufactured pipelines and this could be attributed to the lack of methods which could give accurate residual stress values. Additionally, the profile and orientation of residual stresses fluctuate along the length of each pipe joint and may differ greatly from pipe to pipe [58]. It is interesting to note that to date there are no specific residual stress limitation requirements being imposed for inclusion in pipeline and tube manufacturing specifications [58].

2.5.2 Origin and Principles of Residual Stress

In general, residual stresses fall into two main categories, macro and micro levels which indeed can determine the level of measurements to be used for each [55]. Both categories may be present in the structure at any one time [59]. The micro level is further divided into two sub-categories: one which varies from grain to grain in the material, also called meso level, and one which varies within a single grain. The macro level varies over a distance which is large in comparison to the microstructure of the material. Figure 2-19 schematically defines the difference between the residual stress categories. Lu [60] listed a number of processes which can cause the macro stress levels, ranging from welding to metal work treatment processes. Residual stresses can have an equivalent effect on pipe strength as other mechanical stresses, as they account for up to ~25% of Specified Minimum Yield Strength (SMYS) [61]. Liu et al [62] stated that it is common to assume that the residual stresses are as high as the yield stress. They can be added or subtracted from the direct stresses applied on the structure, and as a consequence when unexpected failure occurs, residual stress could potentially combine critically with the applied stresses [55]. There are three main processes which could lead to residual stresses; mechanical, thermal and metallurgical.

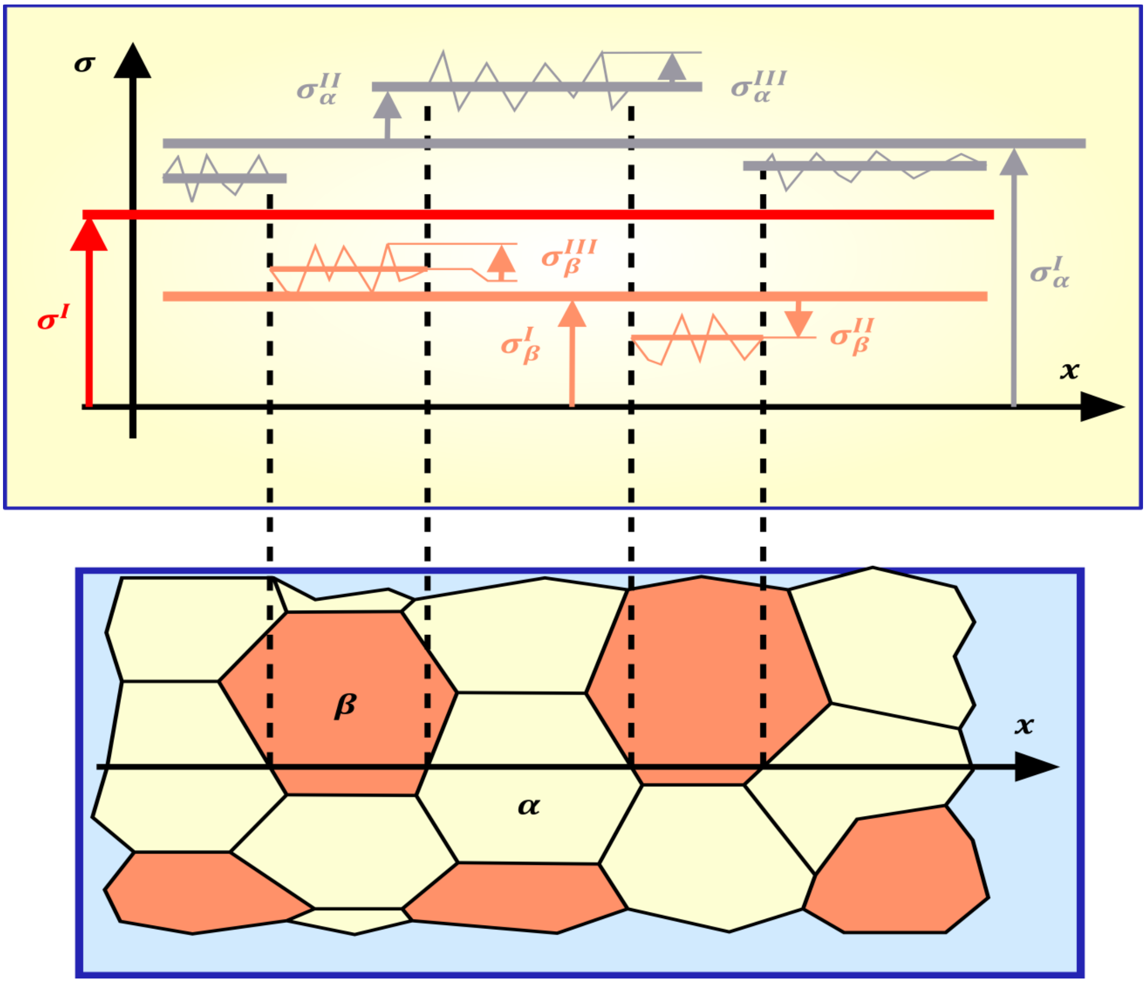

Figure 2-19: Definition of residual stresses categories, 1 (entire structure), 11 (at grain level) and 111 (with the individual grains) [63]

2.5.3 Determination of Residual Stresses Using the FE Method

The use of numerical methods to investigate the residual stress has been widely researched but with limited cases related to pipes with corrosion flaws. Aleshin, et.al [64] have carried FE analysis on pipe manufacturing starting from steel plates and going through various stages of production taking into consideration geometric and material nonlinearities. Part of this analysis was to look at the residual stresses produced at each stage. The authors emphasised the importance of obtaining the values of residual stress required for further accuracies when establishing the remaining strength of pipe systems. The authors concluded by stating that the accuracy of the results obtained from numerical analysis (FE) and the measured data fall well within 1% of each other.

2.5.4 Final Remarks on Residual Stress Consideration in Flaw Assessment

Several papers and experiments have shown some degree of contradiction in results related to the accuracy of the existing defects assessment codes such the modified B31G, RSTRENG and DNV RP F101, and residual stress could be a contributor to this contradiction. The literature review has indicated there is a gap in identifying the effect of residual stress on metal loss and this could be attributed mainly to the challenges faced in determining and quantifying this type of stress at the field sites.

2.6 Summary and Knowledge Gaps

In section 2.4 a review was made of the several assessment methods used for calculating the safe working pressure of corroded pipes. Historically the defects are assumed to fail by plastic collapse in which the remaining strength of the material is assessed in terms of defects through wall thickness depth and axial length by an empirical flow stress parameter. Over recent years, many experimental tests on modern pipes have shown that these flow stress computations are very conservative, which resulted in unnecessary repair or replacement in general.

Based on the relevant needs in the area of metal loss defects interaction roles, the knowledge gaps can be identified as follows:

1. There is still a lack of universally agreed defect interaction rules, and pipeline operators around the world have various rules to pick and choose from.
2. Existing experimental work on pipe metal loss defects is mainly done on single defects with few that are executed on defect interaction which have insufficient details to use and model.
3. Existing experimental work is done on a single defect shape while there is a need to investigate the effect of defect shapes on the interaction roles.
4. Existing methods mainly use empirical equations for deriving safe working pressure of pipes. Today's high advancement of data storage and processing capabilities makes FE analysis a good assessment tool to choose for assessing interacting defects thus proving a cost saving when it comes to pipe repair and replacement.
5. The defect criterion for defining failure in FE analysis is currently based on a single node achieving the highest von Mises stress, while this may potentially give a good

indication of failure for a single defect, applying this criterion for interacting defects still requires further investigation and development.

6. Existing defect assessment methods do not consider the effect of residual stress on metal loss defects and as such an area where further work needs to be concentrated on.

CHAPTER 3: FINITE ELEMENT METHODOLOGY - MODELS SETUP

3.1 Aim

This chapter gives an introduction to FE method and the preliminary work done to validate the experimental work. A nonlinear elastic plastic numerical modelling technique using the FE method is employed in this work to simulate the effect of metal loss in thin-walled pipes using the commercially available FE analysis software code ABAQUS/Standard 6.14 [51]. FE analysis is used to solve for displacements, strains and stresses caused by internal pressure.

3.2 Finite Element Method (FEM) Background

The FE method is used in this work to analyse the failure pressure of metal loss defects, single and interacting, in thin walled pipe joints. FE analysis is a numerical way of solving structural engineering problems which have challenging geometries, loadings, and material properties. It basically provides computed solutions of the stress and strain values in the structure under analysis. In this work, the structure, i.e. pipe, is assembled using a finite number of elements interconnected by nodes. The material properties for the structure are retained by the elements in order to determine the stiffness matrix. The stiffness matrix is calculated for each individual element and then assembled together to form the relationships between the forces and displacements in the model. Boundary conditions, e.g. applied forces and constraints, are applied in order for numerical singularity to be avoided, so that the structure remains stationary during the analysis instead of moving as a rigid body.

3.3 Finite Element Analysis (FEA) Procedure

A schematic diagram of the steps taken to simulate the FE models is depicted in Figure 3-1. Details of the FE models will be presented in the next subsections.

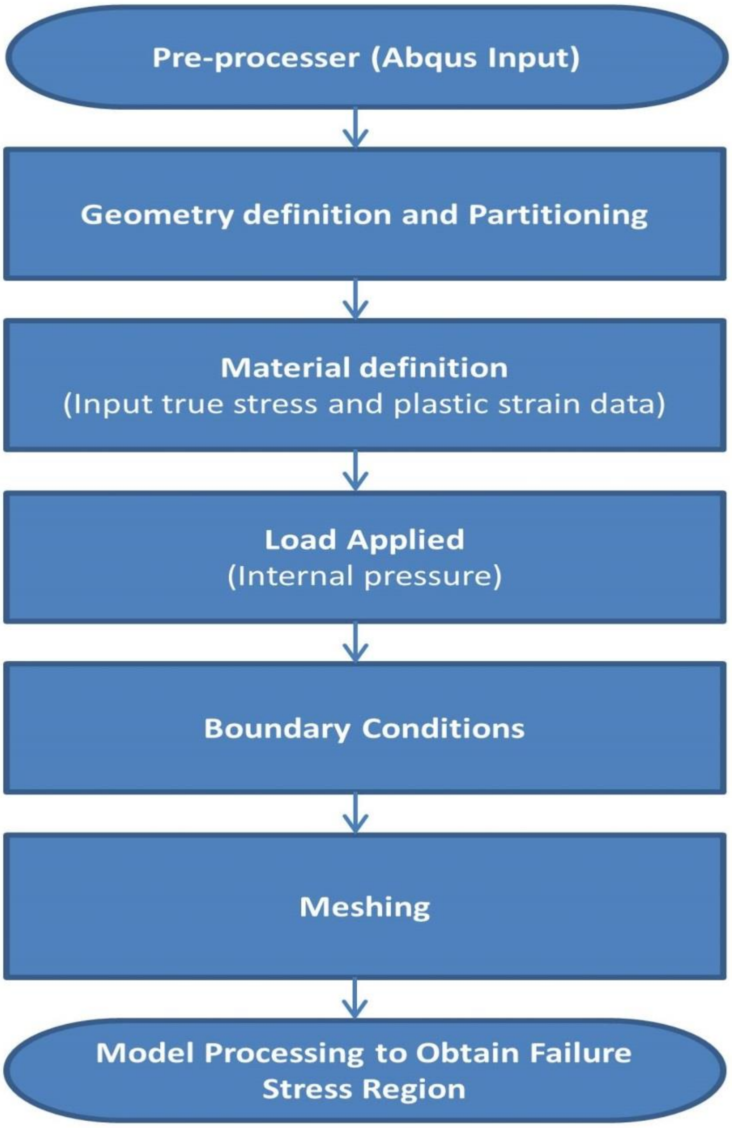

Figure 3-1: Schematic of FEA process

3.3.1 Geometry Definition

A quarter-model of a 20 inch thin pipe with a curved boxed defect is constructed to take advantage of symmetry conditions, where the total pipe length is 1.8 meters. The definition of a thin pipe as per ASME B31.4 code [65] is as follows:

$$\frac{D}{t} > 20 \tag{3-1}$$

For a longitudinal defect, it was relatively easy to construct these within the Abaqus environment. However, for circumferential and diagonal defects; these were constructed in Creo [66] and then transferred into the geometry model as parts using Abaqus built-in Creo associative interface code. Detailed partitioning takes place in this module and later further refined, if needed, in the mesh module. A typical defect shape and partitioning strategy is shown in Figure 3-2.

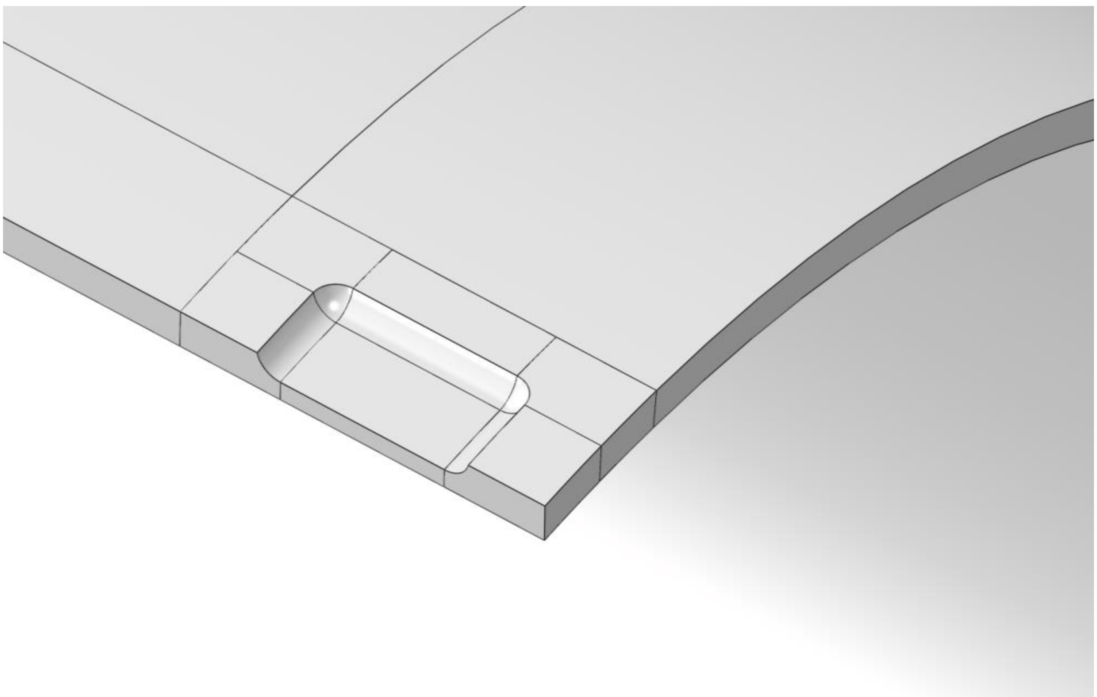

Figure 3-2: Typical Curved Boxed Defect Partitioning Strategy

3.4 Defects Details and Dimensions

Two types of defects on the outer surface of the pipe are modelled; circular defects and curved 'boxed' defects. The circular and boxed defect geometries have been chosen in order to make it practical to machine these defects on actual steel pipes to facilitate future experimental burst pressure tests. For a pipe with a nominal outside diameter of 508 mm, the defect depth tested is 50 % of the wall thickness for all the cases, with a radius of 35 mm for the circular defects and a square of side 35 mm for the curved boxed shaped defects. For the curved boxed defects, the radius of the groove throughout the defects edge is 5 mm, as shown in Figure 3-3. The curvature arc is created at a 45^{o} degree from the corner of the defect. Figure 3-4 shows a schematic of a typical circular defect which was adopted for the models created in the study. The distance between the defects is shown as (S) and is expressed as multiples of the wall thickness (t).

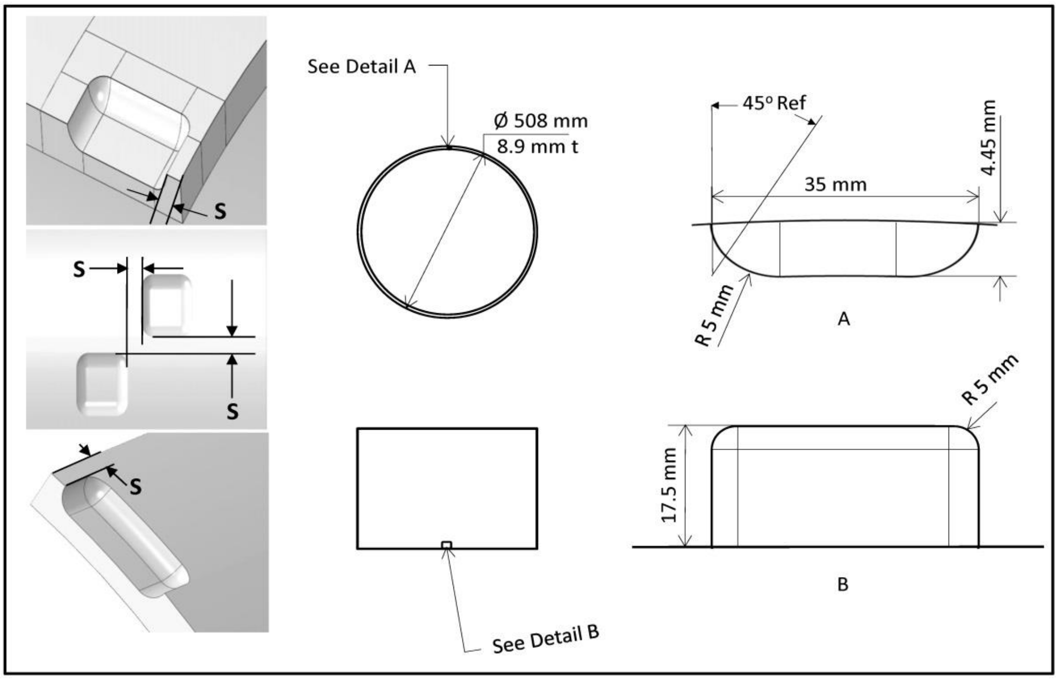

Figure 3-3: Detailed views of the curved boxed shaped defect

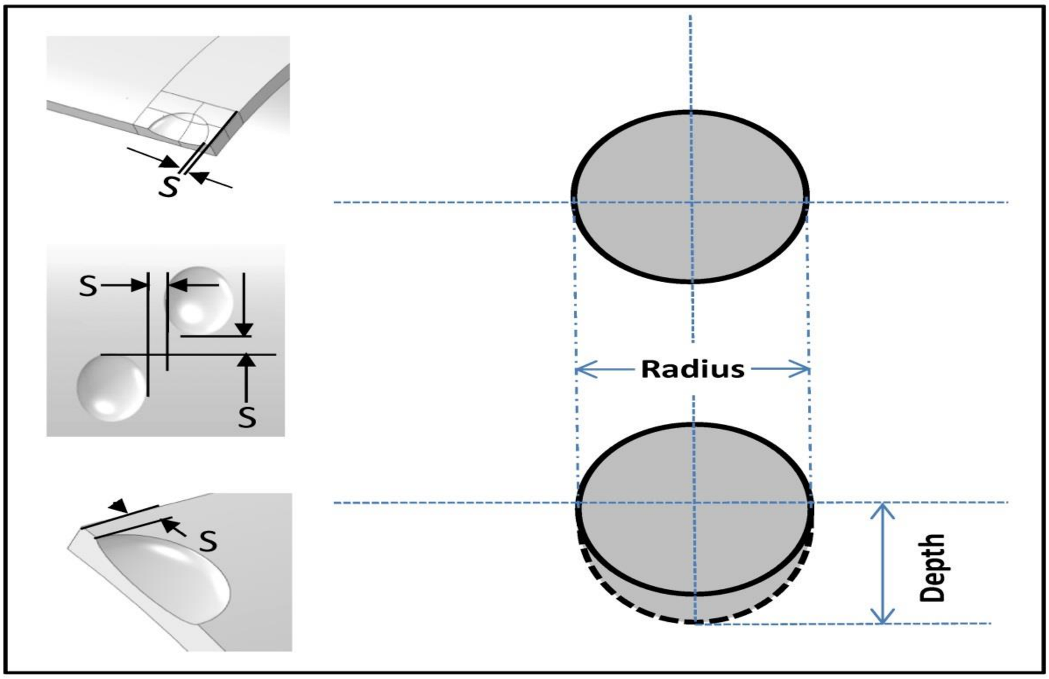

Figure 3-4: Schematic view of the circular shaped defect

3.4.1 Material definition

Ductile carbon steel pipe materials conforming to ISO 3183 [67] are used for the models constructed in the research work. These types of material are widely used in the oil and gas sector as they offer a wide range of properties such as strength, toughness and weldability. They are mainly composed of 98-99% iron, 0.001-0.24% carbon, 0.3-1.9% manganese and other alloys which have effects on strength and toughness [67, 68]. As the name suggests, ductility involves plasticity which in this case both the elastic and plastic properties are to be entered in the properties module. Poison ratio of 0.3 as per ASME B31.4 code [65] and the modulus of elasticity, as determined from tensile tests at ambient temperature, are entered into the elastic part. True stress and plastic strain values are entered into the plastic part of the Abaqus material module.

The material is modelled as an isotropic elasto-plastic material and true stress-true strain data are employed within Abaqus. It is acknowledged that some anisotropic behaviour does exist in the pipes as a result of the manufacturing processes; however, considering that the isotropic behaviour has yielded accurate results in terms of predicting failure pressure as reported by many researchers in the past [8, 11, 15, 16, 19-21], only isotropic behaviour is used in this work. The true stress-strain and plastic strain values are obtained from the engineering uniaxial stress-stress data using equations 3.2 to 3.4 which are only valid up to necking where the loading situation is no longer uniaxial throughout the gauge length [69]:

$$\varepsilon_{true} = \ln\left(1 + \varepsilon_{eng}\right) \tag{3-2}$$

$$\sigma_{true} = \sigma_{eng}(1 + \varepsilon_{eng}) \tag{3-3}$$

$$\varepsilon^{p} = \ln\left(1 + \varepsilon_{eng}\right) - \left(\frac{\sigma_{true}}{E}\right) \tag{3-4}$$

where σ_{eng} and ε_{eng} are the engineering (nominal) stress and strain respectively, while σ_{true} and ε_{true} are the true stress and strain respectively and ε^{p} is the plastic strain.

True stress and plastic strain values are recommended for a non-linear analysis as when the strains become large, i.e. more than 10%, the true stress/strain definitions are more accurate than the engineering stress/strain definitions which consider the original cross-sectional area and length rather than the instantaneous cross-sectional area and length.

For elastic-plastic analysis, the Abaqus material input module requires the user to input the Modulus of Elasticity (E), Poisson's ratio, yield stress and plastic strains of the material obtained from the uniaxial stress-strain curve of the material. Table 3.1 shows the values inputted for the pipe materials used in this work as inputted in Abaqus.

Table 3.1: True stress and plastic strain values

API 5L X60 (t= 5.7mm)		API 5L X60 (t= 8.1 mm)		API 5L X52 (t= 9.5 mm)		API 5L X60 (t= 8.9 mm)		API 5L X60 (t= 9.5 mm)		API 5L X60 (t= 10.5 mm)	
True Stress (MPa)	Plastic Strain	True Stress (MPa)	Plastic Strain	True Stress (MPa)	Plastic Strain	True Stress (MPa)	Plastic Strain	True Stress (MPa)	Plastic Strain	True Stress (MPa)	Plastic Strain
435	0.000	601	0.000	372	0.000	478	0.000	456	0.000	506	0.000
500	0.016	652	0.011	460	0.030	520	0.030	530	0.033	560	0.040
525	0.024	683	0.021	500	0.046	550	0.048	560	0.049	590	0.060
550	0.036	708	0.038	520	0.058	570	0.063	580	0.065	610	0.078
575	0.053	726	0.054	530	0.066	580	0.072	590	0.074	620	0.088
600	0.077	731	0.063	560	0.099	600	0.095	610	0.097	640	0.113
610	0.090	738	0.075	570	0.114	610	0.108	620	0.112	650	0.127
618	0.101	743	0.080	600	0.172	630	0.140	640	0.148	670	0.160
630	0.122	746	0.086	607	0.199	636	0.161	645	0.167	678	0.183

Both material non-linearity and geometric non-linearity (NLGEOM parameter in Abaqus) were invoked in the analysis. Geometric non-linearity takes place when the changes in the geometry of a structure as a result of its displacement under load are taken into account in analysing its behaviour. Geometrical nonlinearities have been entered into the FE analysis because of the extra nonlinear terms added into the strain-displacement relations and the effect of deformation on the equilibrium equations. In geometric non-linearity, the equilibrium equations take into account the deformed shape, whereas in linear analysis the equilibrium equations are always based on the original (unreformed) shape [70, 71]. In the cases studied in this work, geometric non-linearity was taken into consideration due to the highly non-linear behaviour of the metal loss defects which is characterised by large strain at the defect area, i.e. more than 10% strains.

3.4.2 Loads

The maximum pressure that a defect free thin pipe can withstand is normally calculated using Barlow's formula. Internal pressure loading is applied over the whole internal section of the pipe including the defect area. In Abaqus, the pressure is ramped where it increases gradually at each load step. Abaqus terminates the numerical simulation if convergence is not achieved within a pre-set number of iterations.

3.4.3 Boundary Conditions

Pipes are normally manufactured in average lengths of 12 meters. However, the numerical simulation study uses pipe lengths of 1.8 m which has been demonstrated in the literature to be sufficient to cater for the end effects [50, 72]. The 1.8 m pipe length is chosen here as a practical pipe length to enable the experimental laboratory tests of pipe burst pressures discussed in Chapter 5.

Symmetry conditions were applied to reduce the size of the model which results in better computational efficiency. Figure 3-5 and Figure 3-6 show the boundary conditions for both longitudinal and circumferential defects. For the longitudinal and circumferential defects, half the pipe length was modelled due to symmetry, whereas for the diagonal defects which are made with 45^{o} angle, the full pipe length was modelled. This resulted in a quarter-symmetry model for the longitudinal and circumferential defects and a half-symmetry model for the diagonal defects.

To simulate a pipe with end caps and to restrain the pipe from expanding or contracting in the longitudinal direction, plane strain conditions were assumed at the free end of the pipe, i.e. the pipe end was restrained in the axial (Z) direction. To avoid rigid body motion, one node was fixed in all directions. No axial load was applied and internal pressure loading was applied monotonically within Abaqus. This is in line with other FE simulations in the literature [23, 46, 50, 72-75] .

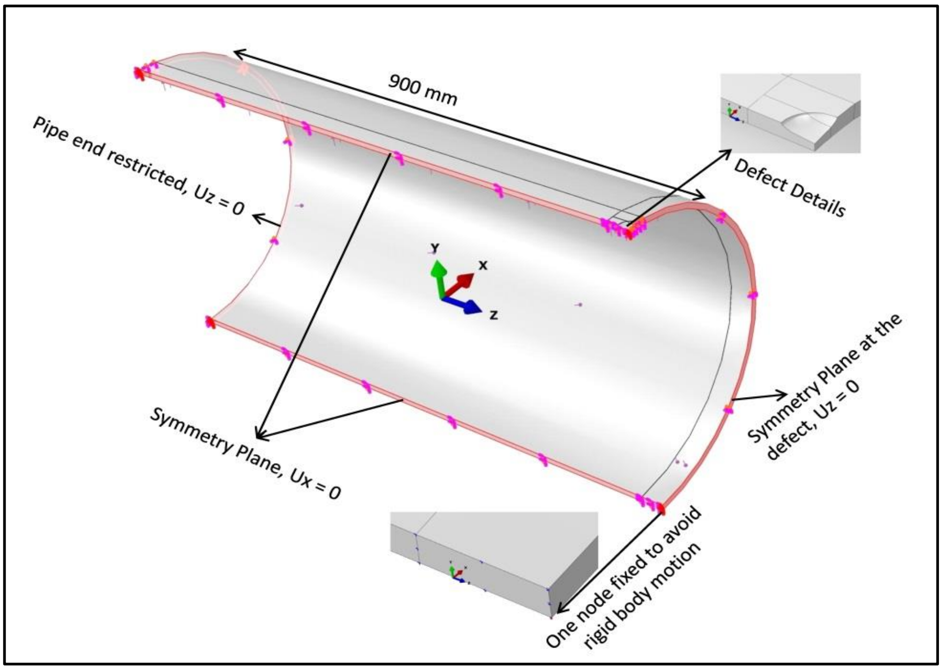

Figure 3-5: Boundary conditions typical for all longitudinal and circumferential oriented defects

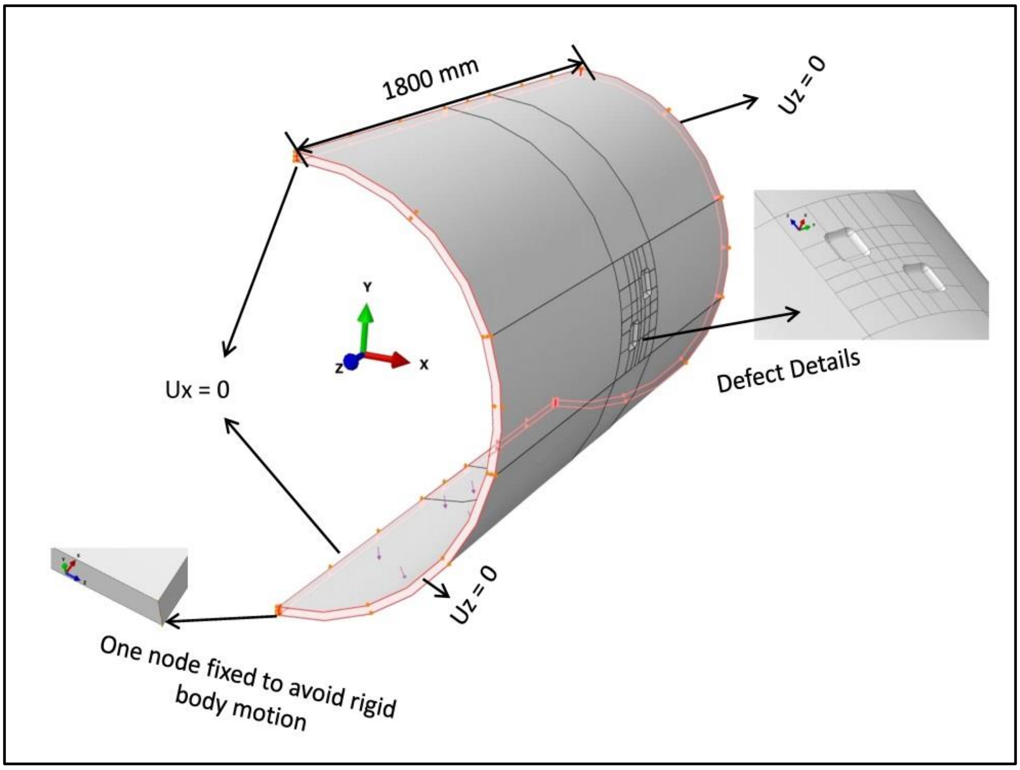

Figure 3-6: Boundary conditions typical for all diagonally oriented defects

3.4.4 Closed End (Plane strain) vs Open End Condition (Axial Load)

To examine the effect on the behaviour of the pipe with closed or open ends, two boundary conditions, with and without axial load, are analysed. The case details are further summarised in Table 3.2: Pipe and Defect Details.

Table 3.2: Pipe and Defect Details

No	D	t	Material	Defect type	Defect dimension
1	508	9.5	X60	Circular	R = 35 mm d = 5.25

The parameters and the mesh size were kept the same for both with and without axial load. The effect of the axial load, $\boldsymbol{\sigma}_L$, is schematically represented in Figure 3-7 and calculated as per equation 3-4 below, based on the thick cylinder theory to provide an accurate representation of a pipe with closed ends.

$$\sigma_L = P\,\frac{D_i^2}{D_o^2 - D_i^2} \tag{3-5}$$

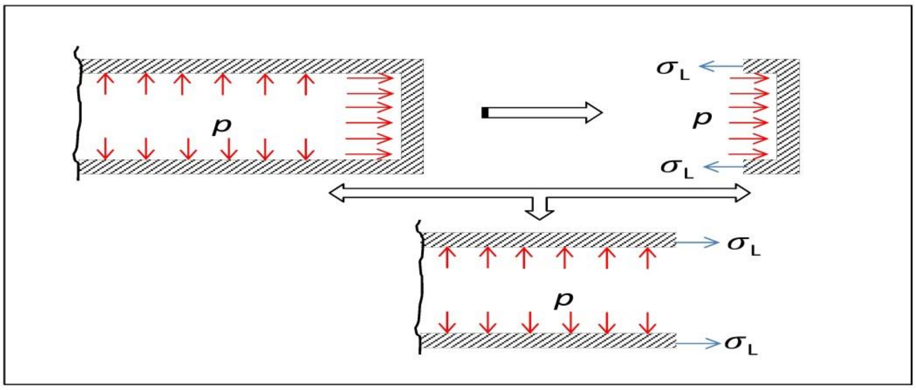

Figure 3-7: Axial load representation of a pipe with closed end (capped)

The boundary conditions for the two cases, i.e. where axial load is applied and where the axial load is replaced by displacement restriction in the axial direction are presented in Figure 3-8.

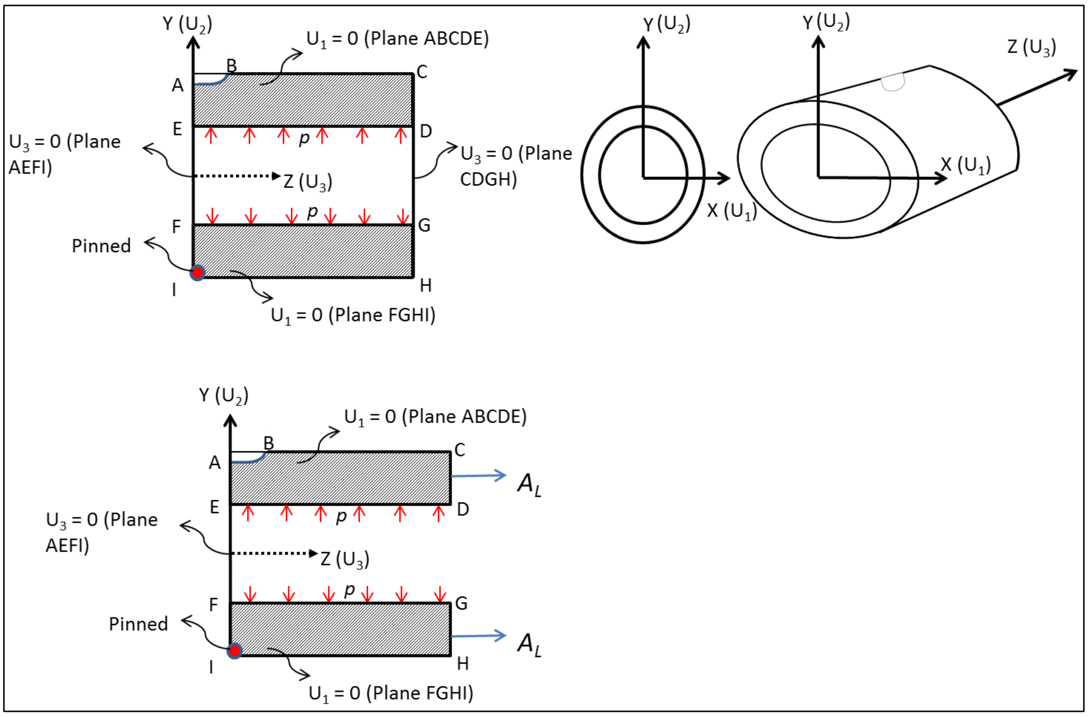

Figure 3-8: Schematic representations of the boundary conditions showing two cases; with axial load (bottom) and without axial load (top)

The failure pressure is defined here as the pressure which results in a node reaching the true UTS of the modelled material, however, a more sophisticated failure criterion will be presented in Chapter 4. Figure 3-9 shows that at the node located at the centre of the defect, the von Mises stress value tends to initially exhibit a small drop and then flattens after reaching the yield point before increasing gradually as the pressure is increased. This trend is observed regardless of the mesh density in this region, as shown in Figure 3-13. This behaviour is clearly different to the uniaxial stress-strain curve where hardening occurs after the yield point. This may be due to the immediate tri-axial post-yield stress redistribution in the other nodes around the node located at the centre of the defect as the pressure is gradually increased [76]. This trend has also been exhibited in [7, 14, 52, 77].

The difference in the failure pressure between the models with and without axial loading is only 1%. This result demonstrates that the failure pressure in these pipes is mainly governed by the hoop stress and plane strain conditions can be chosen for the pipe ends, i.e. no axial loading but with the free end restrained in the axial direction. This was also considered by many researchers in the past [23, 46, 50, 72-75]. One needs to take into account the length of pipe and the end effect to consider the plane strain solution. In all the cases studied in this work, the full length of the pipe is 1.8 meters which was demonstrated in the literature to be sufficiently long to overcome the end effect [50, 72].

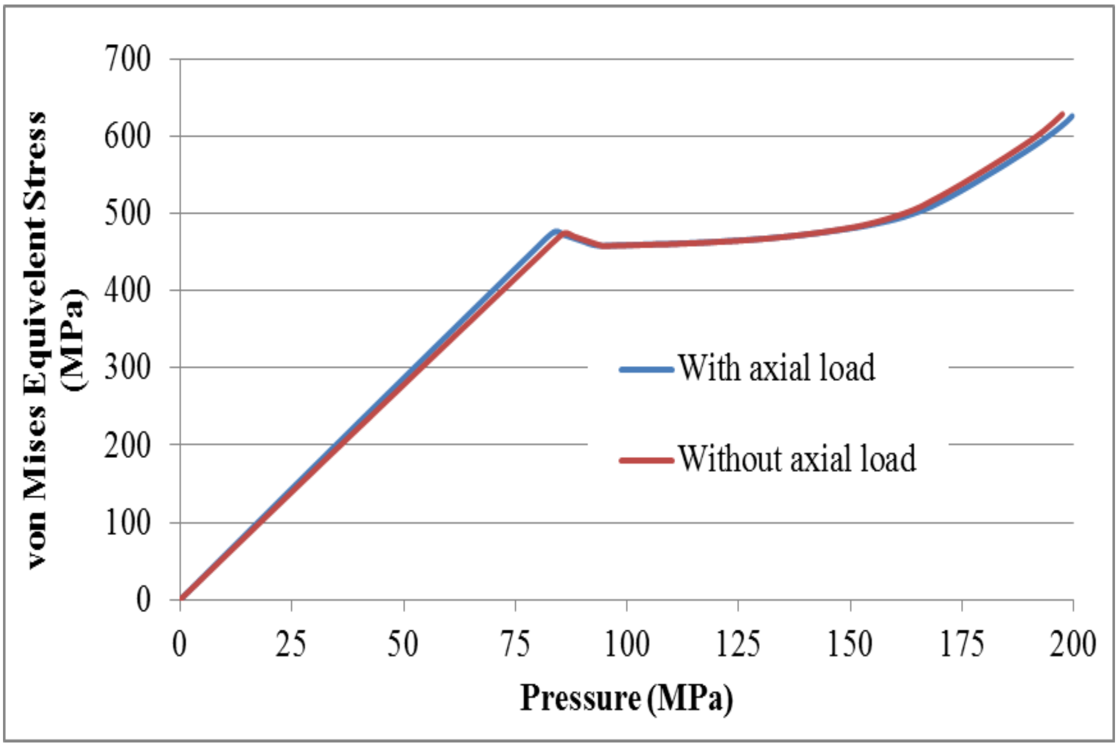

Figure 3-9: Pressure vs von Mises at the node placed at the centre of the defect showing the failure pressure for models with and without axial loading

Figure 3-10 shows a typical ruptured pipe (see Chapter 5) where the failure is clearly far from the pipe ends and the failure zone is approximately 700 mm from the pipe end flange. This was typical for all the cases where rupture has taken place, as discussed later in Chapter 5.

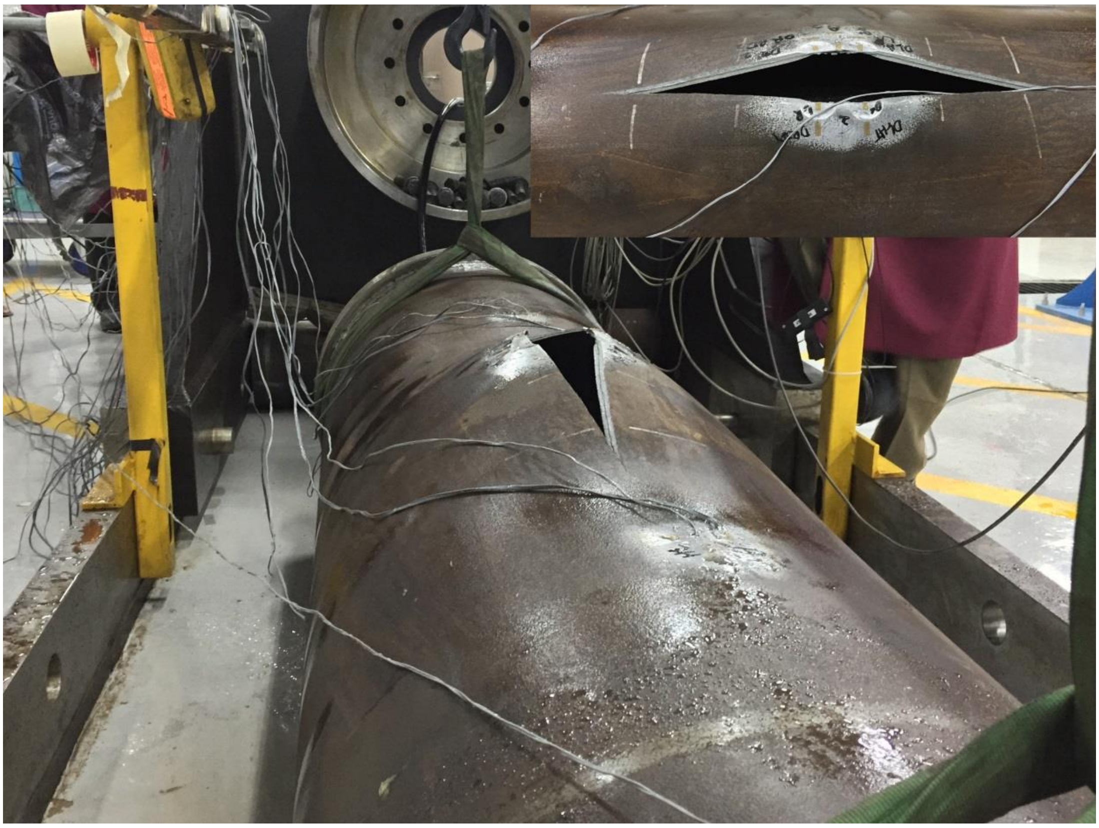

Figure 3-10: Pipe rupture image of X60 (9.5 mm) pipe with circular defects– further magnified on the top right corner.

3.4.5 Meshing and Elements

The types of elements used in this work are quadratic elements where quadratic approximation of the geometry and the displacement field are assumed. C3D20R elements in Abaqus are used which are 3D continuum quadratic elements with 20 nodes with reduced integration points. As the name suggests, reduced integration elements employ less number of integration points when solving for the integrals and are therefore more economical than full integration elements. The main reason for using quadratic elements in this work is the presence of severe changes in the geometry (at the defect site). As the work presented in the research work involves plastic behaviour, using reduced integration elements is favourable as the displacement-based FE formulation tends to overestimate the stiffness matrix and thus in using reduced integration points yields less stiff elements, and FE solution gets closer to the real life behaviour of the structure under analysis [78].

3.5 FE Models and Associated Sensitivity Studies

3D models were created in order to investigate the model's mesh sensitivity. Different cases were tested at the defect location of a curved boxed defect in order to compare against experimental data from the literature [50]. The first case was simulated with quadratic tetrahedron elements (C3D10 in Abaqus) at the defect base while the surrounding zones were all meshed with quadratic hexahedron elements (C3D20R in Abaqus). The second case was simulated using quadratic tetrahedron elements at the defect corner while all the surrounding areas were meshed with quadratic hexahedron elements (C3D20R in Abaqus). The third case was simulated using quadratic tetrahedron elements throughout the model. The Fourth case was simulated with quadratic hexahedron elements throughout the model. In all cases, a coarser mesh was used away from the defect location to reduce the total number of elements and nodes. The details of each mesh are shown in Figure 3-11 and the results of the analysis showing the stress contours are presented in Figure 3-12. While it is very clear to see the defect high stress distribution in the longitudinal direction, compressive stress develops at the edge of the defect in the circumferential direction as a result of the defect deformation and bending effect.

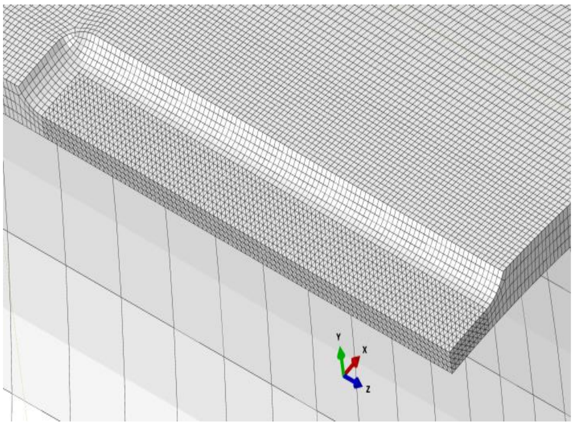

Case 1

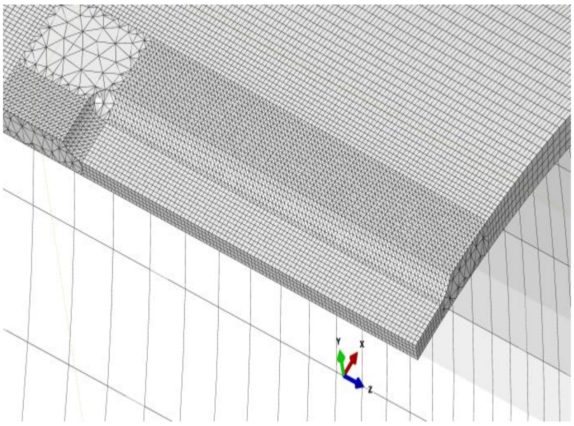

Case 2

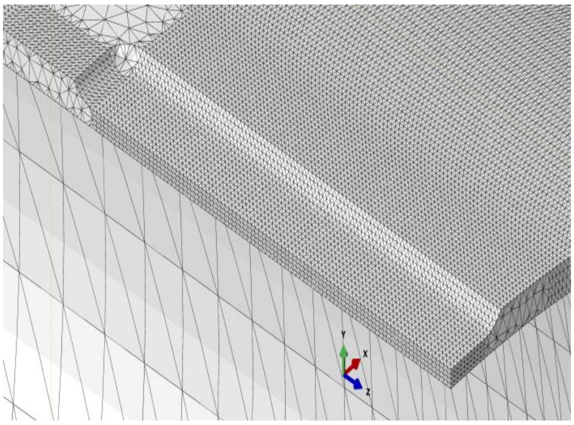

Case 3

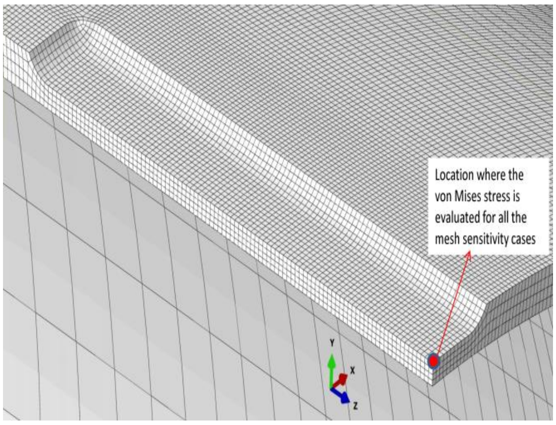

Case 4

Figure 3-11: Mesh details of different cases (case 4 indicates the position where the von Mises stress is evaluated for all the cases)

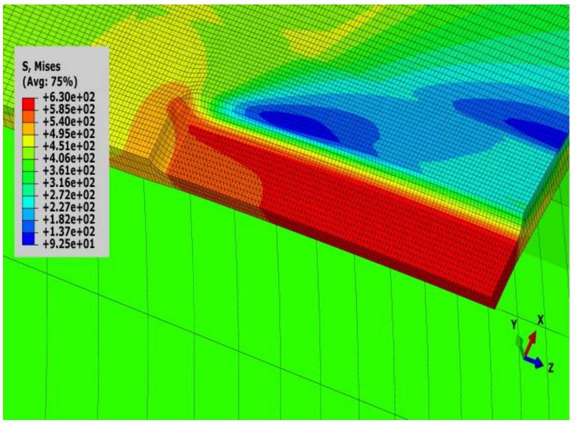

Case 1

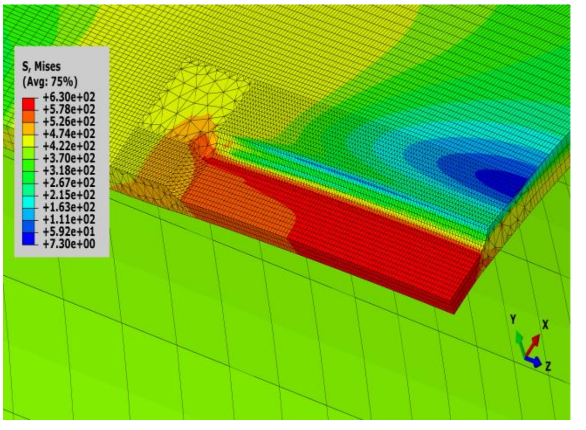

Case 2

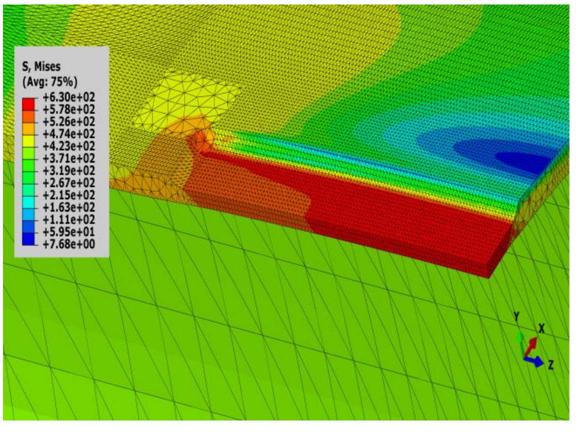

Case 3

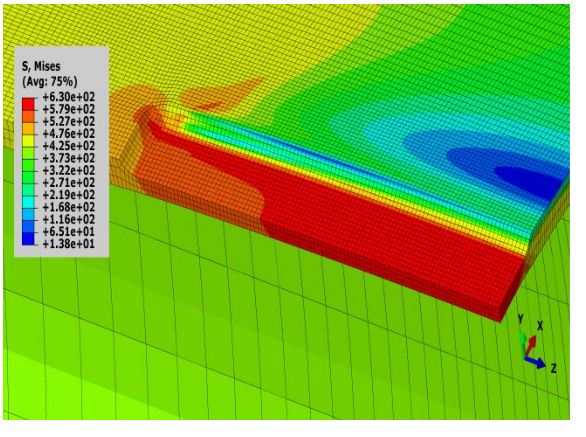

Case 4

Figure 3-12: Mesh and von Mises stress contour details in different cases

The results obtained are further summarised in Table 3.3, keeping in mind that all input parameters are the same for all the cases. The predicted failure pressure in Table 3.3 and Table 3.4 is obtained at a single node, shown in Figure 3-12 (case 4), reaching the material maximum true ultimate tensile stress of 630 MPa [50] .

Table 3.3: Mesh sizes and run time details

Mesh type	Mesh case	von Mises equivalent stress (MPa)	Maximum plastic strain at the same node (indicated in Figure 3-11 case 4) (mm/mm)	Element size at defect area (mm)	No of model elements	Analysis Time (hr:m)
Tet. quadratic elements at defect base (all hex quadratic elements at other areas)	1	630	0.10	1.0	75702	1:36
Tet. quadratic elements at defect corner (all hex quadratic elements at other areas)	2	630	0.10	1.0	118488	1:30
Tet. quadratic elements throughout mesh	3	630	0.10	1.0	281972	2:06
Hex quadratic elements throughout mesh	4	630	0.10	1.0	59173	1:09

The above results indicate that the models made with either full hexahedron elements everywhere or the combined tetrahedron elements with hexahedron elements at the defect part produce the same failure pressure, suggesting that if the mesh at the defects is sufficiently refined, the choice of elements does not significantly affect the results.

A mesh density study considering Case 4 was also carried out where the number of elements was varied through the thickness of the pipe. The study was conducted by placing 3 to 7 quadratic elements through the wall thickness, as shown in Figure 3-13 where the stresses were all taken at the node located at the centre of the defect. The results show that increasing the number of elements beyond 3 elements across the wall thickness has a very small effect on the stress values. At the node located at the centre of the defect, the von Mises stress tends to flatten after reaching the yield point and then increases gradually as the pressure is increased. This may be due to the post-yield stress redistribution around the node located at the centre of the defect.

Table 3.4 shows that as more elements are added across the wall thickness, the total number of elements in the FE mesh increases substantially. The run time for the FE analysis increased from about 1 hour for 3 elements across the wall thickness to more than 7 hours for 7 elements. It is worth mentioning that all the cases were run on a High Performance Computing (HPC) facility using a single 8-core (Intel Sandybridge 2.6 GHz) machine with 30 GB of memory.

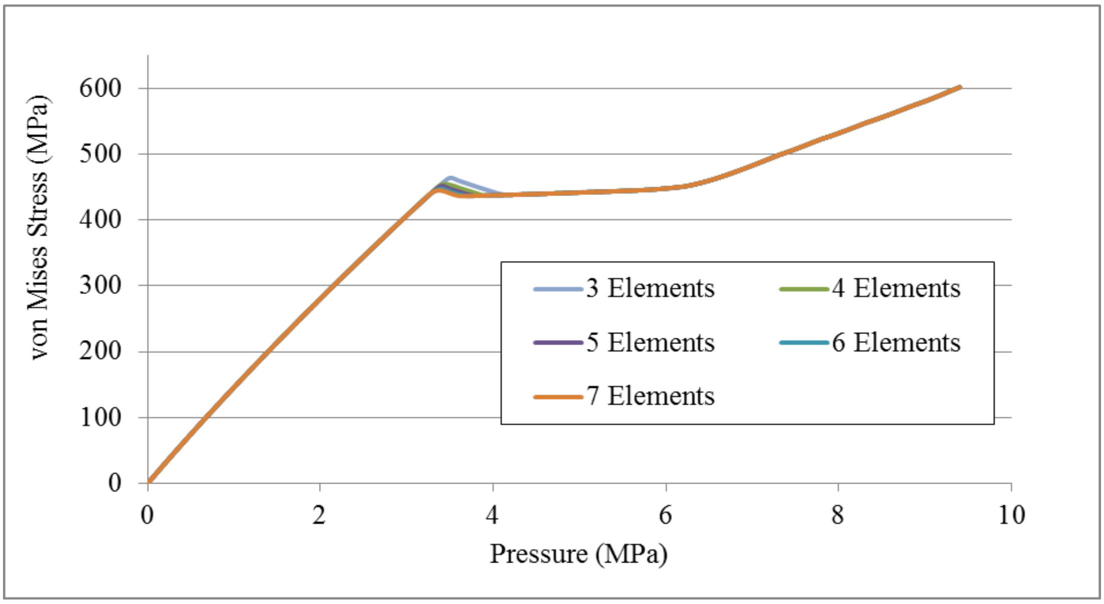

Figure 3-13: Plot of von Mises stress variation with pressure for various elements placed across the wall thickness at the node located at the centre of the defect

Table 3.4: Details of the mesh size in the through thickness cases

No. of element through thickness	von Mises equivalent stress at a node located at the centre of the defect (shown in Figure 3-11 case 4) (MPa)	No of model elements	Analysis Time (hr:mn)
3	630	59173	1:09
4	630	78859	2:00
5	630	98545	2:57
6	630	118231	5:01
7	630	137917	7:24

The outcome of this sensitivity assessment gives a clear direction that the number of through-thickness elements should be kept as small as possible considering the required time to complete the analysis. The FE solutions in this study are all based on 3 to 5 elements through the thickness. A study by Cronin [45] has also shown that more than two elements across the wall thickness are sufficient for accurate analysis.

3.6 Conclusion

The theoretical understanding of FE analysis, required parameters to be used in Abaqus [51] and the subsequent sensitivity analysis of the numerical models presented in this section pave the way to using similar models with high confidence in the subsequent analyses. The next chapter will further elaborate on the failure criterion adopted in this research work so that it can be used along with the FE models tested in this section for single defects and defect interaction cases.

CHAPTER 4: PIPE FAILURE CRITERIA AND VALIDATION

4.1 Pipe Failure Criteria

Pipe failure pressure is normally defined as a pressure above which the pipe will fail either through leak or rupture. The majority of pipes in the oil and gas sectors are made of ductile steel and operate in such a way that failure occurs in a ductile manner unless toughness is compromised. The failure criteria used in this work follow the stress-based failure criterion which has been widely used and shown to predict the collapse pressure of corroded pipes with good accuracy by various researchers [8, 11, 13, 16, 40, 42, 52, 79].

Although there is a general agreement on the use of the stress-based failure criterion for predicting the failure pressure in pipes, there are various opinions on how the highest value of the true UTS within the corroded area leads to failure. Adilson et. al [11] and Freire José et al. [26], considered two criteria for the failure pressure to occur within the simulated model, one is local in which failure is reached when the von Mises stress at any point of the defect region attains the true UTS of the material while the second one which is global considers failure to take place when the nonlinear analysis algorithm in the FE software does not attain convergence. Filho et. al [16] used a similar failure criterion as suggested by Adilson et. al [11] where the pipe is considered to have failed when any element reaches stresses equal to the material's true UTS value. Bedairi et. al [50] stated that failure pressure within the FEA model was reached when the von Mises stress at the defect bottom reached the true UTS of the material. Ma Bin et. al [23] considered failure to take place once the von Mises equivalent stress at the mid surface of the corroded ligament reaches the true UTS of the material. Fekte et. al [20] considered the failure pressure of the corroded pipes to occur when the von Mises equivalent stress at the deepest point of the defect area reaches the true UTS of the considered pipe material.

The choice of using a stress-based failure criterion also follows the pipe design codes such as ASME B31.4 [65] and ASME B31.8 [80] which are based mainly on stress-based designs considering various assumptions such as plane stress using isotropic, linear elastic and homogeneous materials where displacements are small. The strain-based approach which postulates that failure occurs when the applied strain exceeds the maximum strain value during burst was refuted by Chouchaoui [8] as it reveals large scatters in the prediction of the pipe failure pressure. Additionally, failure of the local wall-thinned pipe under internal pressure is a failure by load-controlled loading rather than displacement-controlled loading [13]. The stress-based failure criterion, which is based on the von Mises criterion, suggests that failure is initiated when the stress at the metal loss site reaches the pipe material's true UTS. The stress-based failure criterion is used below to predict yielding of the pipe material based on results obtained from the experimental uniaxial tensile test. The choice of von Mises stress criterion is further imposed by the requirements of ASME B31.4 [65] and B31.8 [80] which are used for designing oil and gas pipes.

The von Mises equivalent stress and equivalent plastic strain equations are given by:

$$\sigma_e = \left[\frac{(\sigma_1 - \sigma_2)^2 + (\sigma_2 - \sigma_3)^2 + (\sigma_3 - \sigma_1)^2}{2}\right]^{1/2} \qquad \textbf{(4-1)}$$

$$\varepsilon_e = \frac{\sqrt{2}}{3}\left[(\varepsilon_1 - \varepsilon_2)^2 + (\varepsilon_2 - \varepsilon_3)^2 + (\varepsilon_3 - \varepsilon_1)^2\right]^{1/2} \qquad \textbf{(4-2)}$$

Two failure criteria are adopted in this work. The first failure criterion is used for a single defect and it predicts failure pressure, P_{Defect}, to occur when the von Mises equivalent stress in the pipe wall ligament (line AB in Figure 4-1) reaches a stress value between the engineering ultimate tensile strength (UTS) obtained from the uniaxial tensile test and the true UTS based on the true-stress-true strain definitions. Therefore, in an FE analysis, failure is assumed to occur when all nodes in the pipe ligament (line AB in Figure 4-1), rather than a single node, have reached the engineering von Mises UTS and are below or equal to the true von Mises UTS. This is considered more effective than judging failure by a single node reaching the true UTS, which may be sensitive to the mesh refinement around the highly stressed region around the defect.

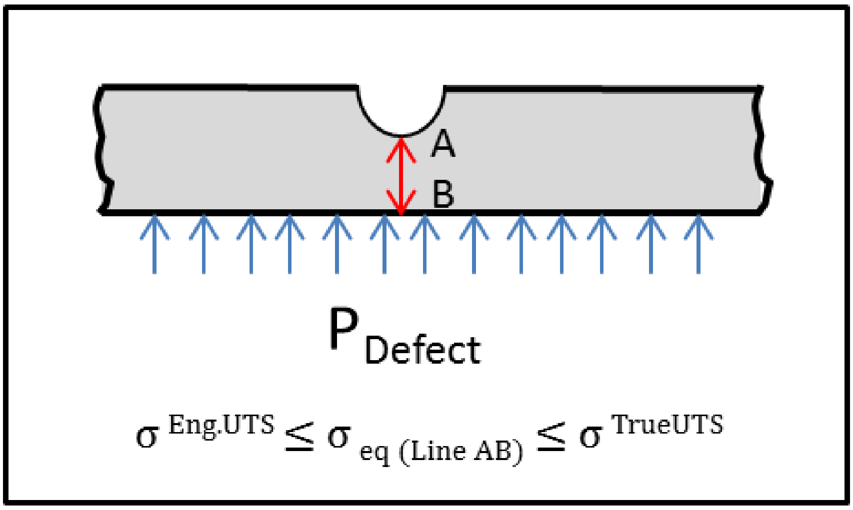

Figure 4-1: Failure criterion for a single metal loss defect

The second failure criterion is used for interacting defects and it predicts failure pressure, P_{Multi}, to occur when the failure criterion above is reached on the spacing between the defects at or before reaching it in the through-thickness ligament. In other words, the von Mises equivalent stress along the length between the two defects (line CE in Figure 4-2) reaches a stress value between the engineering UTS and the true UTS at or before the through-thickness space denoted by the line AB. Therefore, interaction will not occur if von Mises stress reaches the true UTS value at any point along the line AB before line CE. In this case, failure will occur due to the presence of a single defect. As the FE analysis considers only a symmetrical quarter of the pipe for the longitudinally and circumferentially spaced defects, the results presented will show the stresses on line CD which is a mirror image of line DE.

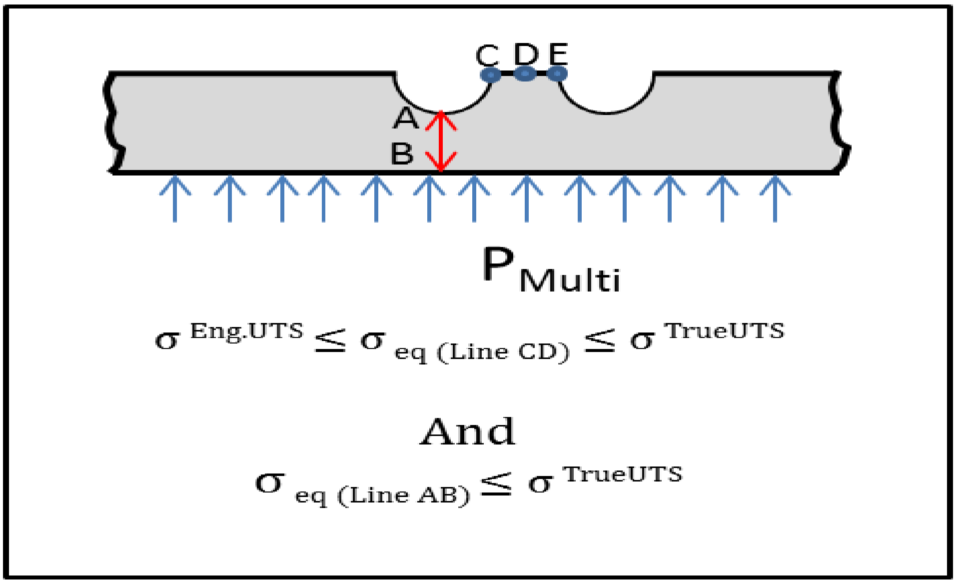

Figure 4-2: Failure criterion for interacting metal loss defects

It is worth noting that FE software is unable to predict the real-life failure pressure of the pipe due to local numerical instabilities that occur once the maximum UTS is reached. This is due to the fact that the true stress-true strain curve used in Abaqus extends beyond the UTS value of the material obtained from a uniaxial tensile test. The Abaqus software would only extrapolate the data forward, so the defected pipe would never actually 'fail' as one would expect during the burst pressure test. In order to overcome this challenge, the pipe is modelled with small pressure steps with higher pressure than that of the experimental failure pressure. In this study, an initial estimate of the failure pressure, obtained using Barlow’s formula, is used in the FE analysis.

4.2 Validation Study

The models created in this work have been validated by comparing the FE failure pressure to the corresponding experimental failure pressure from the literature. The cases stated in Table 4.2 are from studies conducted by Bedairi et al., [50] and Freire José et al., [26]. In [50], a pipe grade of API 5L X60, outer diameter of 508 mm with a wall thickness of 5.7 mm (0.224 inch) was used. A single defect was assessed in this case. In [26], pipe grade API 5L X80, outer diameter of 458.8 mm with a wall thickness of 8.1 mm (0.319 inch) was utilised. A summary of the material tensile properties are shown in Table 4.1 and Figure 4-3 .

Table 4.1: Tensile property data

Material	*Young's Modulus E (GPa)*	*Poisson Ratio, ν*	*Yield Strength, σ_Y (MPa)*	*Engineering Ultimate Tensile Strength, σ^{EngUTS} (MPa)*	*True Ultimate Tensile Stress, $\sigma^{trueUTS}$ (MPa)*
API 5L X60 [50]	207,000	0.3	435	560	630
API 5L X80 [26]	200,000	0.3	601	684	746

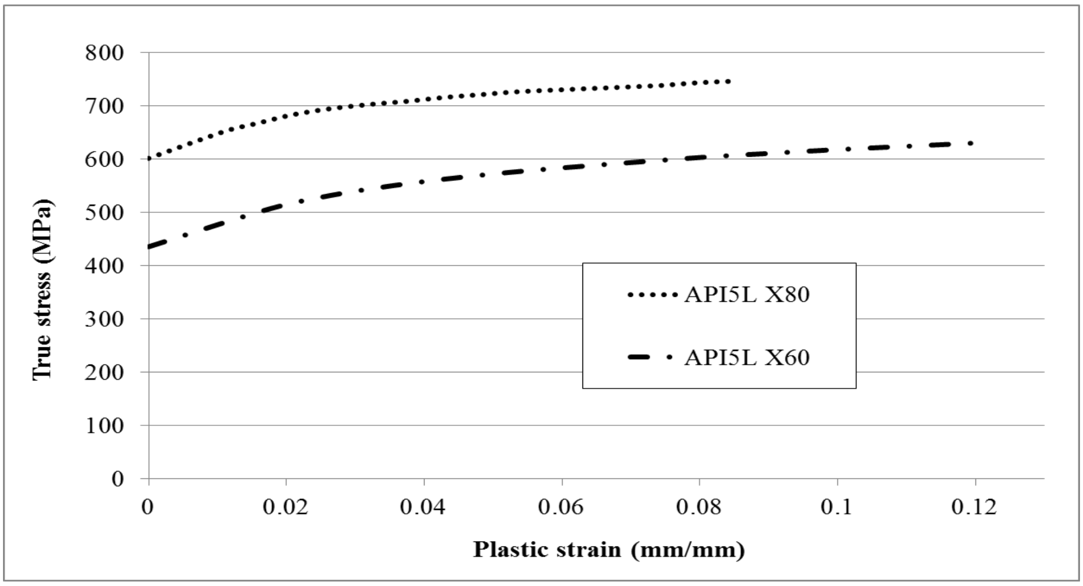

Figure 4-3: True stress-plastic strain values for X80 [26] and X60 Pipes [50]

Table 4.2 further summarises the defect parameters and results of validation work. The failure criteria of both works have been highlighted earlier in the failure criterion section.

Table 4.2: Model validation results

No	Ref.	Pipe Defects Details	Published Experimental Burst Pressure (MPa)	Published FEA Failure Pressure (MPa)	FEA Failure Value in this work (MPa)	Percentage difference	
						Published Experimental Burst pressure	Published FEA Failure Pressure
1	Bedairi et al., [25]	X60 OD: 508 mm t: 5.7 mm Defect type: Rectangular Defect Length: 200 mm Defect Width: 30 mm Defect depth: 45%	9.59	9.42	9.4	2%	0.2%
2	Freire José, et al., [20]	X80 OD: 458.8 mm t: 8.1 mm Defect type: Rectangular Defect Length: 39.6 mm Defect Width: 31.9 mm Defect depth: 5.32 Spacing: 20.5 mm	20.30	19.60	19.33	5%	2%

To further illustrate how the results in Table 4.2 are reached in this paper, test ID no. C1 by Bedairi et al., [50] was used. A high pressure of 12 MPa (higher than the predicted failure pressure) was applied to the pipe. The FE analysis was aborted due to numerical instabilities at a pressure of 9.873 MPa which is 5% higher than the predicted burst pressure. The evolution of the von Mises stress as the pressure is increased is plotted at the 7 nodes placed across the pipe wall thickness (line AB) in Figure 4-4. The location of AB where pressure vs stress evolution is taken is further shown in Figure 4-5. As expected, the highest von Mises stress is initially at point A on the defect surface and then spreads across the pipe wall thickness as the pressure is increased. There is a very slight difference between the final von Mises stress values on line AB. This is due to the post-yield stress redistribution around the defect. As stated in the failure criterion for a single defect in Section 4.1, failure is clearly seen to occur in the through thickness of the defect at a pressure of 9.4 MPa where the stress is bounded by the engineering UTS value of 560 MPa and the true UTS value of 630 MPa.

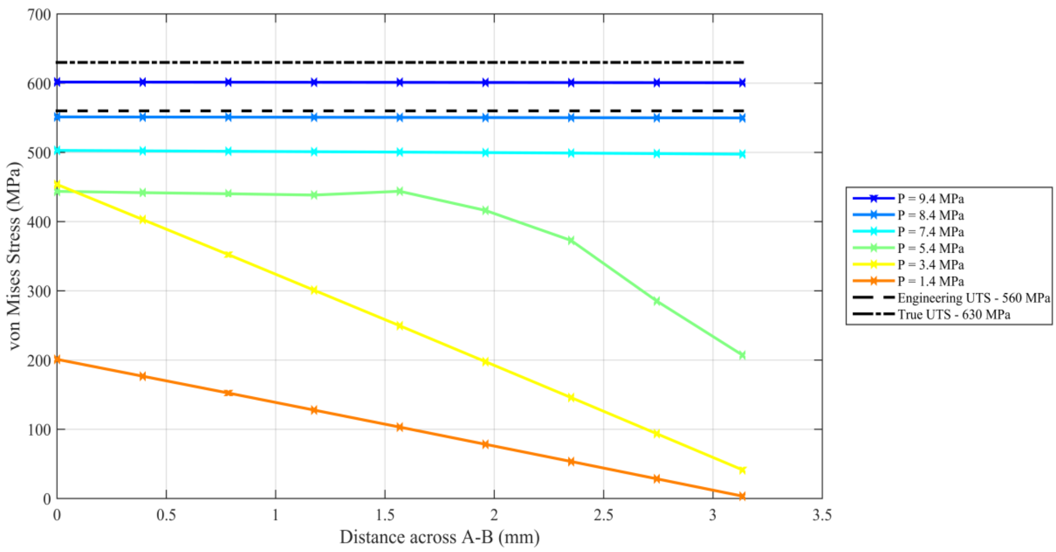

Figure 4-4: von Mises stress curves at different pressure increments across the pipe wall thickness Line (AB) for case no. 1 in Table 4.2

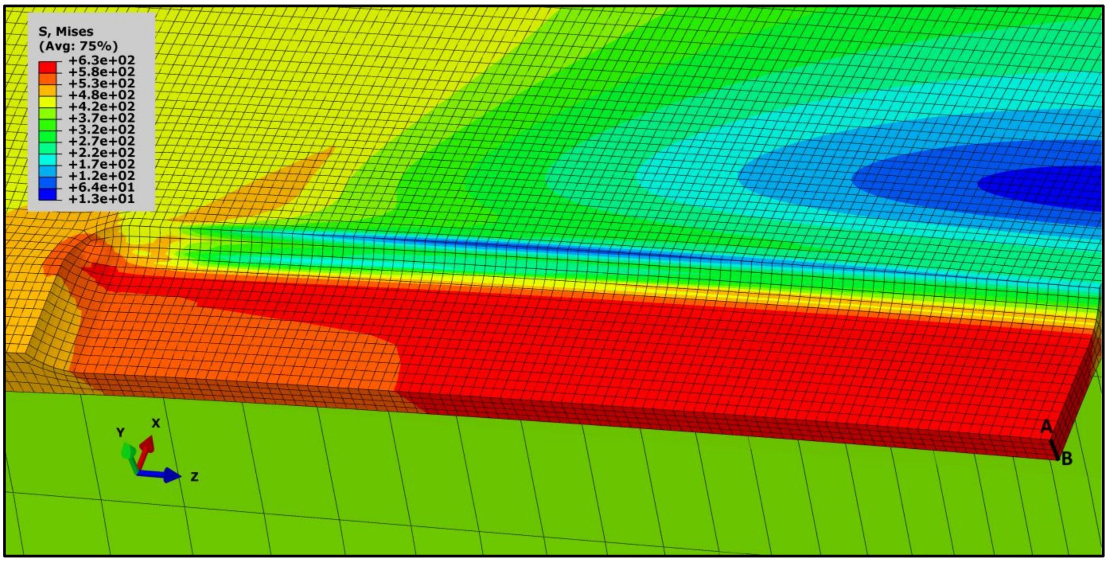

Figure 4-5: Stress contours around the defect area showing the location of line AB

To compare the failure pressure of interacting defects, the study made by Freire José, et al., [26] with case no. IDTS 3 was used. The outcome of the analysis presented in Table 4.2 shows good agreement in terms of the failure pressure although the aim of their study was to look at the path of the failure rather than determining the critical space of interacting defects. The evolution of the von Mises stress as the pressure increases is plotted at the 7 nodes placed across the pipe wall thickness (line AB) in Figure 4-6 and across the ligament between the two defects as shown in Figure 4-7. The choice of the true von Mises UTS value as the highest value in the failure stress range is in line with other failure criteria used in the literature [7, 8, 20, 23, 26, 42, 48-50, 52] which use the true UTS value as an indicator of failure. The true (rather than engineering) definition of the stress at the failure region is appropriate due to the large strains in this region. The engineering UTS value is chosen as the lowest value of the failure stress range as this value is a widely used in engineering failure calculations. Furthermore, the experimental burst pressure tests, discussed in Chapter 5, demonstrate that this failure stress range correlates very well with the numerical data presented in Chapter 6. Using a failure stress range, as opposed to the stress at a single node reaching the true UTS value, is less sensitive to mesh refinement, and choosing a stress range based on the von Mises true and engineering UTS values is practical as it is derived from the uniaxial test data [76].

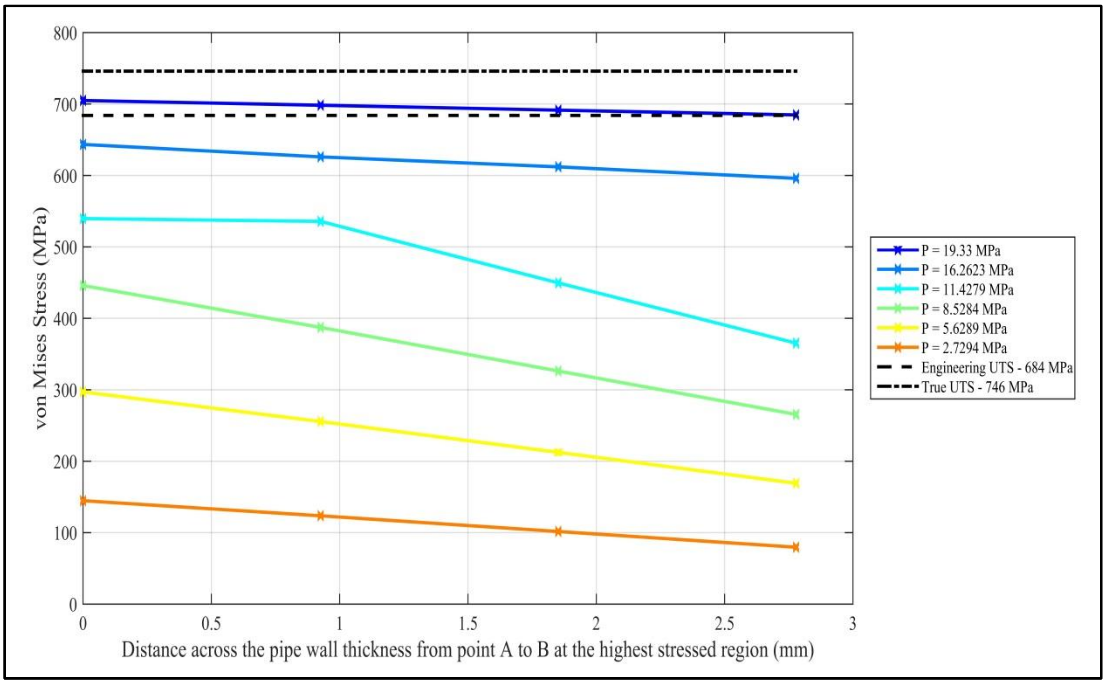

Figure 4-6:: von Mises stress curves at different pressure increments across the pipe wall thickness Line (AB) for case no. 2 in Table 4.2

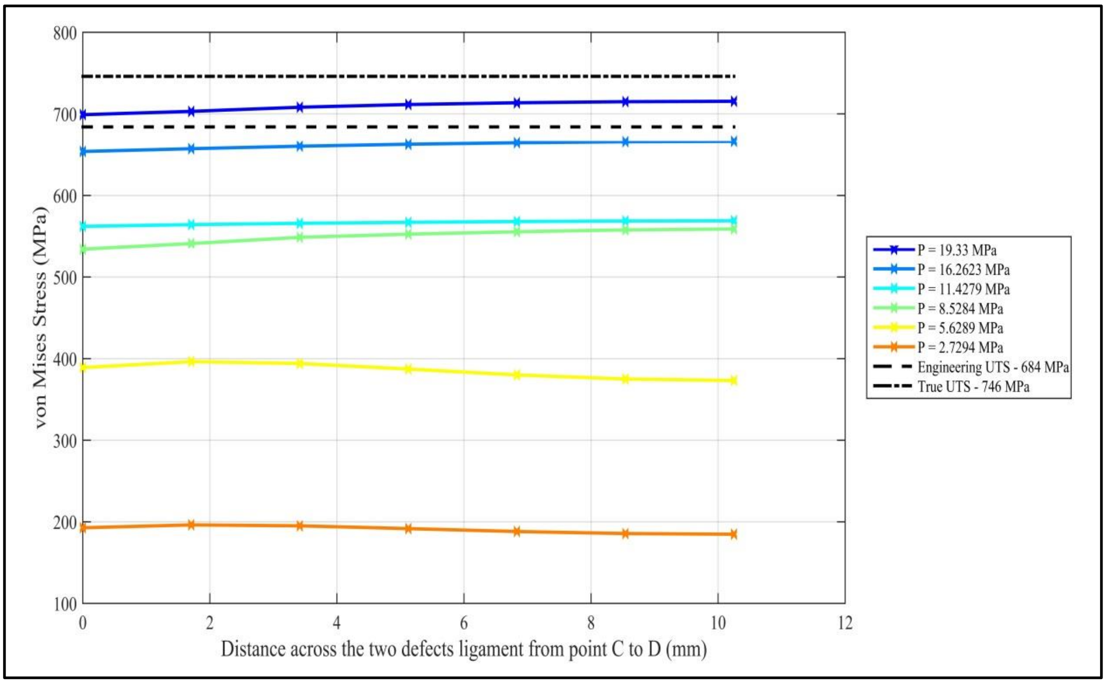

Figure 4-7: von Mises stress curves at different pressure increments across the ligament between the two defects (CD) for case no. 2 in Table 4.2

4.3 Conclusion

The failure criterion proposed in the research work has been validated through existing literature data and will be further tested following the validation of the experimental work presented in Chapter 5. The failure of a single defect is reached when the through-thickness wall ligament is bounded by the engineering and true ultimate tensile stress. Defect interaction occurs when the spacing between the defects is bounded by the engineering and true ultimate tensile before it is reached in the through-thickness wall ligament.

CHAPTER 5: EXPERIMENTAL WORK

5.1 Background

The work described in this Chapter is aimed at, for the first time, investigating experimentally the sensitivity of shapes and orientations of interacting metal loss defects in two different grades of ductile carbon steel, API 5L X52 and API 5L X60. The loading condition considered is an internal pressure load only in a closed ended pipe. The applied load increases the likelihood of failure being controlled by the stress state in and around the vicinity of the machined defects leading to either local leak at the defect or rupture if the defects are interacting.

5.2 Experimental Setup

The experimental work followed the process shown in Figure 5-1.

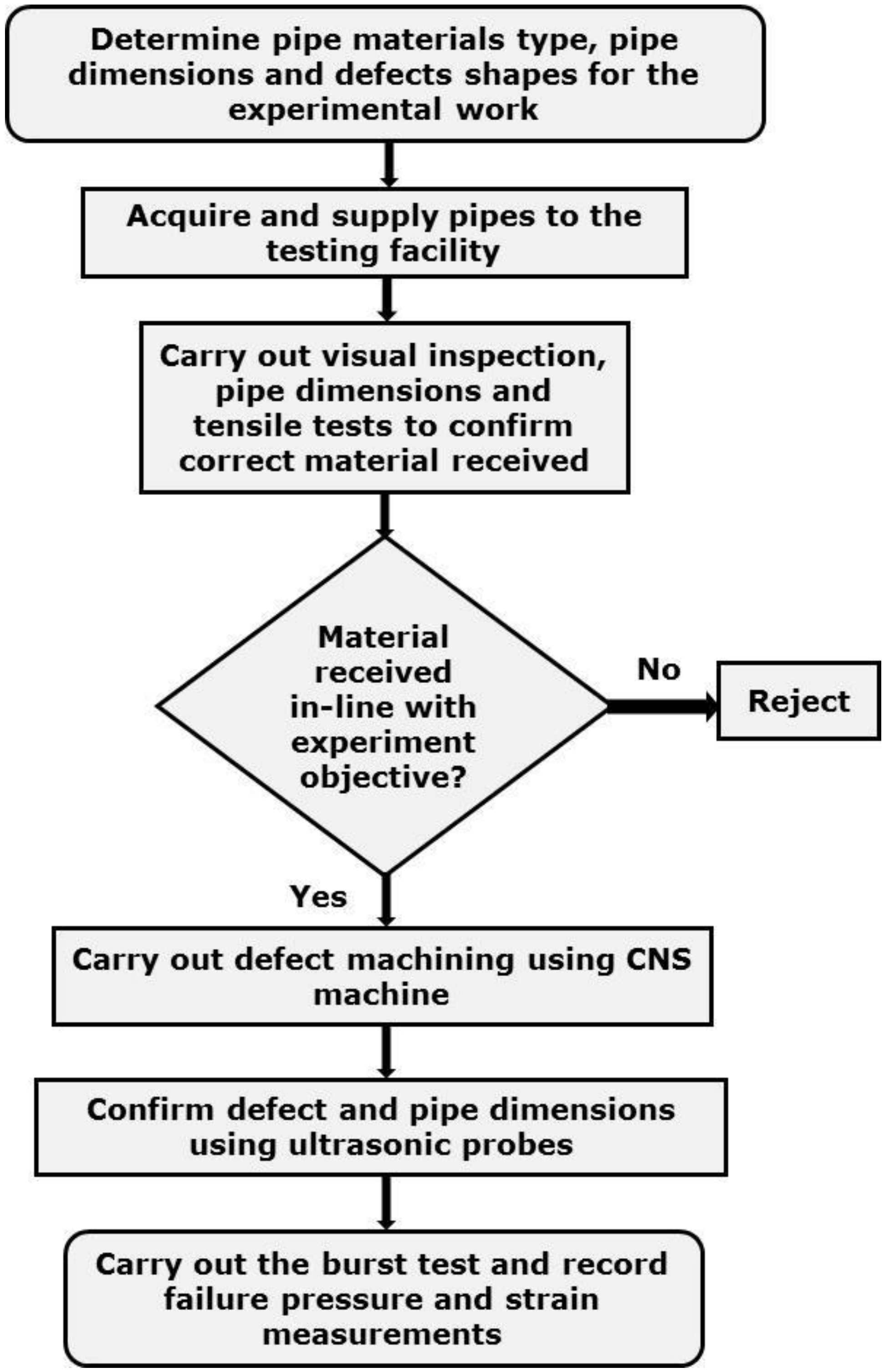

Figure 5-1: Experimental work process

5.2.1 Material Characteristics

Two grades of ductile carbon steel seam-welded pipes (refer to chapter two for details on seam welded pipes) that are manufactured based on API 5L standard (ISO 3183); namely X52 (L360) and X60 (L415), were used in the present work. The thickness used for API 5L X52 is 9.5mm, and for X60 three wall thicknesses were used; 8.9mm, 9.5mm and 10.5mm. Towards achieving the goals set for this study, it was required to do mechanical characterization for the tested materials. This includes the conduction of uniaxial tensile tests in both the circumferential and longitudinal directions. The sample preparation and the tensile tests were performed in accordance with the ASTM-E8 standard.

The tensile tests were carried out on two samples from each pipe type (X52 and X60). Tensile samples, shown in Figure 5-2 have been cut along the longitudinal direction of the pipes according to the ASTM E8 standard. A strain rate of $2.5 \times 10\text{-}4\ s^{-1}$ was used for all tests according to the aforementioned standard. The stress-strain curve of X52 material is shown in Figure 5-3 while for X60 pipes are shown from Figure 5-4 to Figure 5-6. The behaviours of these two materials as seen in the stress-strain curve shows an initial elastic region which progresses into the plastic region. It then starts to strain-harden reaching the ultimate tensile strength. Tables 1 and 2 list the extracted mechanical properties from the true stress-strain curves of X52 and X60 materials respectively. Figure 5-7 shows the fractured tensile samples showing the necking process that takes place in all the tested samples.

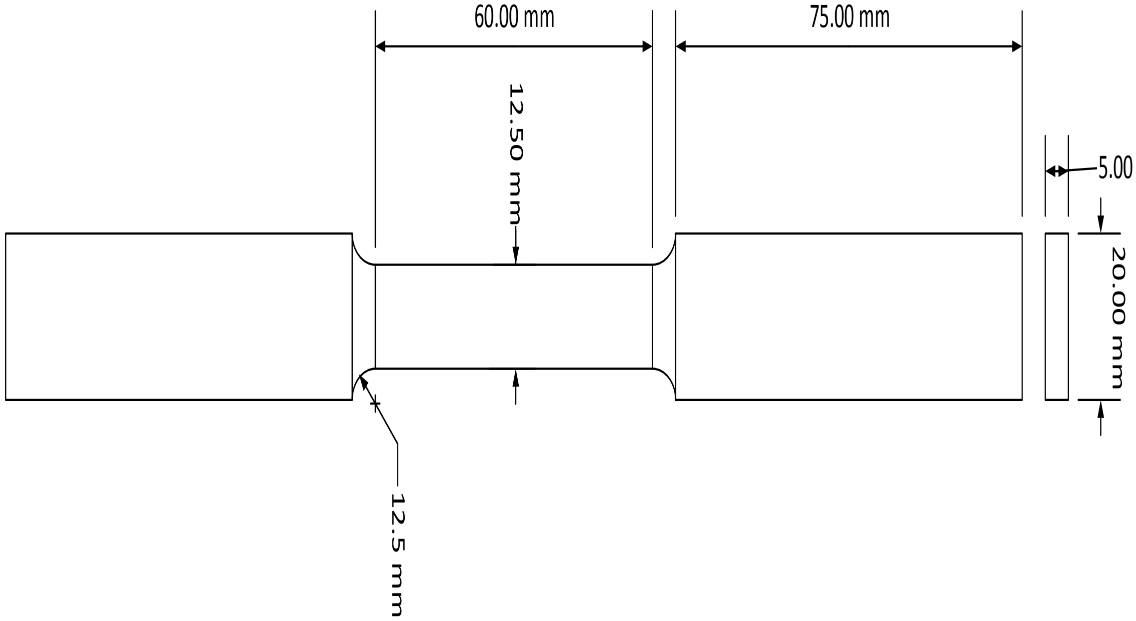

Figure 5-2: Tensile specimen according to ASTM E8 standard.

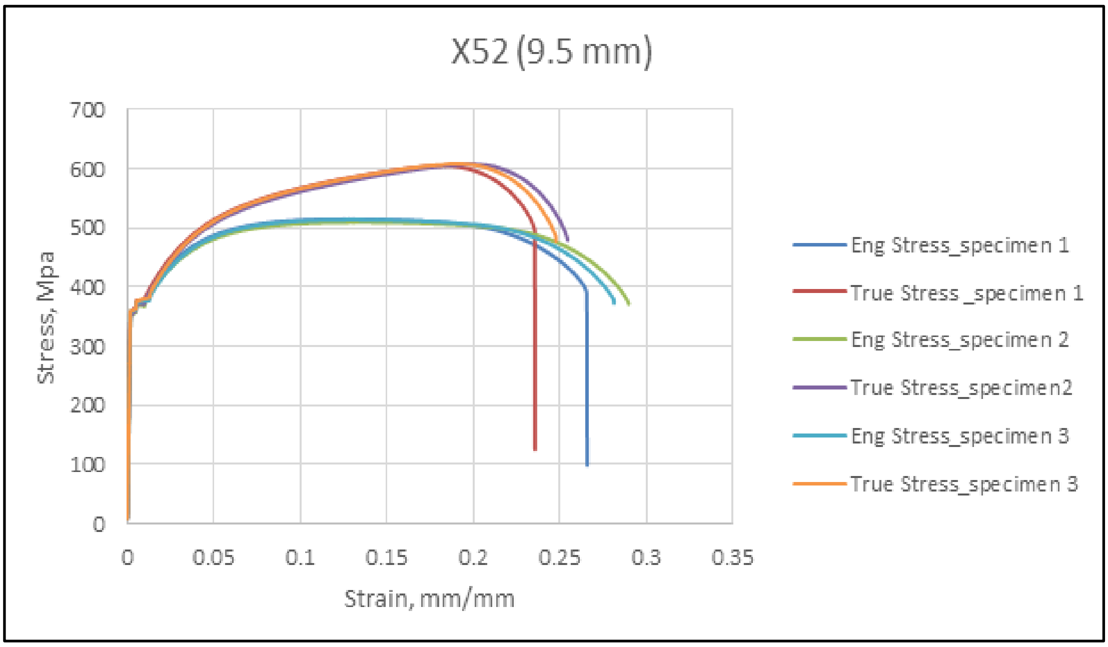

Figure 5-3: Stress-strain curves of X52 material.

Table 5.1: Mechanical properties extracted from the true stress-strain curves of X52 material

Modulus of Elasticity (GPa)	Yield Strength (MPa)	Ultimate Tensile Strength (MPa)
182	372	607

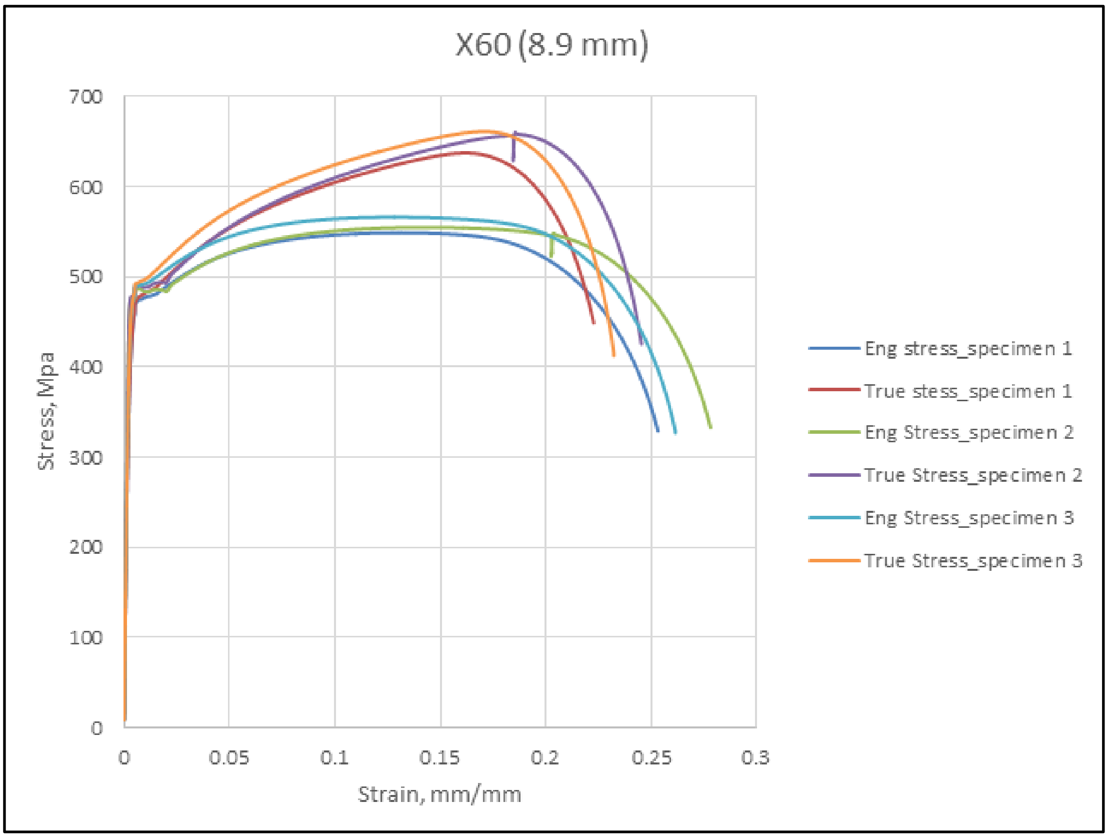

Figure 5-4: Stress-strain curves of X60 material-8.9mm thickness.

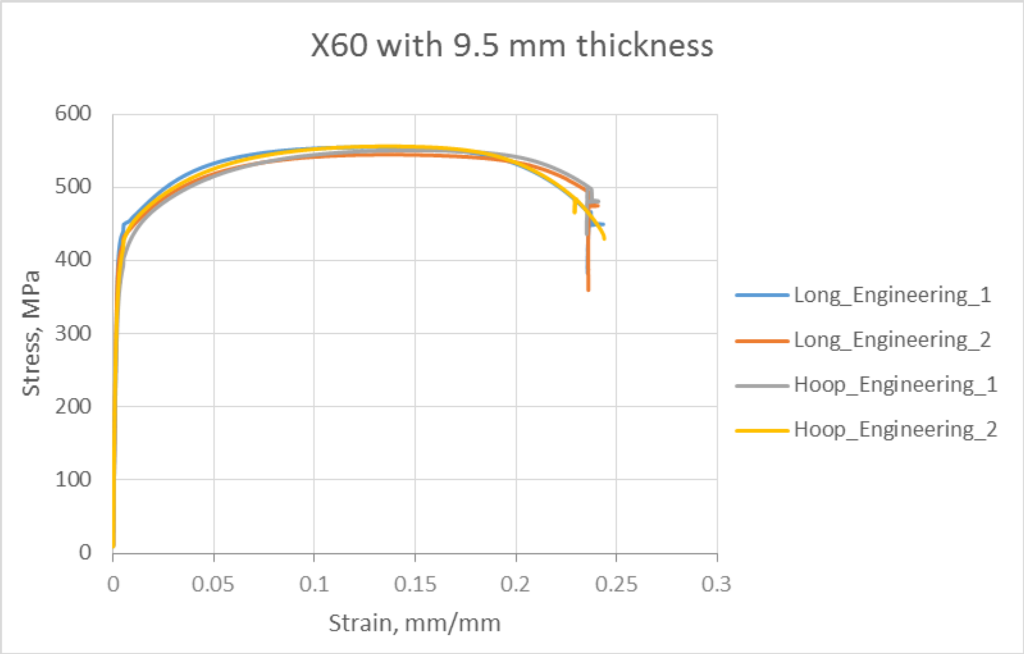

Figure 5-5: Stress-strain curves of X60 material-9.5mm thickness.

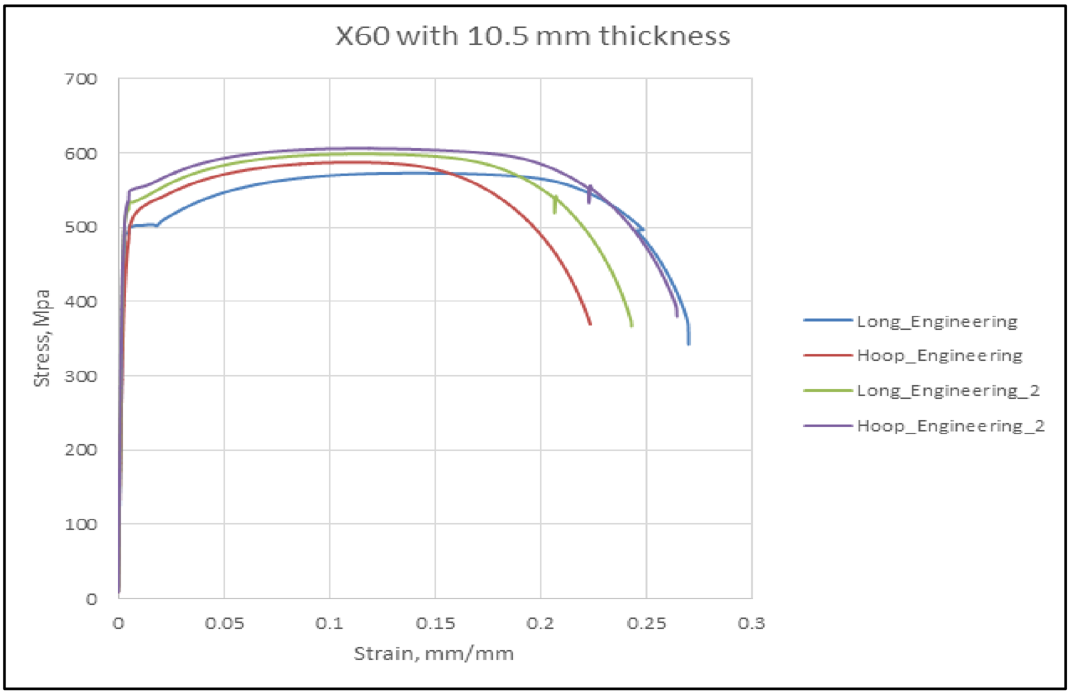

Figure 5-6: Stress-strain curves of X60 material-10.5mm thickness.

Table 5.2: Mechanical properties extracted from the true stress-strain curves of X60 materials

Wall thickness	Modulus of Elasticity (GPa)	Yield Strength (MPa)	Ultimate Tensile Strength (MPa)
8.9 mm	171	478	636
9.5 mm	195	456	645
10.5 mm	183	506	678

Figure 5-7: Tensile specimens of (a) X52 and (b) X60 materials after tensile tests.

5.2.2 Compressive Stress-Strain curves

Compression tests have been carried out on both pipe materials (X52-9.5mm and X60-8.9mm) along the circumferential and longitudinal pipe directions. Stress in the radial direction is of no importance in the test as it plays a minimal role (radial direction variation through the thickness is very small due to the small wall thickness). The compression samples were 4 mm × 4 mm × 8 mm. All tests have been performed without the use of an extensometer. These tests have been carried out using a strain rate of 2.5 × 10-4 s^{-1} and up to a compressive strain of 0.25 mm/mm. It can be clearly seen from the curves in Figure 5-8 and Figure 5-9, that the mechanical behaviours of the material of both pipes along the longitudinal and circumferential directions are quite similar indicating that these ductile steel materials have an isotropic behaviour. Similar findings were also reported in the literature [74].

It can be concluded from the compressive stress-strain curves that the tensile stress-strain curves obtained using tensile tests along the longitudinal direction can be used for the circumferential direction too. It is also clear that the compressive yield strength of X52 is lower than the tensile yield strength. This could be attributed to the presence of residual stresses. The tensile/compression asymmetry is however, smaller in X60 pipes.

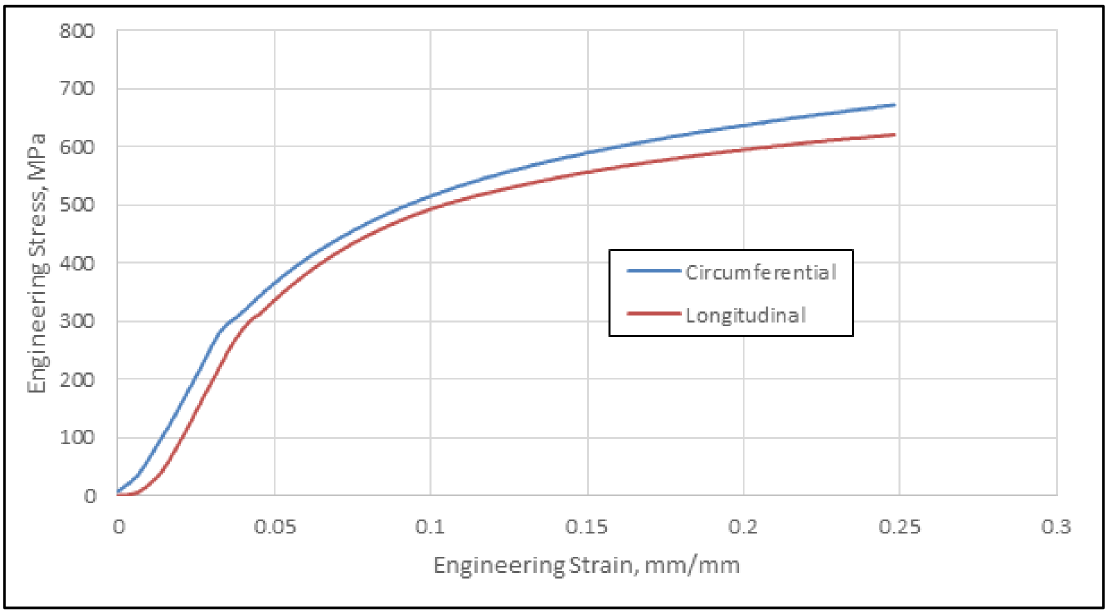

Figure 5-8: Compressive engineering stress-strain curves of X52-9.5 mm material.

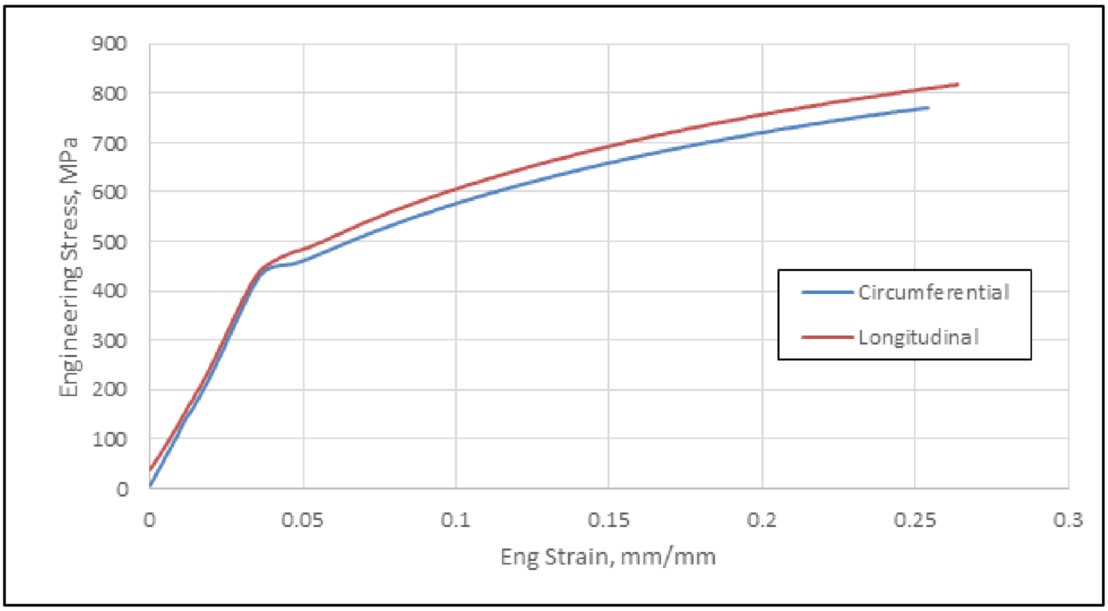

Figure 5-9: Compressive engineering stress-strain curves of X60-8.9mm material.

5.2.3 Charpy V Impact Tests

In order to evaluate the impact of fracture toughness of ductile steel on defect interaction, a Charpy impact test according to ASTM-E23 was conducted. The results of fracture toughness tests are listed in Table 5.3. The fractured samples are shown in Figure 5-9. It is very clear from the measured energy absorption values listed in Table 5.3 that X60 material has higher fracture toughness.

Table 5.3: Charpy V notch fracture toughness results of X52 and X60 materials

Spool	X52	X60
Thickness	9.5 mm	8.9 mm
Specimen1	72 J	224 J
Specimen2	77 J	216 J
Average	74.5 J	220 J

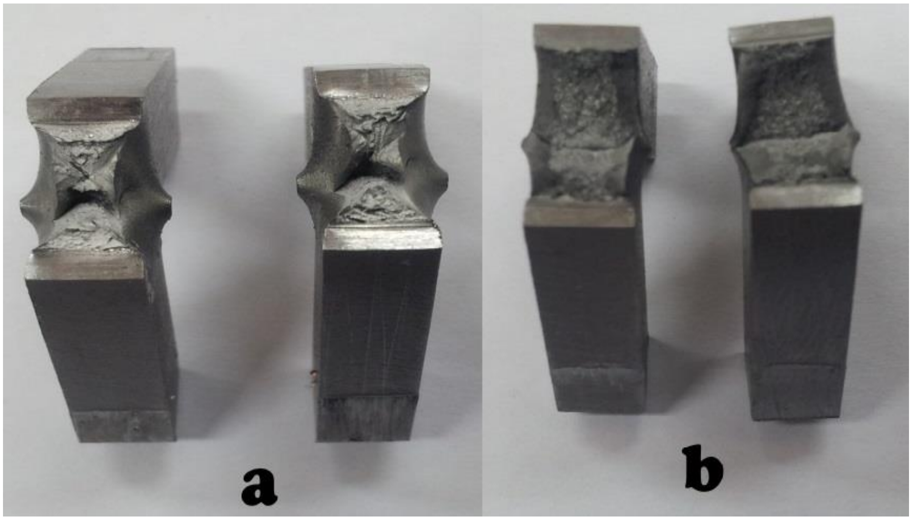

Figure 5-10: Fractured Charpy v notch samples of (a) X60-8.9 mm and (b) X52-9.5 mm materials.

5.2.4 Defect Preparations

For practical reasons, the simulated corrosion defects were machined on the external surface at the centre of the pipe and 180^{o} degree away from the pipe seam weld as to avoid the weld and heat affected zone areas. The circular and the curved box defect geometries have been chosen in order to make it practical to machine these defects on actual steel pipes to facilitate experimental burst pressure tests. For the sake of practicality and to represent real-life defects, the dimensions were chosen to be in line with the pipeline operator forum (POF) [1] for general corrosion, and as such these defect types can be detected and sized, and interaction rules can easily be applied by the existing inline pipe inspection tools [81]. Additionally, such general corrosion defects are widely observed in service in the oil and gas pipes industry and both circular defects and box shape defects have been used in the literature in the past for studying the effect of failure pressure on metal loss defects [8] [26].

It is important to note that metal loss in pipes can take place either internally or externally depending on the corrosion process taking place at the metal site. The surface contour of metal loss defects may not be as smooth as the ones machined for this experimental work; however, the combination of surface profiles that can be introduced to these defects is complex and unlimited and may not add additional benefits to this work. In order to minimise the possibility of stress concentration at the corners, the defects where made with a fillet radius, as shown in Figure 5-11. The defects were machined using computer numerical control (CNC) machines as shown in Figure 5-12 to create a smooth flat bottom defect on the external surface of the pipe. The curved boxed defect machined on the pipe has a length of 35 mm, width of 35 mm and depth of 50% of the wall thickness. The circular shaped defects were also machined with a diameter of 35mm and depth of 50% of the wall thickness. In all the burst cases, detailed measurements of the pipe wall thickness, defects depth, width and length were made. The pressure was monitored by pressure transducers mounted at both ends of the pipe through adaptors welded through the flanges. The exact defect dimensions for the defects tested in the experimental work are presented later in Table 5.4.

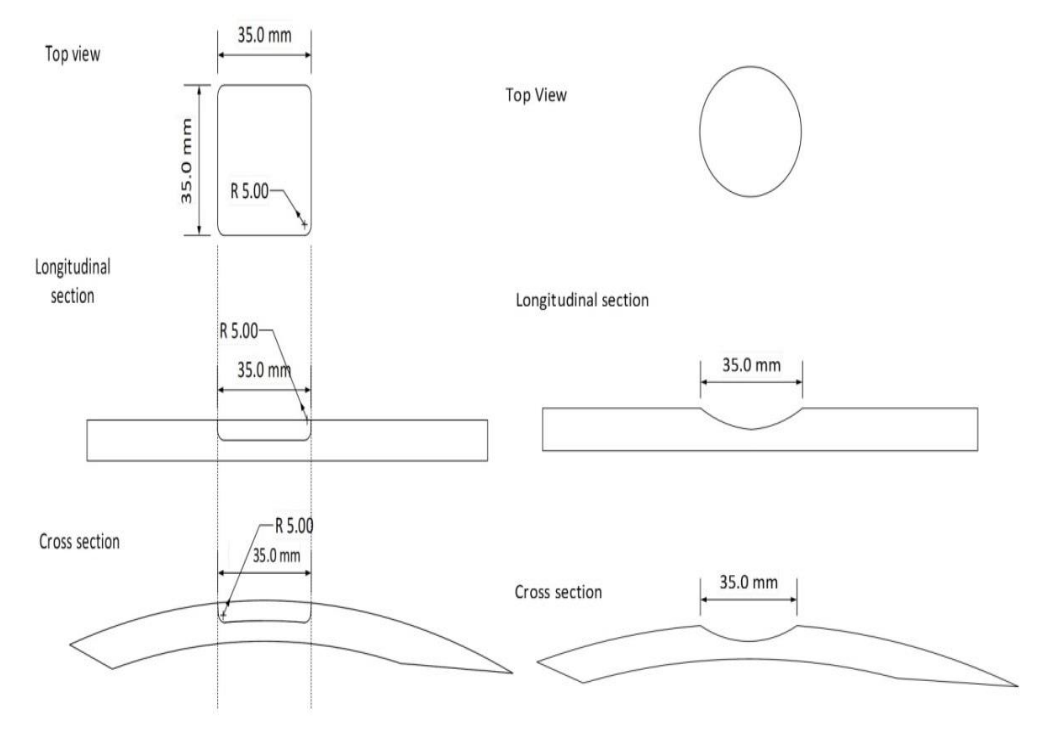

a. Curved boxed defect b. Circular defect

Figure 5-11: Schematic drawing of the defects

Figure 5-12: CNC machine for machining of defects

5.2.5 Test Rig Details

Figure 5-12 shows a schematic diagram of the test assembly. The test setup mainly consists of test specimen, high pressure pump, strain and pressure gauges, and a data logger.

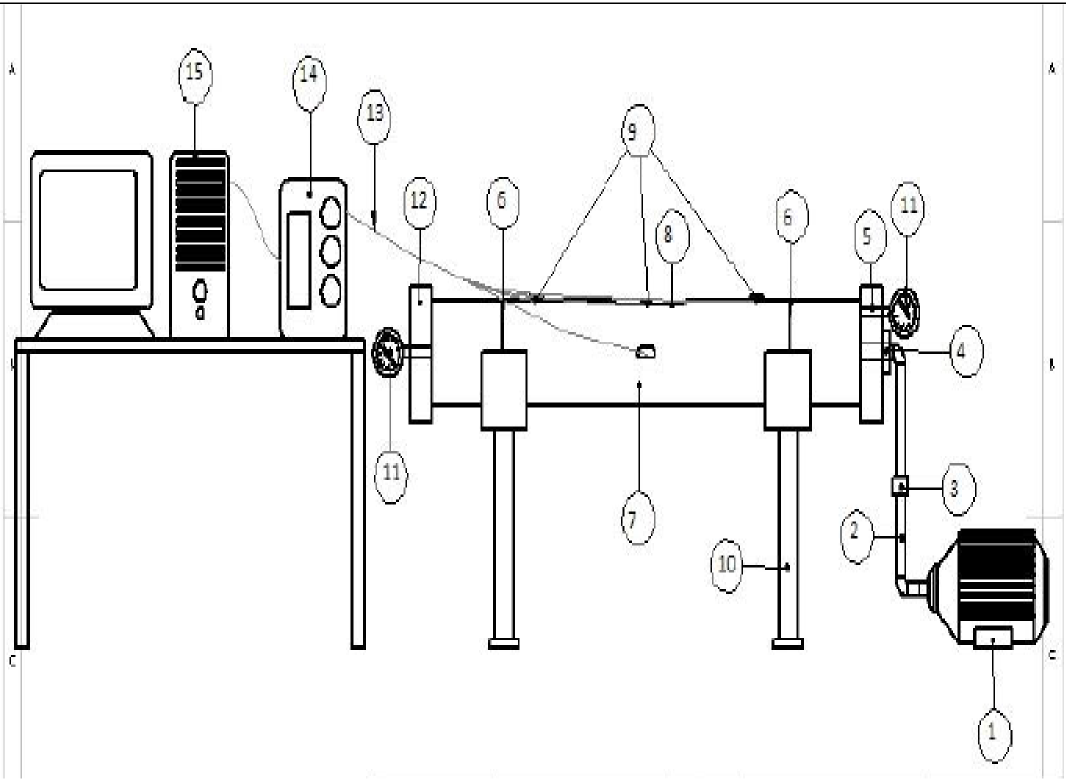

1) High pressure pump 2) Pipe Connection 3) One way valve 4) Coupling 5) Pump End Flange 6) Welded Section 7) Steel Pipe 8) Defect 9) Strain Gauges 10) Stands 11) Pressure Gauges 12) Rear End Flange 13) Electrical Wiring 14) Data Logger 15) PC

Figure 5-13: Burst test setup

Each test pipe consists of 1.8 meter long pipe welded to 50 mm thick flanges made from carbon steel, see Figure 5-14. Two holes were drilled on one flange to provide the fittings for the pump hose and the pressure sensor. Another pressure sensor is installed on the second flange to be used as a backup and to ensure accurate and consistent readings of the applied pressure. Strain gauges were initially used in the first 6 burst tests to gather data for the FE modelling but were disregarded in the consecutive tests.

Figure 5-14: Burst test pipe

5.3 Results and Discussions

A series of 31 hydrostatic burst tests on 1.8 meter pipes containing machined defects, both single and interacting, with a depth of 50% of the wall thickness were conducted. This has provided an exceptional prospect to investigate the defect interaction behaviour of various defects shape, orientation and spacing in relation to the pipe wall thickness. The results are summarised in Table 5.4. The table lists the finding of the 31 burst tests such as the exact dimensions of the machined defects, the actual pipe thickness where defects were positioned, the burst pressure and the occurrence of interaction between defects. These exact dimensions are crucial for reliable comparison between the analytical defect assessment methods and the test measured parameters. These results can be also utilised in the future for other types of research that are focused on pipe metal loss assessments. Shape of the final failure of the defects for all the burst test cases is presented in Appendix A.

Table 5.4: Experimental cases results

Test Case No.	Pipe Details (All with OD of 508 mm)			Defect Type and Orientation CB = Curve Boxed CR = Circular		Actual. Defect Dimensions (mm)			Defect Spacing Xt(mm)	Failure Pressure (Bar)	Defects interaction (Yes/No/NA)
	Grade	Nom t (mm)	Actual t (mm)	Type	Orientation	Length (mm)	Width (mm)	Depth (mm)		Exp	Exp
1	X60	8.9	8.88	CB	Single	35	35	4.44	Single	195.40	NA
2	X60	8.9	8.88	CR	Single	34.1	34.1	4.44	Single	199.70	NA
3	X60	9.5	9.65	CR	Longitudinal	35.5	35.5	4.82	1t (9.65)	190.50	Yes
4	X60	9.5	9.61	CR	Longitudinal	35.4	35.4	4.8	2t (19.2)	193.50	Yes
5	X60	9.5	9.54	CB	Longitudinal	35	35	4.77	1t (9.54)	190.30	Yes
6	X60	9.5	9.54	CB	Longitudinal	35	35	4.77	2t (19.1)	196.10	Yes
7	X60	9.5	9.44	CB	Hoop	35	35	4.72	1t (9.44)	193.20	No
8	X60	9.5	9.58	CB	Hoop	35	35	4.79	2t (19.4)	195.00	No
9	X60	9.5	9.55	CR	Diagonal	35.3	35.3	4.77	1t (9.55)	196.20	No
10	X60	9.5	9.52	CR	Diagonal	35.2	35.2	4.76	2t (19.0)	193.80	No
11	X60	10.5	10.6	CR	Single	37.1	35.1	5.3	Single	246.70	NA
12	X60	10.5	10.7	CR	Longitudinal	37.2	37.2	5.39	3t (32.1)	241.70	Yes
13	X60	10.5	10.7	CR	Longitudinal	37.2	37.2	5.37	4t (42.6)	250.00	Yes
14	X60	10.5	10.65	CR	Longitudinal	37.2	37.2	5.44	5t (53.7)	243.20	No
15	X60	10.5	10.6	CB	Longitudinal	35	35	5.41	3t (32.1)	239.40	Yes
16	X60	10.5	10.7	CB	Longitudinal	35	35	5.39	4t (42.8)	238.40	Yes
17	X60	10.5	10.7	CB	Longitudinal	35.1	35.1	5.54	5t (53.5)	241.00	No
18	X52	9.5	9.7	CR	Single	35.5	33.9	4.87	Single	195.50	NA
19	X52	9.5	9.85	CR	Longitudinal	35	35	4.84	1t (9.90)	191.10	Yes
20	X52	9.5	9.7	CR	Longitudinal	35.5	33.5	4.88	4t (38.7)	195.90	No
21	X52	9.5	9.7	CR	Longitudinal	35.5	33.6	4.84	5t (48.7)	196.50	Yes
22	X52	9.5	9.75	CR	Longitudinal	35.8	33.6	4.9	6t (58.2)	200.80	Yes
23	X52	9.5	9.8	CR	Longitudinal	35.4	33.6	4.84	7t (67.9)	202.70	Yes
24	X52	9.5	9.86	CB	Longitudinal	35	35	4.92	1t (9.70)	184.20	No
25	X52	9.5	9.7	CB	Longitudinal	35	34.9	4.9	4t (39.0)	187.70	Yes
26	X52	9.5	9.7	CB	Longitudinal	35	35	4.86	5t (48.6)	192.80	Yes
27	X52	9.5	9.7	CB	Longitudinal	35	35	4.85	6t (58.2)	199.10	Yes
28	X52	9.5	9.7	CB	Longitudinal	35	35	4.87	7t (68.0)	197.30	Yes
29	X52	9.5	9.8	CB	Hoop	35	35	4.93	1t (9.75)	195.50	No
30	X52	9.5	9.7	CR	Hoop	35.5	33.7	4.8	0.5t (4.80)	206.80	No
31	X52	9.5	9.7	CR	Diagonal	35.5	33.8	4.8	0.5t (4.80)	196.70	Yes

5.3.1 Burst Pressure

Single defects failed locally and no further fracture beyond the defect area was observed. Figure 5-15 shows the failure experienced when testing single defects where failure in the form of a crack occurs at the centre of the defect where the thickness is at its minimum depth. Similar failure behaviours are seen for both circular and curved boxed shapes.

Figure 5-15: Failure of single circular defect

In all the interacting defects, fracture was observed to extend beyond the two defects area. The fracture path appears to occur always along the defect longitudinal axis which is mainly attributed to the stress component perpendicular to the defect.

The extension of the fracture appears to vary from one test to another depending on the state of stress and the material toughness for the tested pipes. Figure 5-16 shows the failure experienced when testing two circular defects spaced by 6t.

Figure 5-16: Failure of circular defects spaced by 6t.

5.3.2 Defect Shapes

The effect of defect shape on burst pressure is clearly seen in Figure 5-17 and Figure 5-18. For the circular shaped defects, the failure seems to occur at the centre of the defect then extends longitudinally through the ligament. The curved boxed defects seem to behave differently where the failure starts to occur at the defects corner then progresses across the defect area. Additionally, pipes with square-shaped defects are seen to have slightly but not significantly lower burst pressure than circular defects.

Figure 5-17: Failure of curved boxed defect spaced by 1t

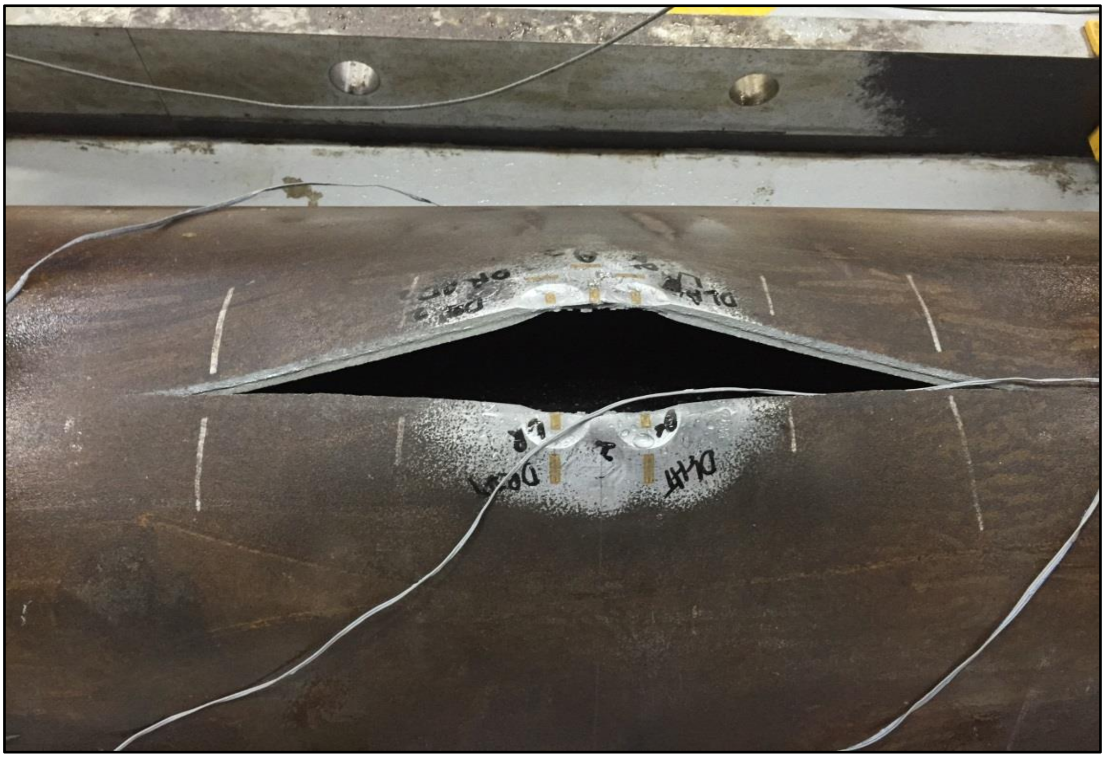

Figure 5-18: Failure of circular defect spaced by 1t

5.3.3 Defect Orientation

The effect of defect orientation is one of the parameters that have been investigated in this work. Defects are either placed in the longitudinal, circumferential or in the diagonal direction. There was no interaction seen to occur for defects placed along the circumferential orientation and this was verified up to a distance of 0.5t. Since the hoop stress dominates over the longitudinal stress, the crack will initiate in the longitudinal direction. For the diagonal direction mode, where the defects are placed along a line making a 45^o angle with the longitudinal direction, the interaction takes place only at a spacing of 0.5t. The shape of the crack has an interesting phenomenon as seen in Figure 5-19. The crack seems to initiate at the centre of one of the defects then extend with 45^o reaching the mid-section of the other defect causing the fracture line to extend beyond the two defects.

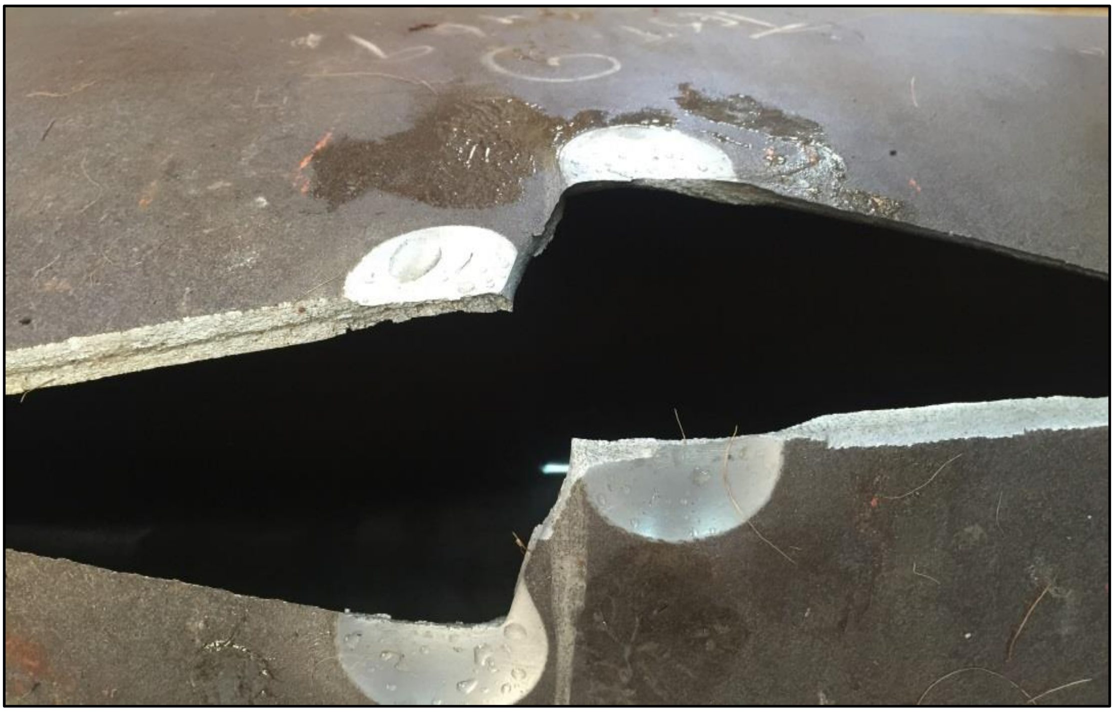

Figure 5-19: Failure behaviour of circular defects with a diagonal orientation spaced by half wall thickness

5.3.4 Defect Interaction

Crack propagation was used as a criterion to judge the interaction between defects for the experimental work. This criterion worked very well for the X60 pipes because of their high fracture toughness and hence high resistance to crack propagation. It was found that spacing between defects equivalent to 4t is sufficient to stop the interaction between defects. The X52 pipes were tested up to spacing equivalent to 7t. Even at this spacing distance, the crack continued to open wide and connected the two defects (both for circular and square defects). This can be caused by the X52 having a lower fracture toughness than that of X60.

5.4 Summary of Burst Tests

The following remarks are made based on the outcome of the burst tests.

- Defect interaction of 50% metal loss defects occurs in defects spaced up to and including 4 wall thickness (4t) for both circular and boxed defects. This was observed in the X60 grade, but for X52, the interaction could not be judged by the crack opening as the material toughness is relatively low which allows the crack to propagate for longer distances.
- Pipes with boxed defects have slightly but not significantly lower burst pressures.
- As spacing between the defects increases, the burst pressure converges to a steady value approaching the burst pressure as of that for single defect.
- Defects placed along the circumferential direction had no interaction even when the spacing was as small as 0.5t.
- Defects spaced diagonally were only observed to interact at 0.5t.
- For the X60 pipe and for both circular and square defects, the interaction stops at a spacing of 5t.

- Pipes of the same grade and from different manufacturers have slightly different material properties and hence different burst pressures.

5.5 Conclusion

Experimental burst tests were conducted to investigate the effect of shape and orientation of metal loss defects in API 5L X52 and X60 pipes with external diameters of 508 mm and with various wall thicknesses. The thicknesses used for X52 is 9.5mm and for X60 three wall thicknesses were used; 8.9mm, 9.5mm and 10.5mm. Scattered values were observed in the material properties in apparently identical pipe materials (due to chemical compositions, rolling, heat treatments and mechanical manufacturing processes such as expanders). The accurate evaluations of whether defect interaction occurs or otherwise are important parts of any defect assessment process.

The burst pressures of the defective pipes tested experimentally showed that interaction is not sensitive to defect shapes and occurs only for defects spaced within 4 wall thicknesses (4t). The tests also showed that defect orientation has an influence when it comes to defect interaction. Defects oriented in the hoop and diagonal directions show no interaction even when spaced by 1t, while defects oriented in the longitudinal directions show defect interaction up to 4t, but no interaction for defects spaced at longer distances. The experimental results will be further utilised in carrying out a parametric study looking in detail at the effects of spacing, shape and orientation in Chapters 6 and 7.

CHAPTER 6: NUMERICAL INVESTIGATION

6.1 Introduction

This chapter presents the details the FE numerical simulations of the pipe burst experiments that were discussed in chapter 5. The details of the FE methodology and models validation have been covered in chapters 4 and 5. All the FE models described in this chapter have been generated using the standard Abaqus package [51]. All the single and longitudinal spaced defects parts were created in Abaqus, the rest of the models were created in Creo [66] and then transferred into the Abaqus software. The following details were used throughout the analysis of this work unless exceptions are stated within the individual cases:

(i) Average pipe thicknesses and actual defect dimension details obtained from the experimental work were used in the FE simulation cases.

(ii) Isotropic material behaviour was used for all the modelled cases.

(iii) All defects created represent the actual location of the defects in the experiments, i.e. the external surface.

(iv) The FE simulation cases were based on 3D solid continuum elements.

(v) The von Mises yield criterion was used as a representation of the stress state for the failure criteria described in Chapter 4.

(vi) One quarter model was used for all cases except for the diagonal defect cases where a half model was utilised as deemed necessary.

6.2 Nonlinear Finite Element Analysis (FEA)

Numerical investigations of the effect of shape and orientation of closely spaced defects were carried out using the Abaqus 6.14 FEA software [23]. The outcomes of all the 31 experimental cases listed in Chapter 5 were numerically modelled and further studied using two analytical methods used for defect assessment, namely DNV RP F101 and ASME B31G. Artificial corrosion defects with the same length, depth and width were used in the models. The length to width ratio was kept the same (35 mm each) while the depth was constant for all defects, as 50% of the wall thickness. All cases were modelled with C3D20R elements with an average number of 90K elements and 400K nodes for both the circular defects models and the curved boxed shaped defects (with a range of 7 to 11 nodes across the wall thickness).

6.3 Material Properties

Details of the ductile carbon steel materials used in this research work are given in chapter 3. The engineering stress and strain values seen in chapter 5, were further converted to true stress-plastic strain as required for the numerical simulation using the Abaqus software. Figure 6-1 shows the true stress vs. plastic strain plot for both X52 and X60 materials.

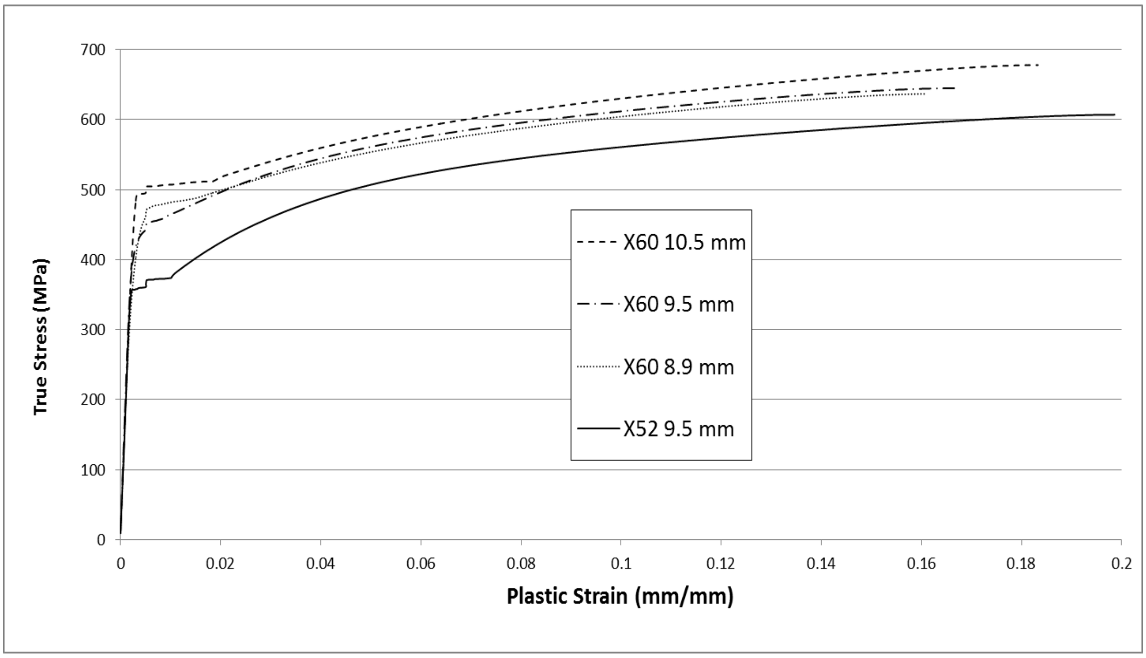

Figure 6-1: True stress vs. plastic strain data for all tested samples (the dimensions shown are the wall thicknesses of the relevant pipes from which the tensile specimens were taken)

6.4 Discussion of Simulation Results

A total of 31 simulation cases were analysed using Abaqus and further analytically calculated using ASME B31G and DNV RP F101 as shown in Table 6.1 (details of each case can be found in Chapter 5 Table 5.4). As stated in chapters 1 and 2, single defects were treated and discussed in detail by several researchers and were experimentally tested and simulated in this work to compare the failure pressure for single defects and for interacting defects. The subsequent sections will give an overview of each of the factors affecting the failure pressure of both single and interacting metal loss defects considering that failure criterion stated in Chapter 4. Efforts were made to compare the strain data obtained experimentally with those obtained via the FE analysis, as seen in Appendix B.

Table 6.1: Comparison of experimental failure pressure of the tested pipes with analytical and numerical methods.

Test Case No.	Failure Pressure (Bar)						Difference % Experimental Vs. Predicted					Defects interaction (Yes/No/NA)	
	Exp	ASME B31G (Single)	DNV (Single)	Modified B31G	DNV (Interacting)	FEA	ASME B31G (Single)	DNV (Single)	Modified B31G	DNV (Interacting)	FEA	Exp	FEA
1	195.40	175.8	187.6	180	NA	193.6	-10.03	-3.99	-7.88	NA	-0.92	NA	NA
2	199.70	176.2	187.9	182.4	NA	195.8	-11.77	-5.91	-8.66	NA	-1.95	NA	NA
3	190.50	183	208	175.5	172.2	199.5	-3.94	9.19	-7.87	-9.61	4.72	Yes	Yes
4	193.50	162.7	181.1	176.3	172	198	-15.92	-6.41	-8.89	-11.11	2.33	Yes	Yes
5	190.30	165.9	186.1	171.1	165.6	193.6	-12.82	-2.21	-10.09	-12.98	1.73	Yes	Yes
6	196.10	182	181.5	172.02	165.5	193.6	-7.19	-7.45	-12.28	-15.60	-1.27	Yes	Yes
7	193.20	178.5	202.6	189	184.7	200.2	-7.61	4.87	-2.17	-4.40	3.62	No	No
8	195.00	181.3	205.8	188.7	184.5	202.4	-7.03	5.54	-3.23	-5.38	3.79	No	No
9	196.20	180.7	205.1	188.6	184.4	206.8	-7.90	4.54	-3.87	-6.01	5.40	No	No
10	193.80	180	204.3	188.7	184.5	206.8	-7.12	5.42	-2.63	-4.80	6.71	No	No
11	246.70	222.4	235.4	232.7	NA	245	-9.85	-4.58	-5.67	NA	-0.69	NA	NA
12	241.70	196.4	202	214.5	196.4	246.8	-18.74	-16.43	-11.25	-18.74	2.11	Yes	Yes
13	250.00	193.5	197.2	215.3	196.3	243	-22.60	-21.12	-10.92	-18.78	-2.80	Yes	Yes
14	243.20	189.8	191.4	215.7	195.6	243	-21.96	-21.30	-10.76	-19.07	-0.08	No	No
15	239.40	195.8	201.9	210	190.5	237	-18.21	-15.66	-13.12	-21.18	-1.00	Yes	Yes
16	238.40	194.6	199.1	211.8	190.5	237	-18.37	-16.48	-12.37	-21.18	-0.59	Yes	Yes
17	241.00	191.5	194.4	211.6	189.3	234	-20.54	-19.34	-12.45	-21.68	-2.90	No	No
18	195.50	144.9	191	160.9	NA	193.6	-25.88	-2.30	-17.70	NA	-0.97	NA	NA
19	191.10	138.3	174.5	148.6	159.3	187	-27.63	-8.69	-22.24	-16.64	-2.15	Yes	Yes
20	195.90	129.4	159.1	149.8	158.3	184.8	-33.95	-18.79	-23.53	-19.19	-5.67	No	No
21	196.50	127.5	155.4	150.2	158	184.8	-35.11	-20.92	-23.56	-19.59	-5.95	Yes	Yes
22	200.80	126.5	153	151.2	157.5	185.9	-37.00	-23.80	-24.70	-21.56	-7.42	Yes	Yes
23	202.70	126.2	151.1	152.1	158.1	181.5	-37.74	-25.46	-24.96	-22.00	-10.46	Yes	No
24	184.20	138.5	174.8	143.6	151.8	173.8	-24.81	-5.10	-22.04	-17.59	-5.65	No	Yes
25	187.70	129.5	159.4	146.1	151.9	176	-31.01	-15.08	-22.16	-19.07	-6.23	Yes	Yes
26	192.80	127.8	155.8	147	152.2	180.4	-33.71	-19.19	-23.76	-21.06	-6.43	Yes	Yes
27	199.10	127	153.5	148.56	152.36	180.4	-36.21	-22.90	-25.38	-23.48	-9.39	Yes	No
28	197.30	125.6	150.4	149.1	152.39	179.3	-36.34	-23.77	-24.43	-22.76	-9.12	Yes	No
29	195.50	151.5	193.3	158.9	169.9	184.8	-22.51	-1.13	-18.72	-13.09	-5.47	No	No
30	206.80	149.9	191.2	161.1	172.7	198	-27.51	-7.54	-22.10	-16.49	-4.26	No	No
31	196.70	149.9	191.2	161.1	172.7	192.5	-23.79	-2.80	-18.10	-12.20	-2.14	Yes	Yes
Average difference percentage (Experimental Vs. Predicted)							-21.12	-9.96	-14.76	-16.12	**-2.04**		

6.4.1 Strain Analysis of the Burst Pipes

Several strain gauges were placed on the burst pipes in order to measure the strain data and compare them with the strain data obtained from the FE analyses. Of the total 31 burst tests, six pipes were fitted with strain gauge rosettes in and around the defect area. The dimensions of the strain gauge are 10 mm in length by 3 mm in width.

In order to obtain an average strain value covering the area of the strain gauge rosette, the nodes positioned within the area of the strain rosette were identified. The same set of nodes was then entered into Abaqus to retrieve the maximum principal strain values and von Mises stress values. The strain values of all the nodes lying within the area of the strain rosette were then averaged and used for comparison purposes.

X60 pipe which has a wall thickness of 9.5 mm with two circular defects spaced by 2t was selected for comparison. The strain gauges were placed at various locations as shown in Figure 6-2. The shape of the failure is shown in Figure 6-3.

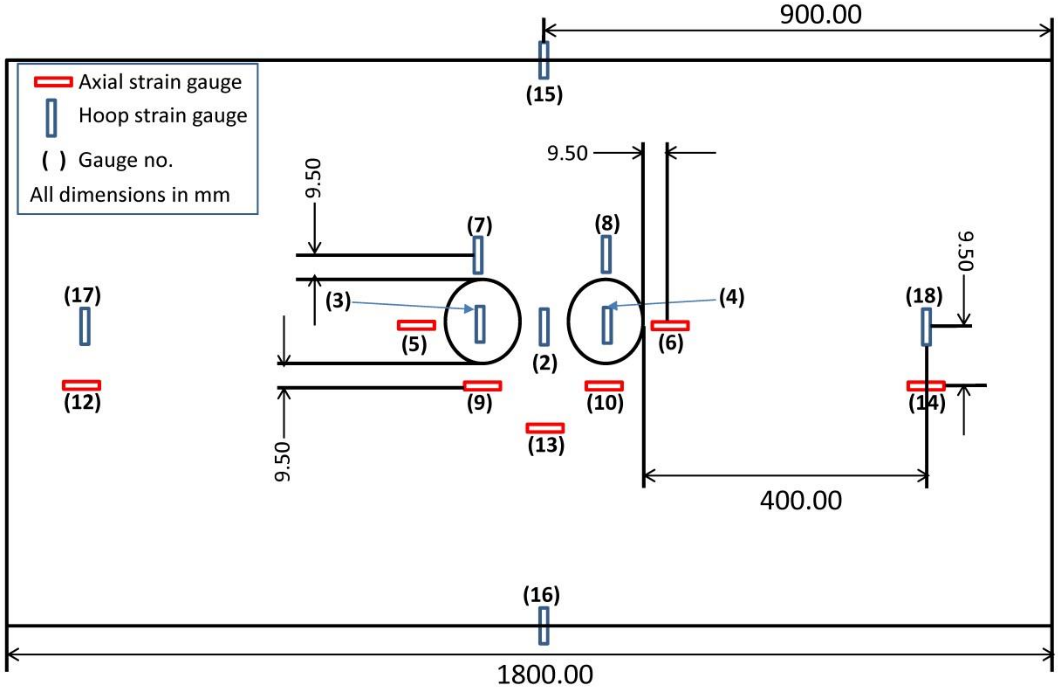

Figure 6-2: Strain Gauge Locations (X60 pipe)

Figure 6-3: Defects failure shape (length of rupture line is 227.5 mm) for X60 pipe

The strain gauge data vs those obtained from the FE analysis are shown in Figures 3 to 8. Since the gauge measures the total strain (the elastic and plastic strain), the maximum principal total strain in Abaqus was used for comparison. Figure 6-4 shows the results for gauge 3 (inside the defect), while Figure 6-5 shows only the initial readings up to pressure of 8.4 MPa. There is a good agreement (less than 10% difference) between the hoop strain gauge data and the FE averaged values at the defect area up to a pressure of 8.4 MPa (von Mises stress of 458 MPa). However, the readings deviate from the FE solutions after a pressure of 13.44 MPa which may be caused by the strain gauges losing contact with the pipe surface as the pipe rapidly approaches the burst pressure. This deviation has also been observed by Medjo et al [82] who also compared strain gauge data to the corresponding FE solution for a similar pipe defect.

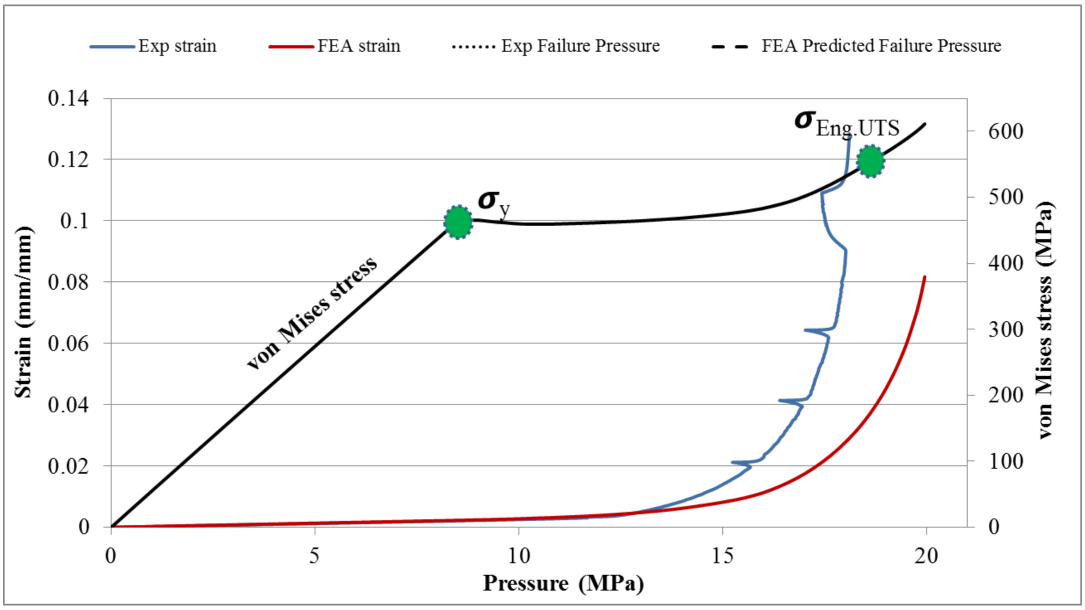

Figure 6-4: Experimental vs FE hoop strain values inside the defect (gauge no. 3)

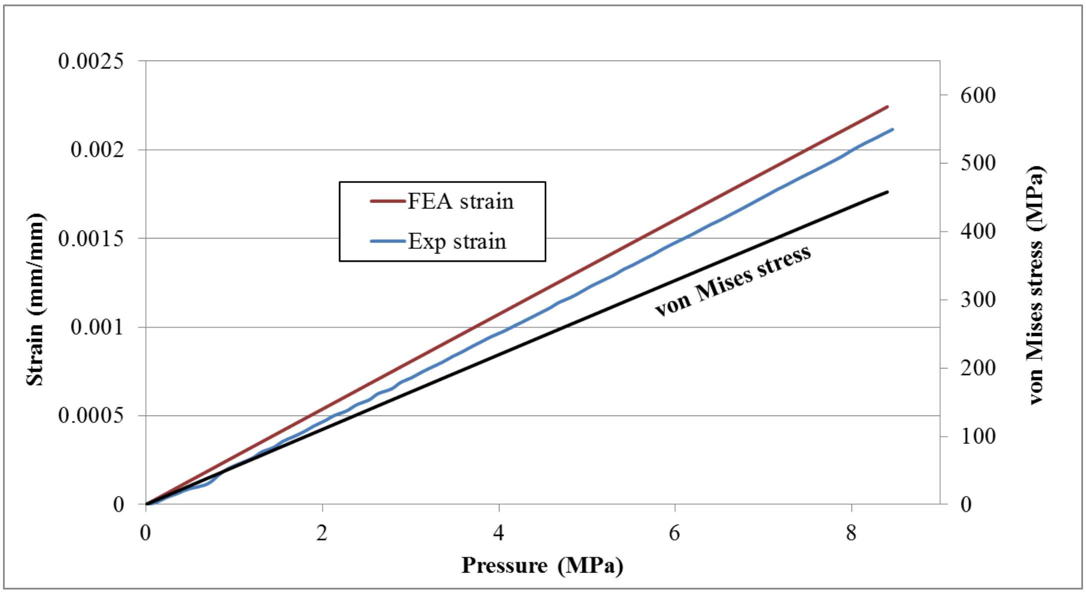

Figure 6-5: Experimental vs FE elastic hoop strain values inside the defect (gauge no. 3)

Figure 6-6 shows the hoop strains for gauge 17 (400 mm away from the defect edge) which are further magnified to show the elastic strains in Figure 6-7. Since this gauge is far from the defect, it is expected that elastic behaviour is mainly dominant. A similar deviation of the FE solutions is observed around a pressure of 13.65 MPa. The same pattern is observed in Figure 6-8 which shows the longitudinal strains for gauge 12 (400 mm away from the defect edge) which are further magnified to show the strains in Figure 6-9. The difference between the experimental strain gauge reading for the longitudinal direction and that obtained from the FE analysis is about 15% at around a pressure reading of 14.5 MPa.

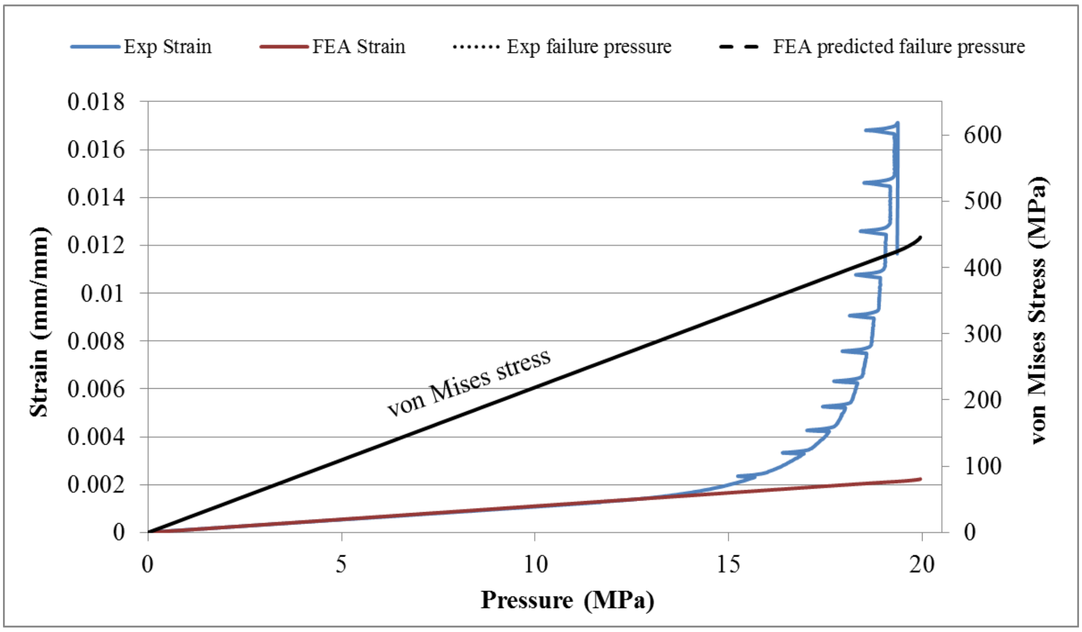

Figure 6-6: Experimental vs FE hoop strain values at 400 mm from the defect corner (gauge no. 17).

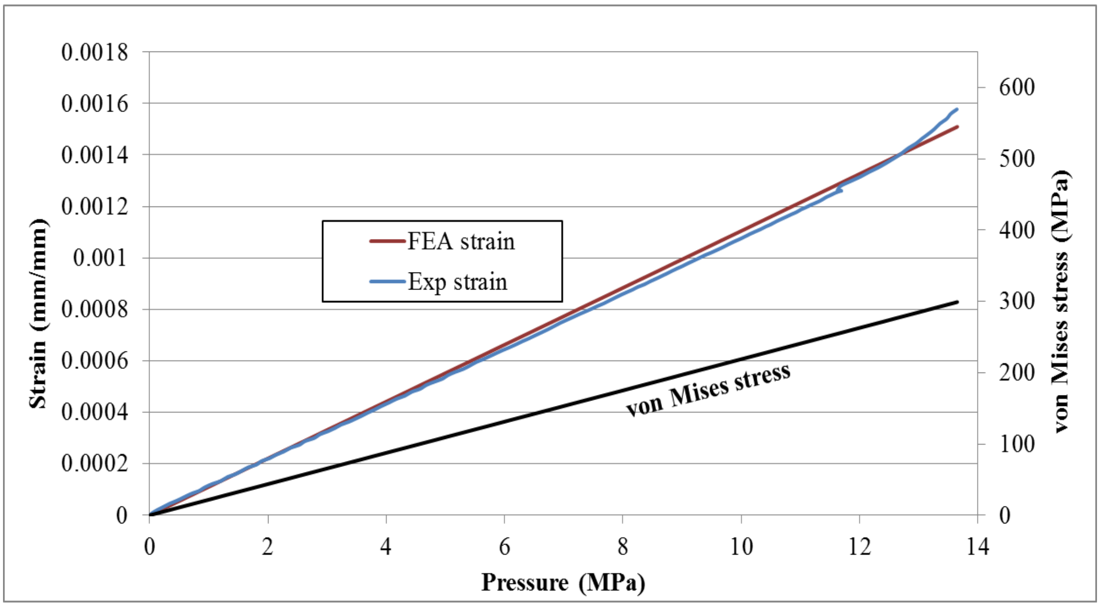

Figure 6-7: Experimental vs FEA elastic hoop strain values at 400 mm from the defect corner (gauge no. 17)

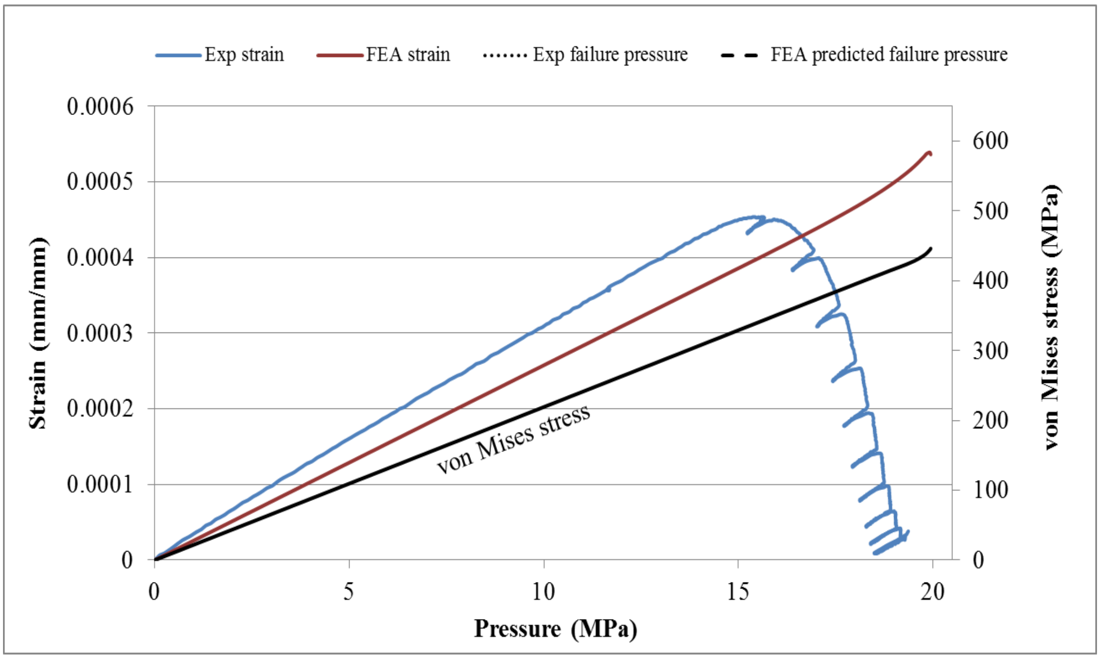

Figure 6-8: Experimental vs FE longitudinal strain values at 400 mm from the defect corner (gauge no. 12).

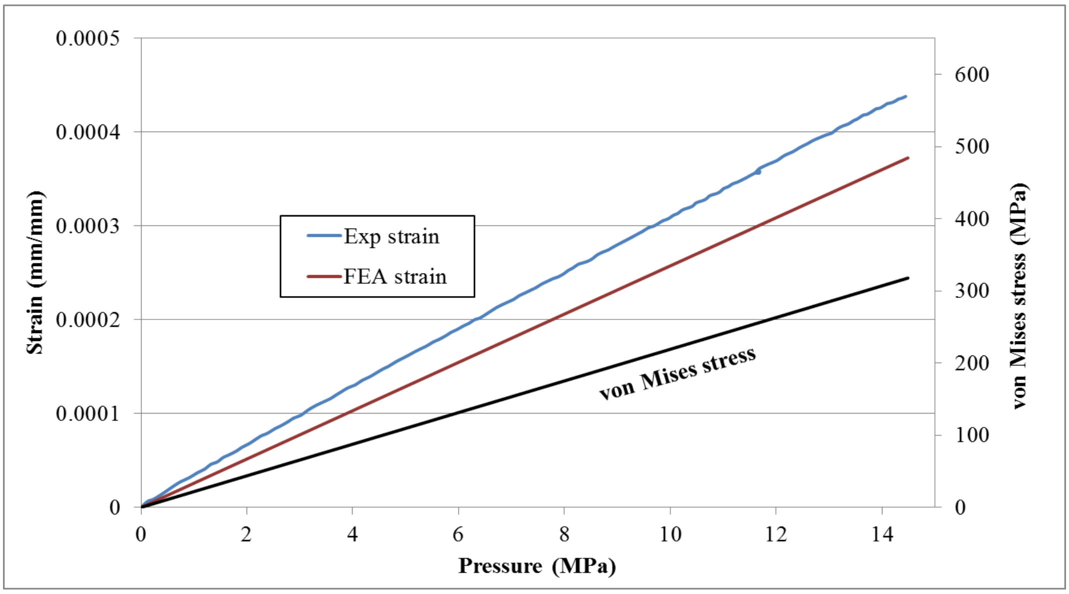

Figure 6-9: Experimental vs FE elastic longitudinal strain values inside the defect (gauge no. 12)

6.4.2 Effect of Spacing on Circular Defects

6.4.2.1 Spacing in the Longitudinal Direction

Figure 6-10 to Figure 6-13 present examples of the stress evolution for circular defects spaced by one wall thickness for two grades of steels API-5L-X52 and API-5L-X60 with 9.5 mm wall thicknesses and 50% defect depth. The example presented in Figure 6-14 is for API-5L-X60 with 10.5 mm wall thicknesses and 50% defect depth. The interaction criteria stated in Chapter 4 clearly show that the von Mises stress along line CD reaches the failure criterion before the von Mises stress in the through-thickness line AB, i.e. the defects will interact and failure occurs locally at the defect as well as through the ligament between the two defects. The case presented in Figure 6-14 is also in line with the outcome of the experimental work where no interaction is observed, giving further indication that the proposed failure criterion is robust in terms of interaction prediction. The stress level across the CD line when failure is predicted in Figure 6-13 varies only slightly between points C and D which is attributed to the fact that the CD line is only 9.8 mm (1t). The stress levels, however, vary with noticeable change in Figure 6-14 as the distance C-D between the two defects is 26.9 mm (5t).

Simulation cases were carried out for both materials until interaction has ceased to occur. The results of the analysis show that the defect interaction (i.e. 100% of line CD reaching the failure criterion before line AB) occurs for defect depths of 50% of the wall thickness for distances up to 6t for the X52 pipe. However, for the X60 pipe material, the interaction effect occurs up to 4t. The outcome of the FEA for both cases is in line with the experimental work.

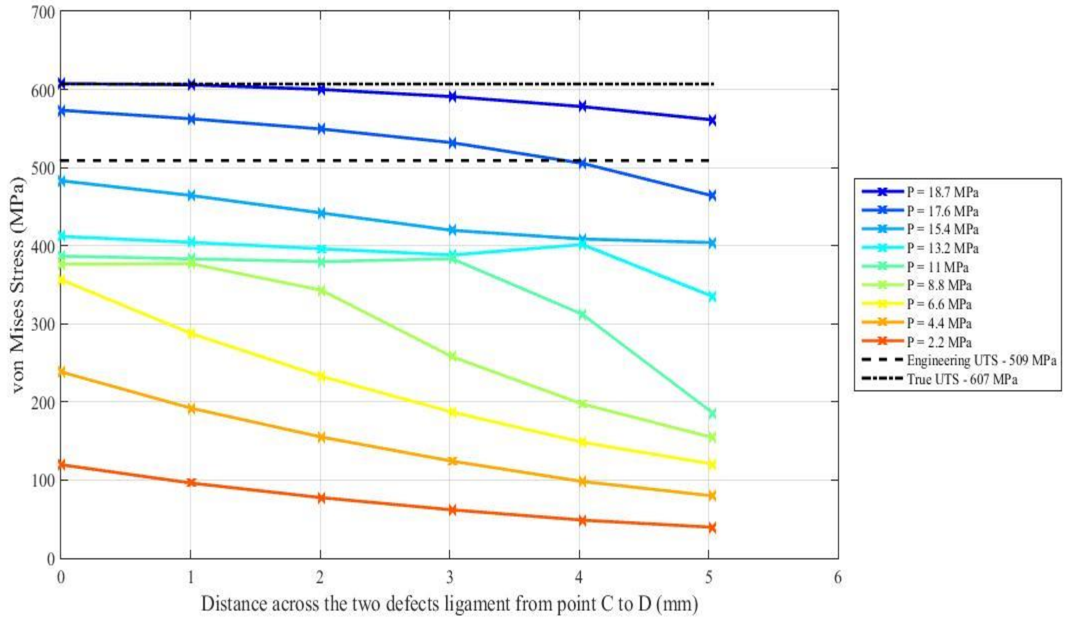

Figure 6-10: von Mises stress curves at different pressure increments across the pipe wall thickness Line (CD) spaced by 1t and with a depth of 50% for X52 pipe for circular defects in the longitudinal direction

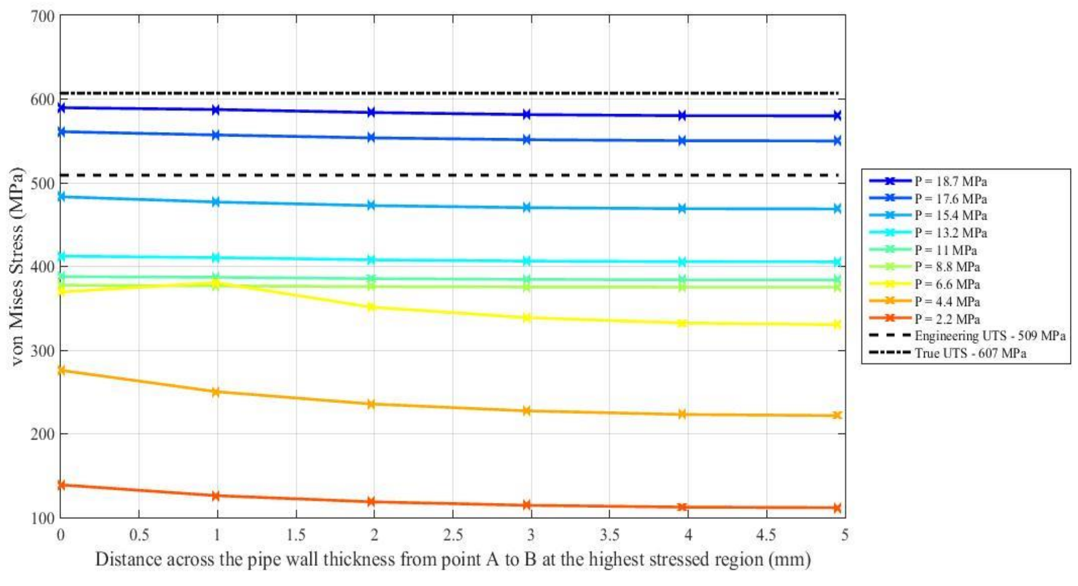

Figure 6-11: von Mises stress curves at different pressure increments across the ligament between the two defects (AB) spaced by 1t and with a depth of 50% for X52 pipe for circular defects in the longitudinal direction.

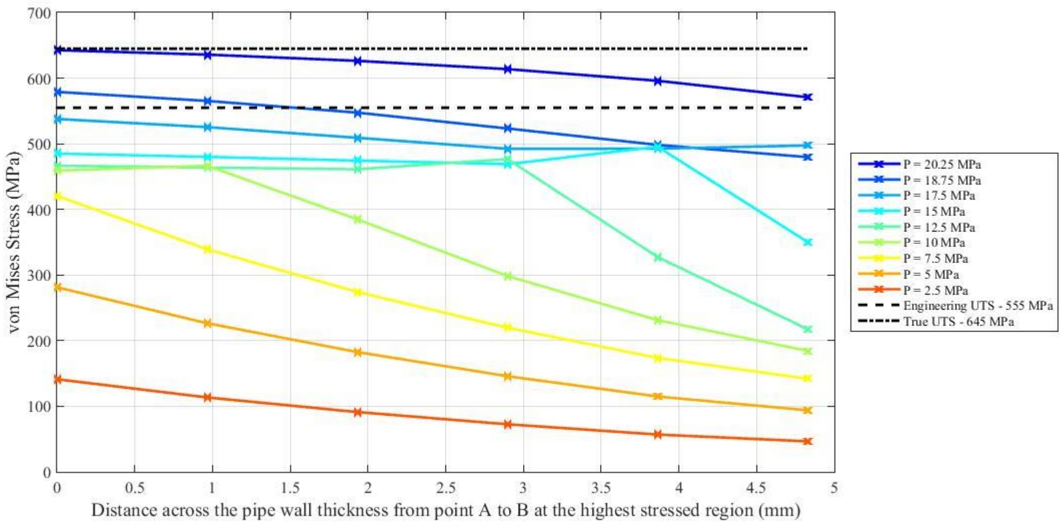

Figure 6-12: von Mises stress curves at different pressure increments across the pipe wall thickness Line (AB) spaced by 1t and with a depth of 50% for X60 pipe for circular defects in the longitudinal direction

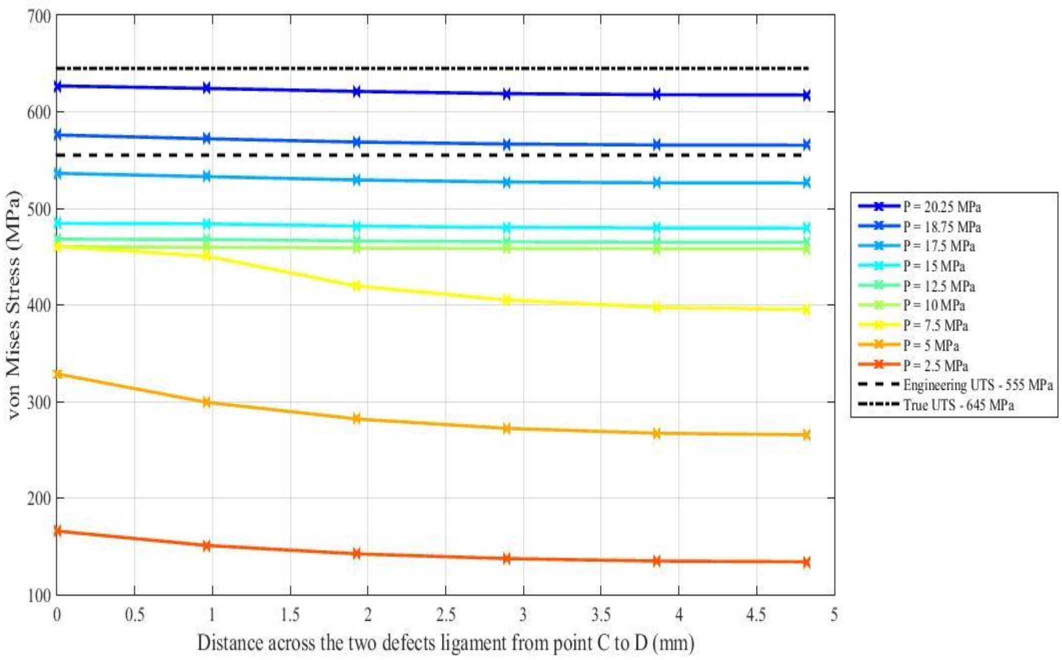

Figure 6-13: von Mises stress curves at different pressure increments across the ligament between the two circular defects (CD) spaced by 1t spacing in the longitudinal direction

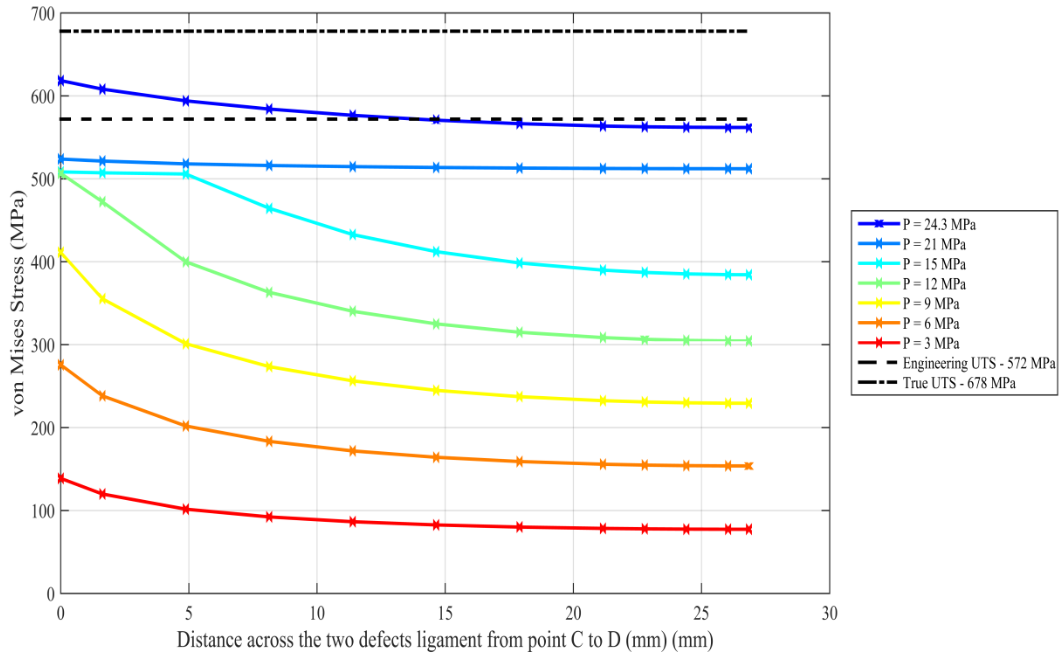

Figure 6-14: von Mises stress curves at different pressure increments across the ligament between the two circular defects (CD) spaced by 5t spacing in the longitudinal direction for X60 pipe

Comparison of the experimental results with those obtained numerically and via analytical methods was done for X52 pipe with 9.5 mm wall thickness containing circular defects. Due to the limited number of cases for the X60 pipe, the comparison was carried out only for the X52 material. Results shown in Figure 6-15 reveal that FE predicted failure pressure values are less conservative than those obtained from analytical methods. Generally, as spacing increases so does the failure pressure which starts to flatten once the defects reach a pressure similar to that of single defect. At spacing of 6t and 7t, it was realised that the experimental failure pressure is higher than that of single defects which could be attributed to the variation in wall thickness (permissible tolerance for wall thickness as per ISO 3183 is 0.1t). The difference seen between the experimental and the FEA results at 7t is mainly attributed to the 10% variation in the wall thickness of the experimental pipe compared to that of the FEA model which has a constant wall thickness across the modelled pipe.

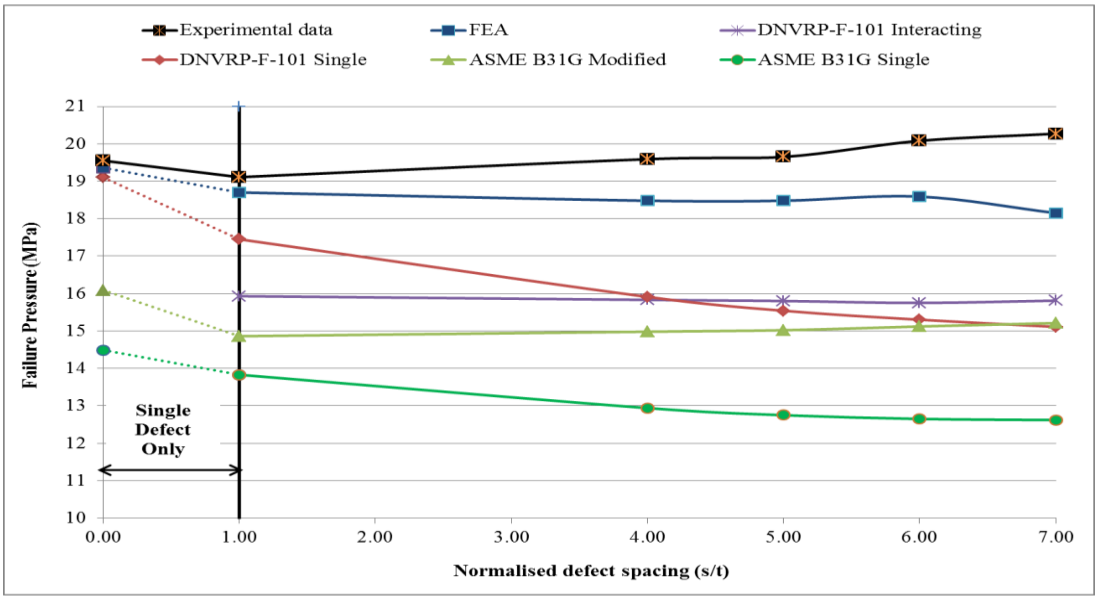

Figure 6-15: Comparison between experimental results and both numerical and analytical methods for X52 circular defects longitudinally spaced.

6.4.2.2 Spacing in the Circumferential Direction

As seen in Table 6.1, simulation was carried out for all the circumferential cases and the outcomes were similar to those seen in the experimental work. Figure 6-16 shows typical von Mises stress contours around the circular defects in the circumferential direction for API-5L-X52 with 9.5 mm wall thickness, 50% defect depth and 0.5t spacing. As with the experimental work, the FE analysis shows that defects in the circumferential direction do not interact even when the spacing is reduced to 0.5t. The prediction of the fracture path from the numerical simulation shows good results as can be seen in Figure 6-16. Though both defects in the simulation results had the same stress values at the centre of the defect, in the experimental work only one defect has failed which could be possibly attributed to geometry imperfection.

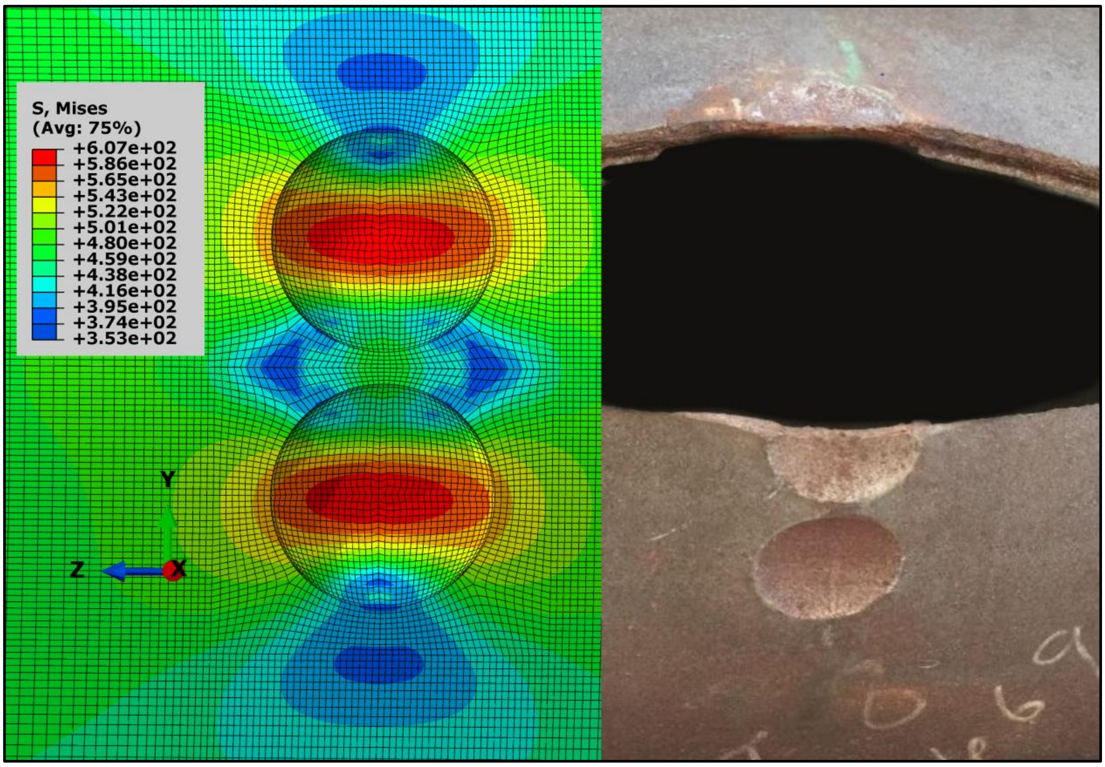

Figure 6-16: Effect of circumferential spacing on circular defects in X52 (9.5 mm) with 50% defect and 0.5t spacing (the right side shows actual burst failure)

6.4.2.3 Spacing in the Diagonal Direction

The simulation results obtained for circular defects in the diagonal orientation for the two grades of steel shows that defect interaction does not occur when the defects are spaced by 1t or longer and with a defect depth of 50%. In this case, the failure will be local by leak at the centre of each of the two defects rather than a crack line joining the two defects which was observed both experimentally as well as numerically. The only case where interaction is possible for the 45^{o} diagonally spaced defects is when they are spaced by 0.5t which was the case seen experimentally as well as numerically which can be seen in Figure 6-17.

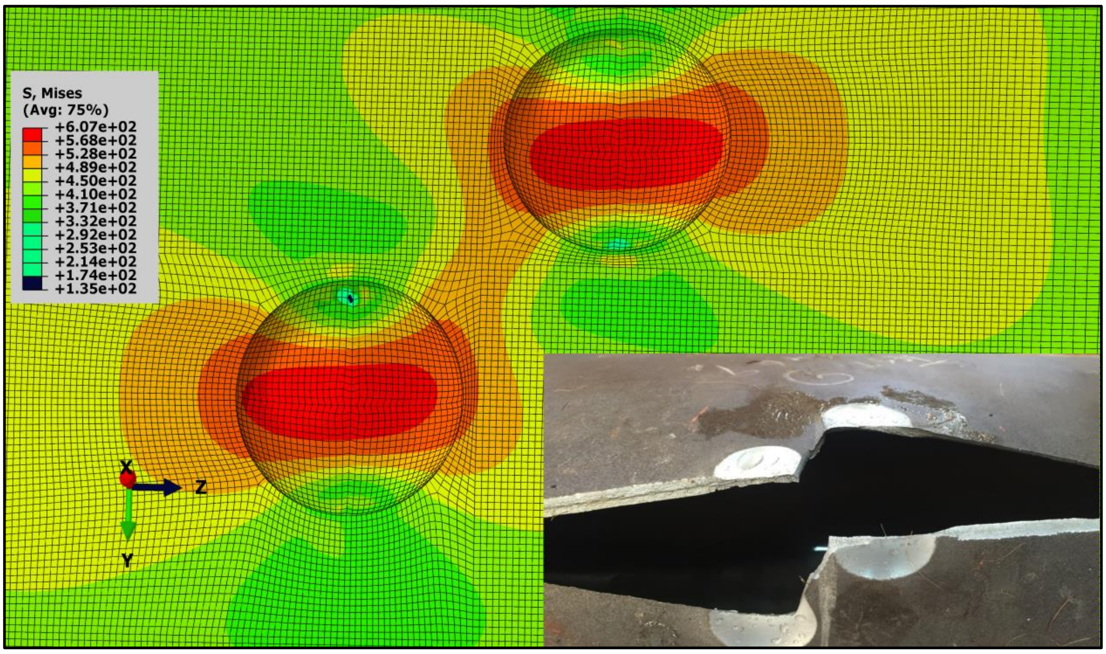

Figure 6-17: Effect of diagonal spacing on circular defects in X52 (9.5 mm) with 50% defect and 0.5t spacing (the right image shows actual burst failure)

6.4.3 Effect of Spacing on Boxed Shape Defects

6.4.3.1 Spacing in the Longitudinal Direction

Figure 6-18 and Figure 6-19 present the stress contours for boxed defects spaced by 4t in the longitudinal direction for both pipe materials with 50% defect depths. The results presented were analysed by varying the defect spacing and investigating the impact on defect interaction as seen in the experimental work. Defect interaction in the longitudinal direction was present in the X60 pipe for spacing up to 4t, similar to that seen for the circular defects in the same material. Similar findings were also observed for defects interaction of 4t in X52 pipes. The experimental results, seen in Table 6.1, show that curved boxed defects spaced by 1t in the longitudinal direction did not interact and one of the defects failed locally. This could be attributed to a pre-existing either intergranular crack or surface crack which caused this to happen as it was evident from the subsequent tests that interaction was present for defects spaced by 2t up to 4t.

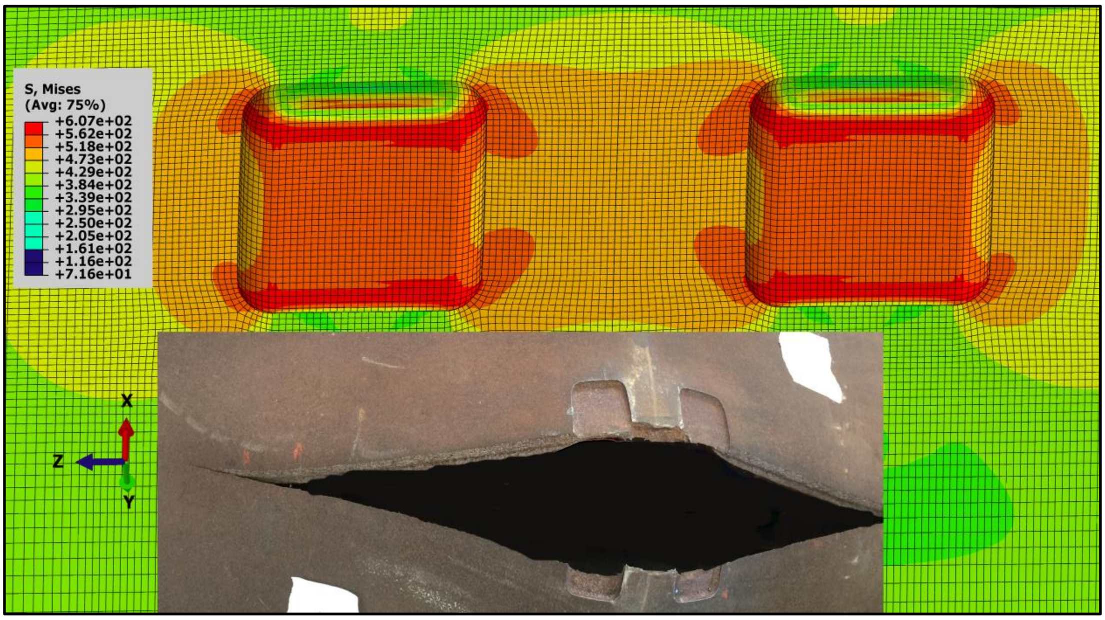

Figure 6-18: Effect of longitudinal spacing on curved boxed defects in X52 (9.5 mm) with 50% defect and 4t spacing (the lower image shows actual burst failure)

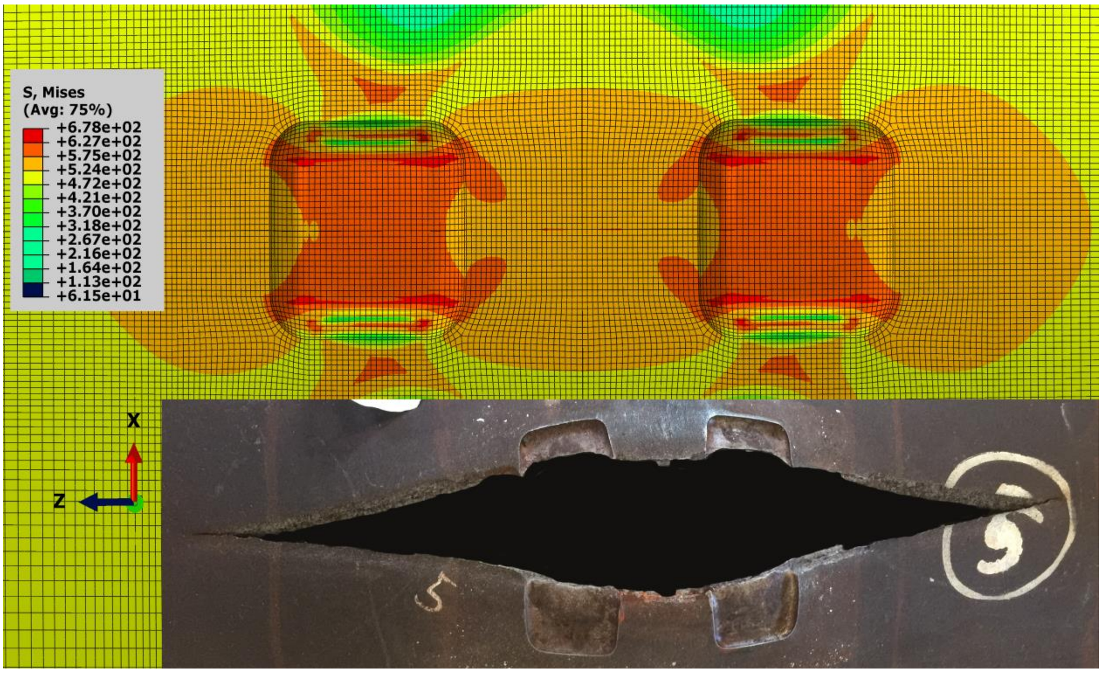

Figure 6-19: Effect of longitudinal spacing on curved boxed defects in X60 (10.5 mm) with 50% defect and 4t spacing (the lower image shows actual burst failure)

Figure 6-20 below shows a comparison between the methods used within this study to arrive at the failure pressure of X52 material with curved boxed defects spaced in the longitudinal direction. As spacing increases, so does the failure pressure which starts to flatten once the defects reach a pressure similar to that of single defect. It can be also observed from Figure 6-20 that the analytical methods have yielded conservative failure pressure values compared to those obtained numerically.

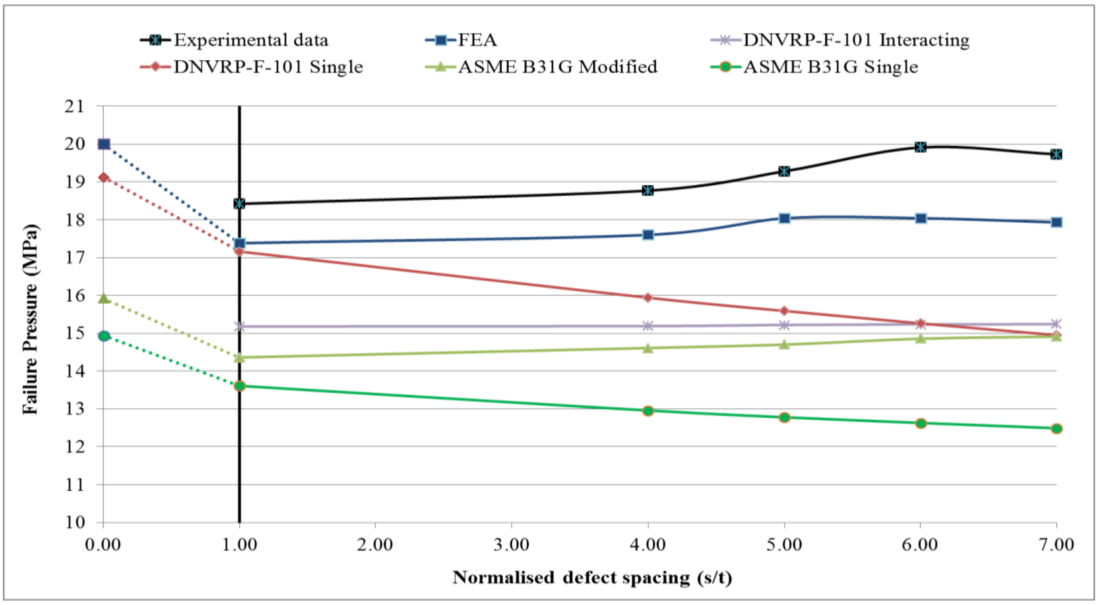

Figure 6-20: Comparison between experimental results and both numerical and analytical methods for X52 curved boxed defects longitudinally spaced.

6.4.3.2 Spacing in the Circumferential Direction

The simulation results for both grades of steel, X52 and X60, with curved boxed shape defects show the same trend of behaviour as that observed with circular defects spaced in the circumferential direction. Due to budget constraints, the burst test was performed only for a spacing of up to 1t. The stress contours from the FE analysis show that the highest von Mises stresses occur within the defect area, rather than across the wall thickness, indicating that failure will always occur at the defect rather than in the ligament area. From

Figure 6-21, for the experimental tested pipes and FE model, failure tends to occur at the bottom corner of the defect where there is a higher stress concentration effect despite the efforts taken to reduce this affect by introducing the curvature.

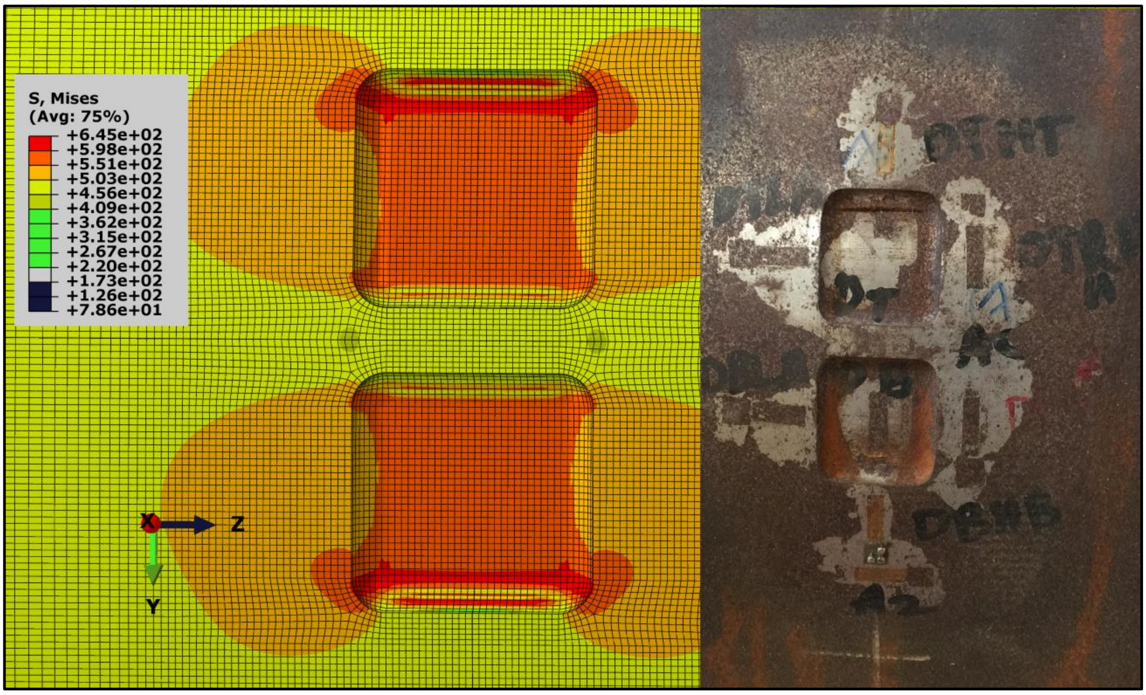

Figure 6-21: Effect of circumferential spacing on curved boxed defects in X60 (9.5 mm) with 50% defect and 1t spacing (the right image shows actual burst failure)

6.4.3.3 Spacing in the Diagonal Direction

Due to constraints on resources, the effect of Curved Boxed defects spaced on the diagonal orientation was not carried out experimentally. However, a parametric study will be carried out instead for this type of defect in the diagonal direction, as discussed in Chapter 7, section 7.8.

6.5 Conclusion

The numerical results in this study relating to metal loss defects for two common pipe grades of API 5L X52 and X60 with an outer diameter of 508 mm and wall thicknesses of 9.5 mm and 8.9/9.5/10.5 mm respectively were presented. Defect interaction occurs when the spacing between the defects is bounded by the engineering and true ultimate tensile before it is reached in the through-thickness wall ligament. Interaction leads to a rupture line joining the defects while its absence will lead to only local leak at each individual defect.

The FE results clearly show that the predicted failure pressure values are less conservative than those obtained analytically and there is a good correlation with the experimental cases which paves the work for further parametric studies which will consider the effect of different parameters as discussed in chapter 7.

CHAPTER 7: PARAMETRIC STUDY

7.1 Introduction

The work is this chapter is an extension to the numerical modelling performed for the experimental cases in chapter 6. As seen from chapters 5 and 6, defect interaction is governed mainly by defects spaced in the longitudinal orientation. As a result, the parametric work presented in the subsequent sections of this chapter will mainly look at one grade of steel, X60 (10.5mm) and defects oriented in longitudinal direction. Comparisons with X52 pipe material will also be carried out for one variable to further test the derived failure pressure equations and to investigate the impact of materials. The failure criterion proposed in chapter 4 and verified both experimentally and numerically in chapters 5 and 6 will be used throughout the work prescribed in this chapter. Material properties used earlier in chapter 6 will be used throughout the numerical models. Past research work has indicated that burst pressure depends mainly on the defect geometry rather than the overall pipe restraint conditions, i.e. whether the pipe is modelled with or without end caps [83, 84]. As a result of this conclusion, no further analysis of the modelling of the effects of end caps is attempted.

More than 160 FE models and subsequence numerical analyses were performed to estimate the failure pressure of pipes with both single and interacting defects in this parametric study. The interaction spacing (clustering under one long defect) is defined as the space between defects where the stress levels correspond to the failure criterion stated in chapter 4. Since there is non-existence of "ideal" corrosion defect shapes within the complex nature of the corrosion process, the parametric study is carried out within the envelop of the tested defect shapes in the experimental work, i.e. either half or double the dimensions of the defects tested experimentally are used. Table 7.1 shows the parameters covered in this work and the main variables which are the burst pressure (MPa) and defect spacing (mm) which varies until no defect interaction occurs. Numerical models made for each case are further presented in Appendix B.

Table 7.1: Parametric study details

Case study	Material	Outer diameter, D (mm)	Wall thickness, t (mm)	Defect depth, d (mm)	Defect Length, DL (mm)	Defects Types
1P -a	API 5L X60 True UTS= 678 MPa	254	10.5	5.25 (50%)	Variable (17.5, 35, 70)	Both circular and curved boxed
1P -b	API 5L X52 True UTS= 607 MPa	254	10.5	5.25 (50%)	Variable (17.5, 35, 70)	Both circular and curved boxed
2P	API 5L X60 True UTS= 678 MPa	254	10.5	Variable (25%, 50%, 75%)	35	Both circular and curved boxed
3P	API 5L X52 True UTS= 678 MPa	Variable (254, 508 and 762)	10.5	5.25 (50%)	35	Both circular and curved boxed
4P	API 5L X60 True UTS= 678 MPa	254	Variable (6.35, 10.5, 15)	5.25 (50%)	35	Both circular and curved boxed

In addition to the cases listed in Table 7.1, further three cases were analysed; first, a single internal defect was analysed to evaluate the failure pressure and compare with that of an external defect. Second, two curved boxed defects when they are in contact with each other to form a single (lengthier in the longitudinal direction) defect to determine the failure pressure and compare with a single curved boxed defect having the same length as the two combined defects. Finally, curved boxed defects spaced diagonally were analysed as to compare the interaction outcome with those seen for the circular defects in Chapter 6.

The results of the FE analyses were normalised by dividing by P_n which is the pressure obtained from Barlow's formula (see equation 7-1) using the true UTS values (For X60, the value used is 678 MPa and for X52 607 MPa) and relevant pipe parameters where needed.

$$P_b = \frac{(2 * t * \sigma_{UTS})}{\mathrm{D}} \quad \textbf{(7-1)}$$

7.2 Effect of Defect Length (For X52 and X60)

A study on the effect of the length of defects was conducted. For this parameter only two materials (API 5L X52 and X60 detailed in chapter 5 and 6) were analysed to look at the failure pressure trend as well the critical defect spacing when materials are varied. The outcome of the analysis for both of the materials with different shapes is shown in a two dimensional schematic as shown in Figure 7-1 to Figure 7-4. The defect interaction stops when the failure pressure remains the same as the interaction is increased, i.e. the failure pressure curve becomes horizontal. This is indicated by a dark circle in the relevant figures. It can be seen from the results obtained that pipes with short defect lengths fail at a higher pressure, as expected due to the higher stiffness created at the surrounding ligament. It is also noted that failure pressure for the curved boxed defects is lower than that for circular defects in both of the studied materials which could be as a result of less material in the defect ligament due to the shape of the defect. The difference in spacing between circular defects and that of the curved boxed defects is almost similar, suggesting that shape of defects has a minimal if not negligible effect for the cases 1P-a and 1P-b. However, it was observed that spacing between circular and curved boxed defects was slightly different for X60 17.5 mm as the circular defects stopped interacting after reaching 4t while it was 3t for the curved boxed defects. The same was also noticed for the 70 mm length defects in X52 as defect interaction ceased to occur after 6t in circular defects while it was possible for defects to interact up to 7t in the curved boxed defects. These slight differences could be attributed to the inherent FEA model approximation. Both of the X52 and X60 pipe materials have very similar defect spacing trends postulating that the material strength of these pipe materials has minimal effect. As stated earlier, as the interaction ceases to exist, it is observed that the predicted failure pressure tends to flatten out and defects will fail individually.

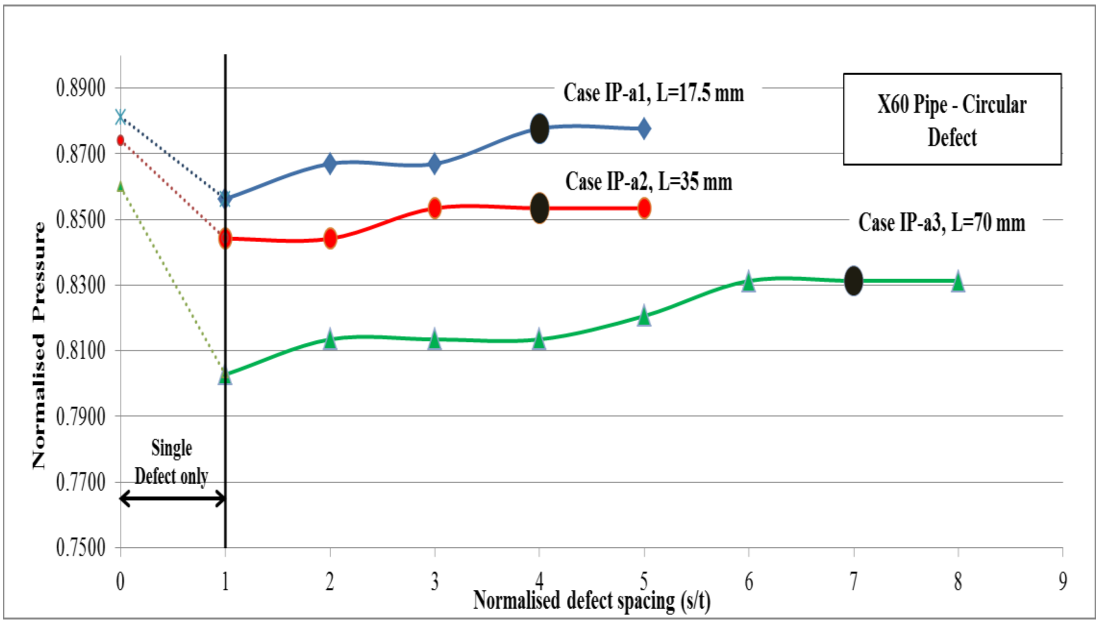

Figure 7-1: Normalised pressure vs defect spacing for X60 pipe circular defects with various defect lengths (Note: dark circles denote last possible interaction space)

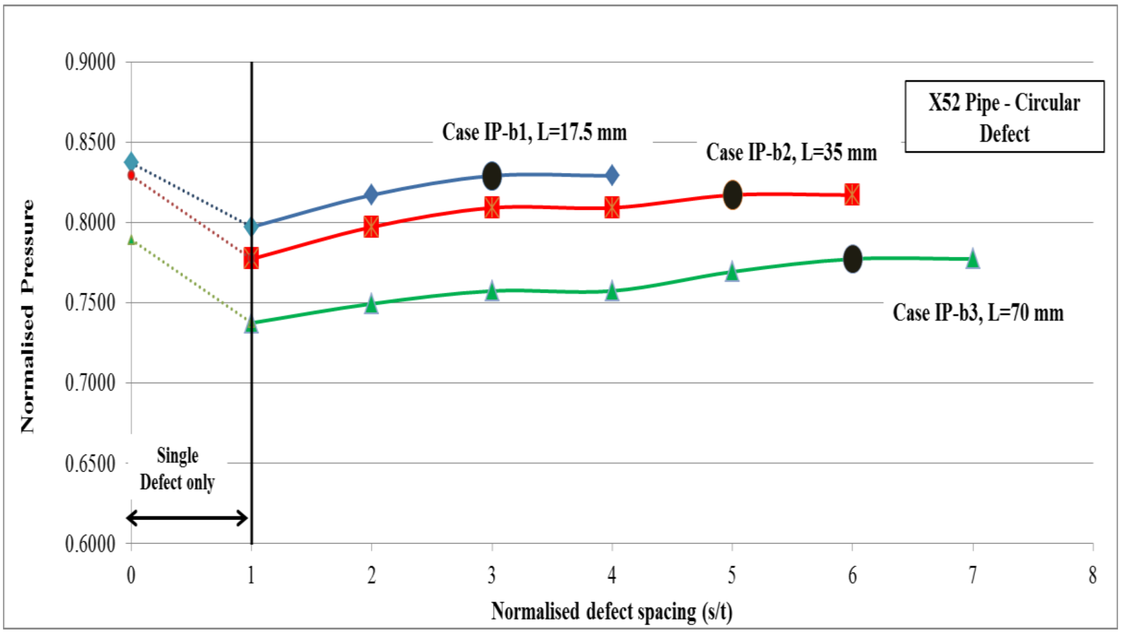

Figure 7-2: Normalised pressure vs defect spacing for X52 pipe circular defects with various defect lengths (Note: dark circles denote last possible interaction space)

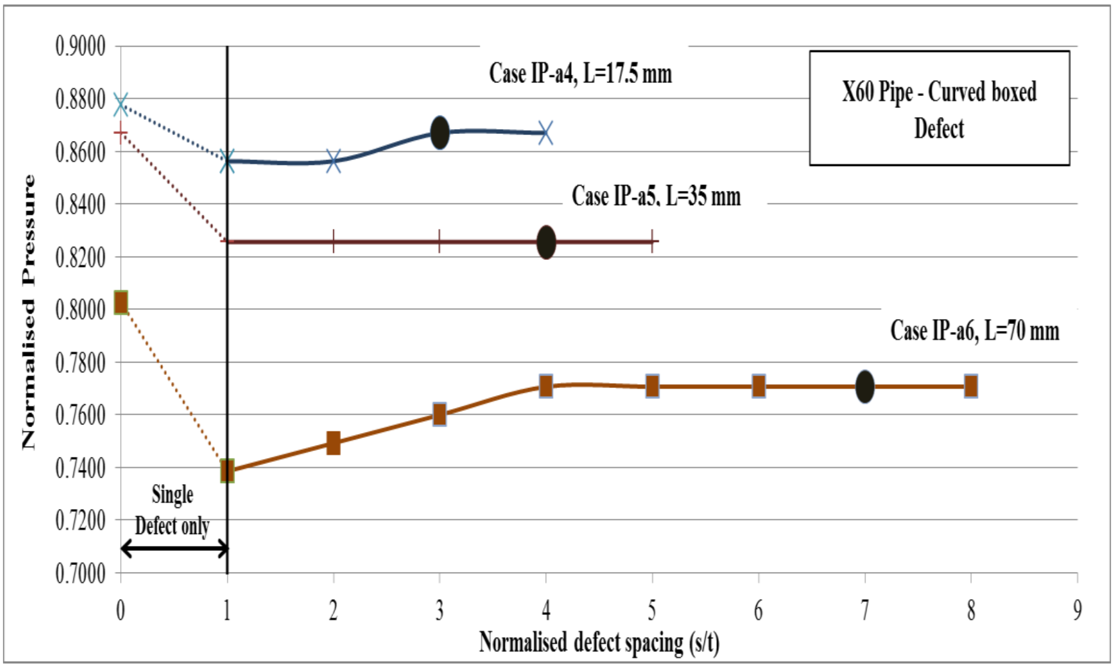

Figure 7-3: Normalised pressure vs defect spacing for X60 pipe curved box defects with various defect lengths (Note: dark circles denote last possible interaction space)

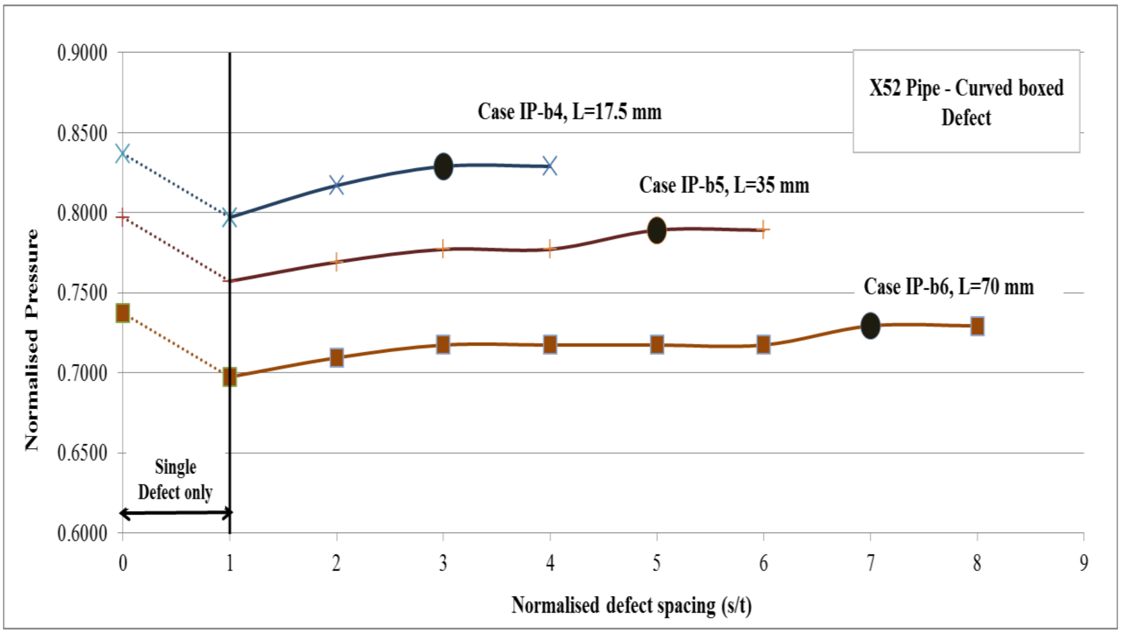

Figure 7-4: Normalised pressure vs defect spacing for X52 pipe curved boxed defects with various defect lengths (Note: dark circles denote last possible interaction space)

Recognizing that defect length has the highest impact in terms of failure pressure and critical spacing between defects due to the fact that more material is removed from the ligament (pipe becoming less stiffer), a generalised evaluation equation obtained from a surface fitting curve similar to the one shown in Figure 7-5 for interacting defects was developed for predicting the failure pressure. It is important to mention that this generalised formula is only valid for the specific pipe geometry investigated in this study (see cases 1P-a and 1P-b in Table 7.1) to predict the failure pressure of interacting defects.

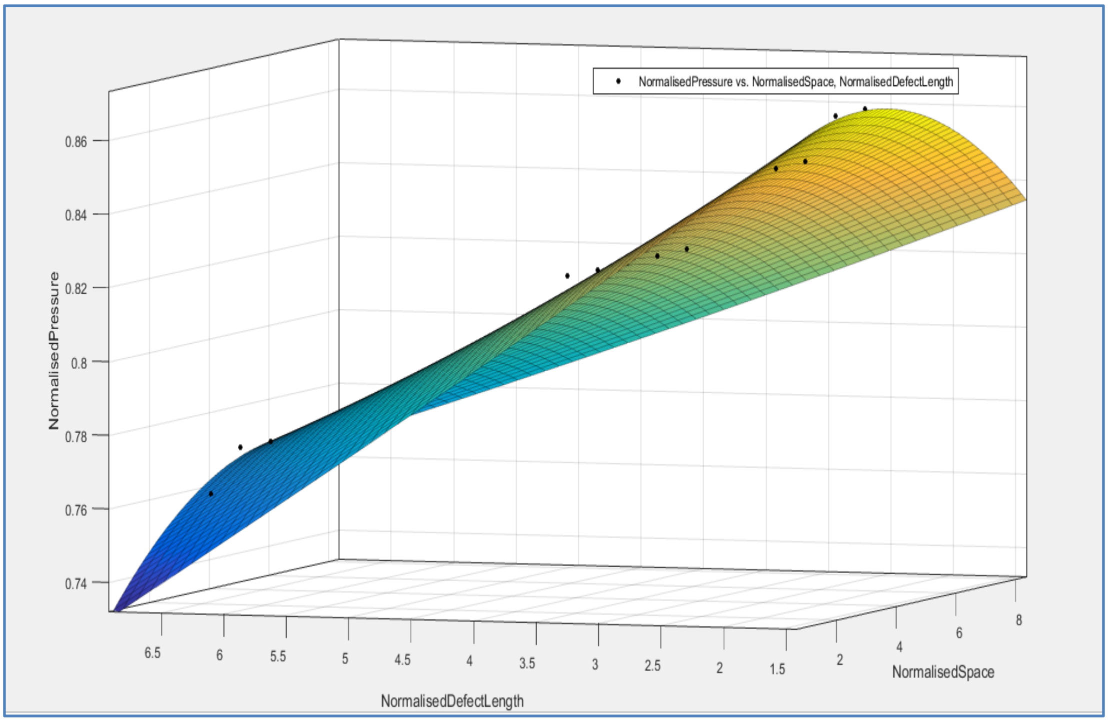

Figure 7-5: Surface fitting for curved boxed defects of X60 materials (variable length parameter)

The developed generalised solution for predicting the failure pressure for circular and curved boxed shaped defects taking into consideration two materials (X52 and X60) and various variable parameters along with defects spacing is proposed as below:

$$P_f\ (x, y) = p00 + (p10 * \mathrm{x}) + (\mathrm{p01} * \mathrm{y}) + (\mathrm{p20} * \mathrm{x}^2) + \mathrm{p11}(\mathrm{x} * \mathrm{y}) + (\mathrm{p02} * \mathrm{y}^2) \qquad \textbf{(7-2)}$$

where,

x = Normalised defect spacing (s/t)

y = Normalised defect length (ratio between defect length and wall thickness)

The coefficients for equation (7-2) are listed in Table 7.2.

Table 7.2: Coefficient values of the failure pressure prediction for the defects length parameter of X52 and X60 materials

Coefficients	X52		X60	
	Circular defects	Curved boxed defects	Circular defects	Curved boxed defects
P00	0.7220	0.7662	0.8758	0.8975
P10	0.0139	0.0103	0.0051	0.0041
P01	-0.0098	-0.0363	-0.0126	-0.0266
P20	-0.0010	-0.0005	-0.0001	-0.0011
P11	-4.29E-06	-4.41E-04	2.49E-05	0.0015
P02	-0.0003	0.0022	0.0002	0.0002

It should be noted that equation (7-1) is only valid for the valid flaw interaction spacing cases.

7.3 Effect of Defect Depth

The effect of defect depth was studied and the results are presented in Figure 7-6 and Figure 7-7. The outcome of the study gives clear indication, as expected, that deeper defects have lower failure pressures as the pipe wall stiffness decreases with deeper defects. It is noticed that circular defects tend to interact when spaced with longer distances than those which have a curved boxed shape. Defects with higher depth tend to have less interaction spacing as they tend to fail locally and failure does not extend outwards through the defect and pipe wall thickness ligament. The effect of spacing on circular defects is higher than that with curved boxed defects, suggesting that the shape of defects plays a role on effect of spacing when defects for the same defect depth. The data presented in Figure 7-6 and Figure 7-7 have fixed pipe outside diameter of 508 mm, wall thickness 10.5 mm and defect length of 35mm.

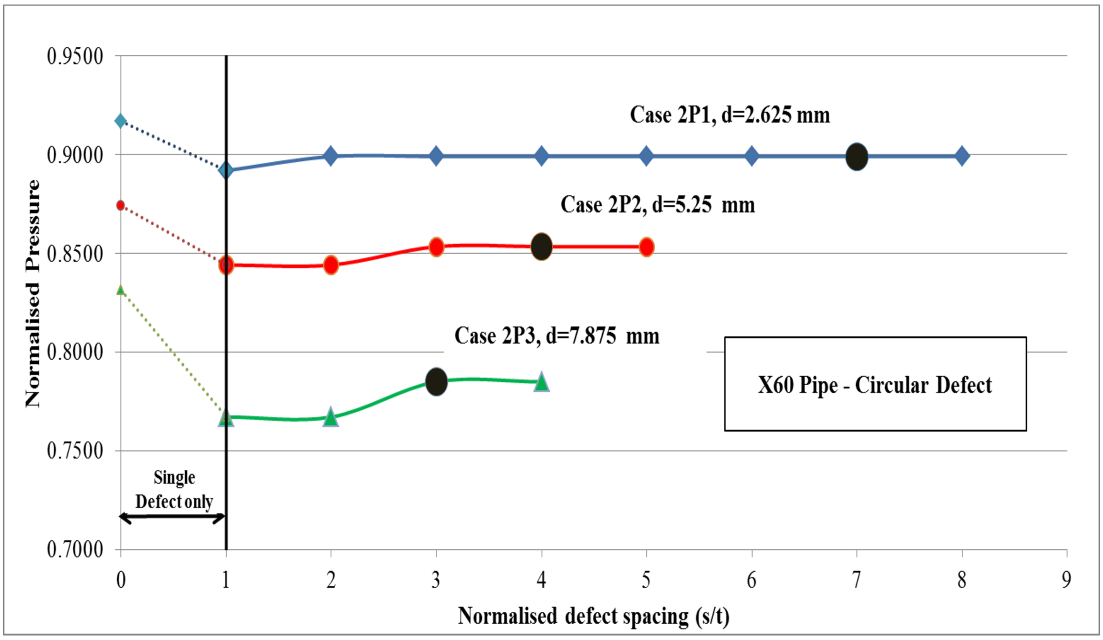

Figure 7-6: Normalised pressure vs spacing for X60 pipe circular defects with various defect depths (Note: dark circles denote last interaction spacing)

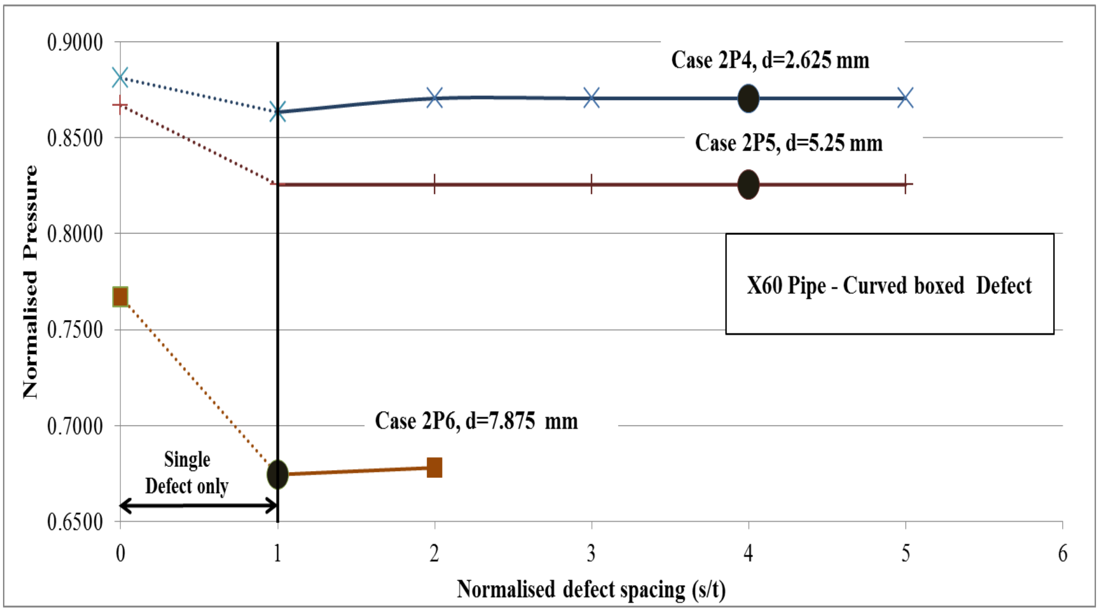

Figure 7-7: Normalised pressure vs spacing for X60 pipe curved box defects with various defect depths (Note: dark circles denote last interaction spacing)

The generalised equation (7.1) is utilised to predict the failure pressure for the defects with the variable depth parameter. The y variable in the equation for this case relates to the defect depth variation (normalised by dividing the defect depth with the pipe wall thickness, i.e. y=d/t) and the coefficient for the circular and the curved box defects are listed below:

Table 7.3: Correction factors for the failure pressure prediction of the defects depth parameter of X60 material

Coefficients	Circular defect	Curved boxed defect
P00	0.9242	0.7942
P10	0.0005924	0.006211
P01	-0.007929	0.04569
P20	-0.0002717	-0.0006413
P11	0.0008932	-0.0004033
P02	-0.001656	-0.007754

Random cases were devised to test the validity of the results obtained from the proposed generalised equation for intermediate values of the parameters, which are then compared to the corresponding FE solutions as shown in Table 7.4. The percentage difference among the cases from 1 to 3 is -0.31, 0.27 and 0.23 respectively. The outcome shows that the generalised equation proposed can be used with high confidence for the particular cases listed in this study.

Table 7.4: Values of normalised pressure obtained analytically vs those obtained from FE analysis

No	Material True UTS (MPa)	D (mm)	t (mm)	d (mm)	DL (mm)	Defects Types	P_n from formulae	P_n from FEA
1	678	254	10.5	4.2	35	CR	0.8693	0.8720
2	678	254	10.5	4.2	35	CB	0.8558	0.8534
3	678	254	10.5	6.3	35	CR	0.8145	0.8163
Average percentage difference (%)							0.27	

7.4 Effect of Outside Diameter

Three pipes' outside diameters of 254 mm, 508 mm and 762 mm were studied. All the pipes in this case have a fixed pipe thickness of 10.5 mm, defect length of 35 mm and defect depth of 5.25 mm (50%). Figure 7-8 and Figure 7-9 show the outcome of the analysis for both circular and curved boxed defects. It is observed that the higher the external diameter size, the more spacing it takes for defects to interact. For circular defects, interaction is possible up to 4t for the 254 mm (10 inch) size pipe, while it is 6t for the 762 mm (30 inch) size pipe. There was no change in spacing between the 254 mm and 508 mm pipe sizes. As expected and in line with the thin pipe failure theory (Barlow's formula), a lower pressure of failure is seen as the outside diameter increases from 254 mm to 762 mm. It is worth noting that the effect of the shape of defects with respect to the change of pipe outer diameter size is negligible.

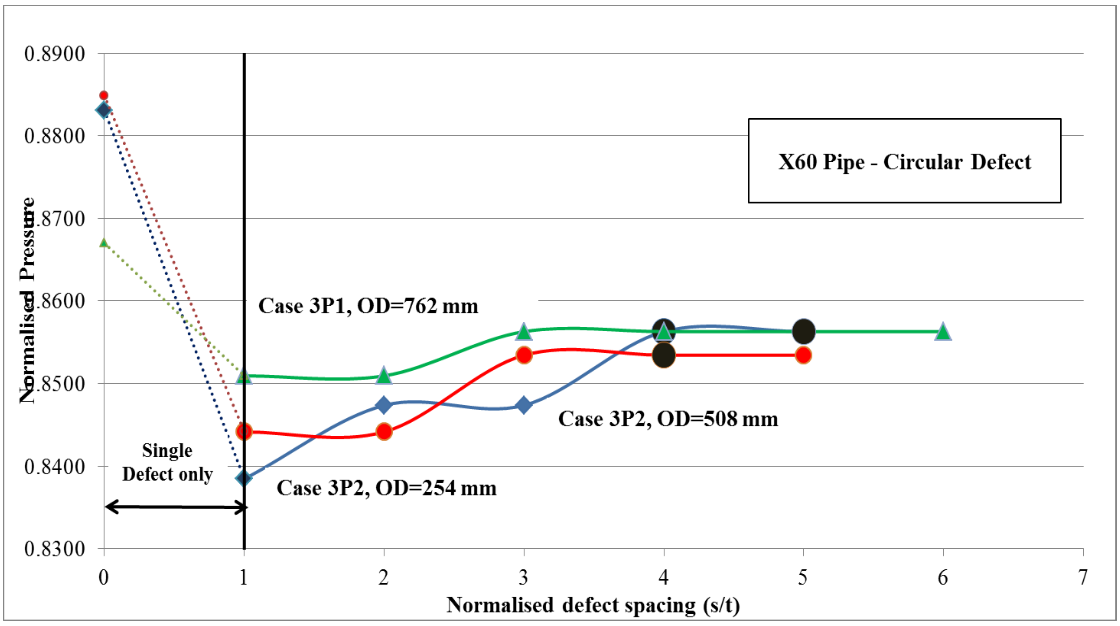

Figure 7-8: Normalised pressure vs spacing for X60 pipe circular defects with various external diameters (Note: dark circles denote last interaction spacing)

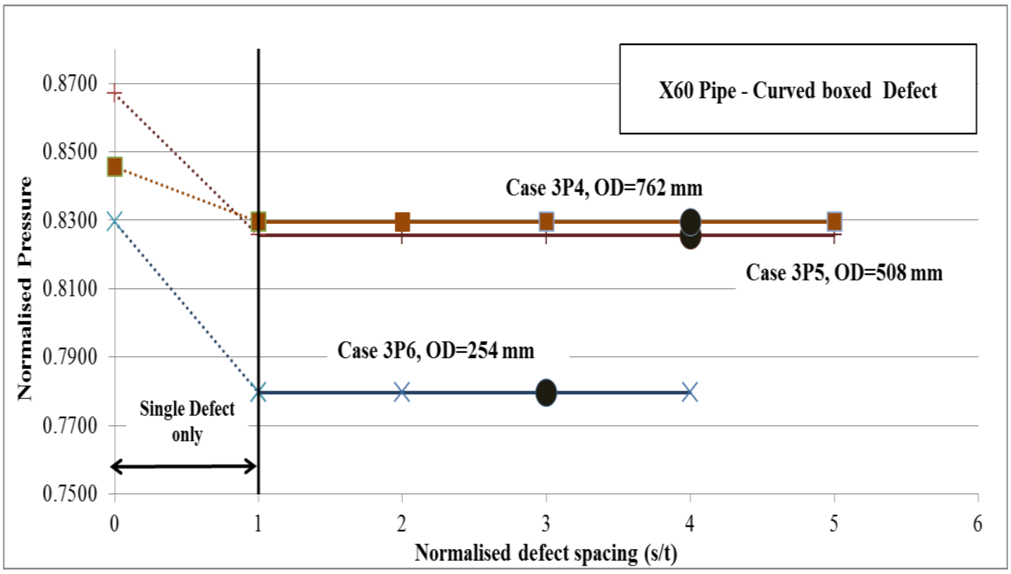

Figure 7-9: Normalised pressure vs spacing for X60 pipe curved boxed defects with various external diameters (Note: dark circles denote last interaction spacing)

The generalised equation (7.1) is utilised again to predict the failure pressure for the defects with the variable depth parameter. The y variable in the equation for this case relates to the outside diameter variation (normalised by dividing the pipe outside diameter with the pipe wall thickness, i.e. D/t) and the coefficients for the circular and boxed defects are listed in Table 7.5.

Table 7.5: Correction factors for the failure pressure prediction of the pipe external diameter parameter of X60 material

Coefficients	Circular defect	Curved boxed defect
P00	0.8321	0.6928
P10	0.0086	0.0023
P01	-5.33E-05	0.0043
P20	-4.81E-04	1.53E-04
P11	-5.60E-05	-5.01E-05
P02	3.38E-06	-3.31E-05

7.5 Effect of Pipe Wall Thickness

Figure 7-10 and Figure 7-11 show the outcome of the parametric study concerning the variation in wall thicknesses for both of the shapes studied, circular and curved boxed defects. It was observed that interaction space between defects tends to decrease as the pipe wall thickness increases which could be attributed to the higher stiffness which needs to be overcome by the internal pipe pressure. Both shapes of defects cease to interact at a spacing of 5t. Circular defects at lower wall thicknesses tend to interact at a higher spacing than those of curved boxed defect shapes. In general, defects spaced in the lower wall thicknesses tend to interact at more spacing distances than those with higher thicknesses. The data presented in Figure 7-10 and Figure 7-11 have a pipe outer diameter of 508mm, defect length of 35mm, defect depth of 5.25mm (50%) for X60.

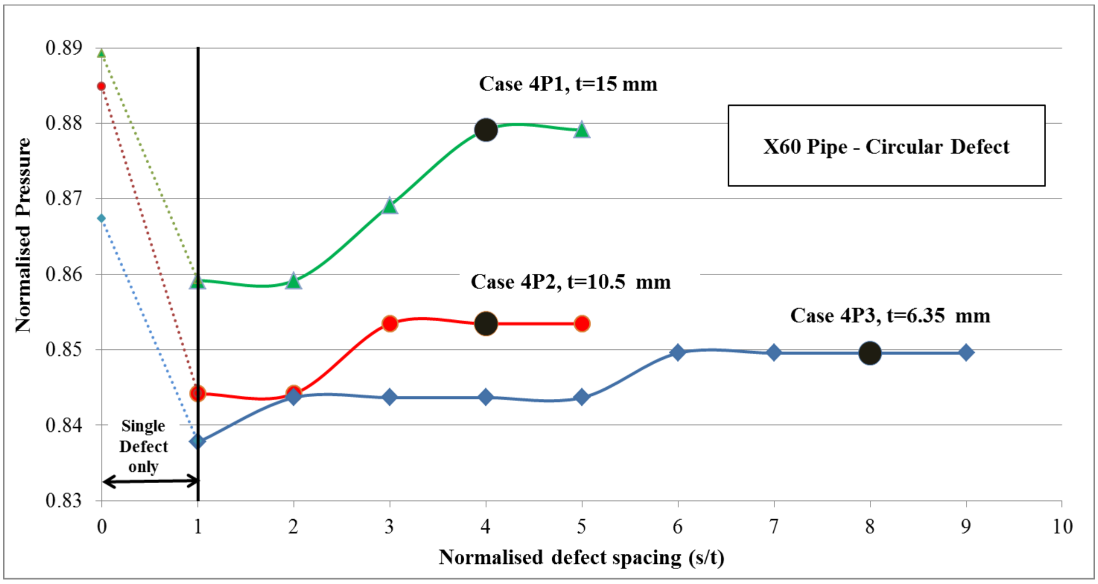

Figure 7-10: Normalised pressure vs spacing for X60 pipe circular defects with various pipe wall thicknesses (Note: dark circles denote last interaction spacing)

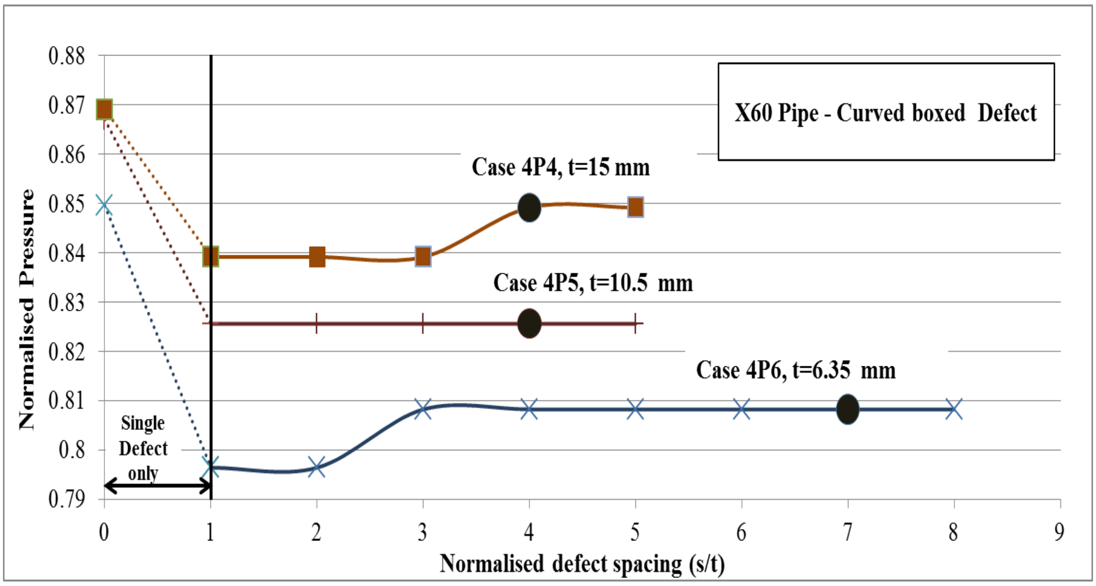

Figure 7-11: Normalised pressure vs spacing for X60 pipe curved boxed defects with various pipe wall thicknesses (Note: dark circles denote last interaction spacing)

The generalised equation (7.1) is utilised again to predict the failure pressure for the defects with the variable depth parameter. The y variable in the equation for this case relates to the pipe wall thickness variation (normalised by dividing the outside pipe diameter with the variable pipe wall thickness, i.e. D/t) and the coefficients for the circular and boxed defects are listed in Table 7.6.

Table 7.6: Correction factors for the failure pressure prediction of the pipe wall thicknesses parameter of X60 material

Coefficients	Circular defect	Curved boxed defect
P00	0.9308	0.8967
P10	0.0082	0.0030
P01	-0.0031	-0.0022
P20	-8.59E-05	-3.37E-04
P11	-7.54E-05	1.92E-05
P02	2.44E-05	1.09E-05

7.6 Effect of Multiple Variables

A failure pressure for the assessment of both single and interacting defects can be further predicted taking into considerations multiple variables similar to the ones stated in Table 7.1. An equation based on curve fitting can then be obtained for future references.

7.7 Effect of Touching Defects

A pair of almost touching curved boxed defects were analysed and compared with a single defect having the same length and width of the touching defects. The details of the two cases are shown in Table 7.7. The results show that the two defects fail within the same failure pressure of that for the lengthier defect indicating that the pair of defects acted as single defect.

Table 7.7 Impact of joint defect vs single long defect

No	Mat.	D (mm)	t (mm)	d (mm)	DL (mm)	DW (mm)	S_n	Defect type	P_f (MPa)
1	X60	508	10.5	4.75	70	35	0	CB	22.6
2	X60	508	10.5	4.75	35	35	10^{-4}	CB	22.6

The FE mesh and stress contours of the two cases are shown in Figure 7-13 and Figure 7-12. It is important to state that the size and through thickness elements in both models were the same.

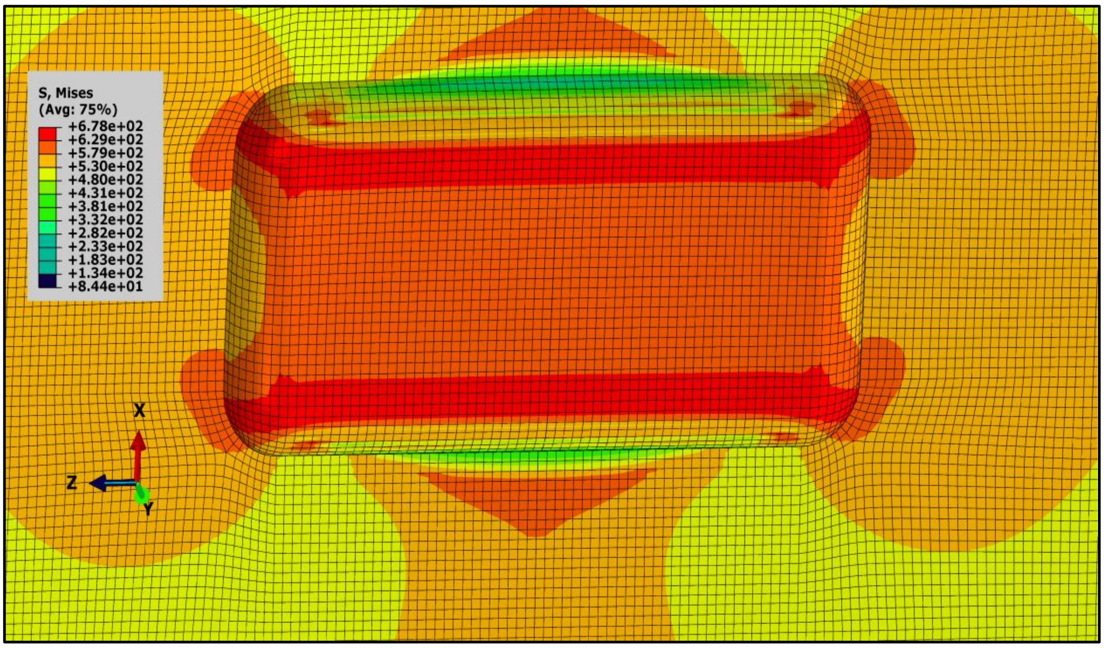

Figure 7-12: FE Mesh and stress contour of the single long defect

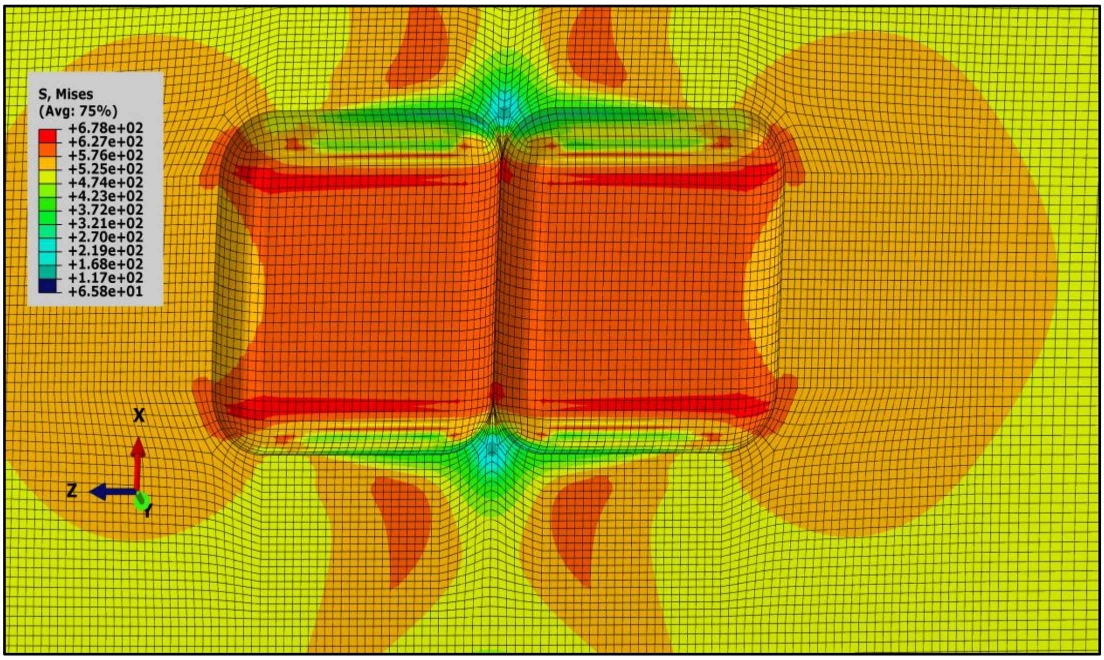

Figure 7-13: FE Mesh and stress contour of two joint defects

7.8 Effect of internal vs external surface defects

As stated in Chapter 5, the defects considered in the experimental work were all manufactured on the external surface as it was more practical to make. This section of the parametric study looks at the impact of failure pressure of both internal and external defects for single and interacting defects. In order to have a comparable result, the type and both surface and through thickness elements were the same for all of numerical models as depicted in Figure 7-14 for single defects and Figure 7-15 for interacting defects. Pipes and defect dimensions are listed in Table 7.8.

Table 7.8: Pipes and defects details

No	Mat.	D (mm)	t (mm)	d (mm)	Radius (mm)	S_n	Defect type	Defect Location	P_f (MPa)
1	X60	508	10.5	4.75	35	0	CR	External	25.7
2	X60	508	10.5	4.75	35	1	CR	External	23.7
3	X60	508	10.5	4.75	35	0	CR	Internal	25.7
4	X60	508	10.5	4.75	35	1	CR	Internal	23.9

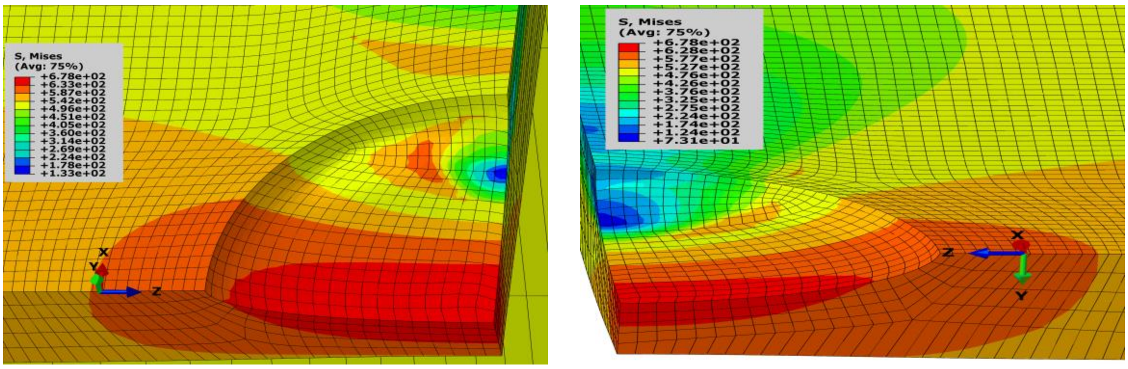

Figure 7-14: FE mesh for single external defect (left) and internal defect (right)

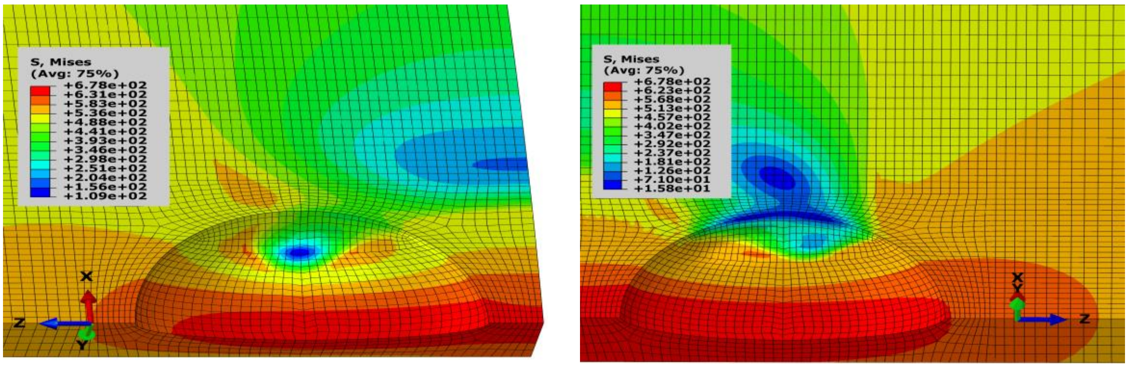

Figure 7-15: FE mesh for 1t interacting external defects (left) and internal defects (right)

Both of the single defects failed at the same failure pressure, though it is noticed in Figure 7-16 that there was a delay in the yield for the internal defect.

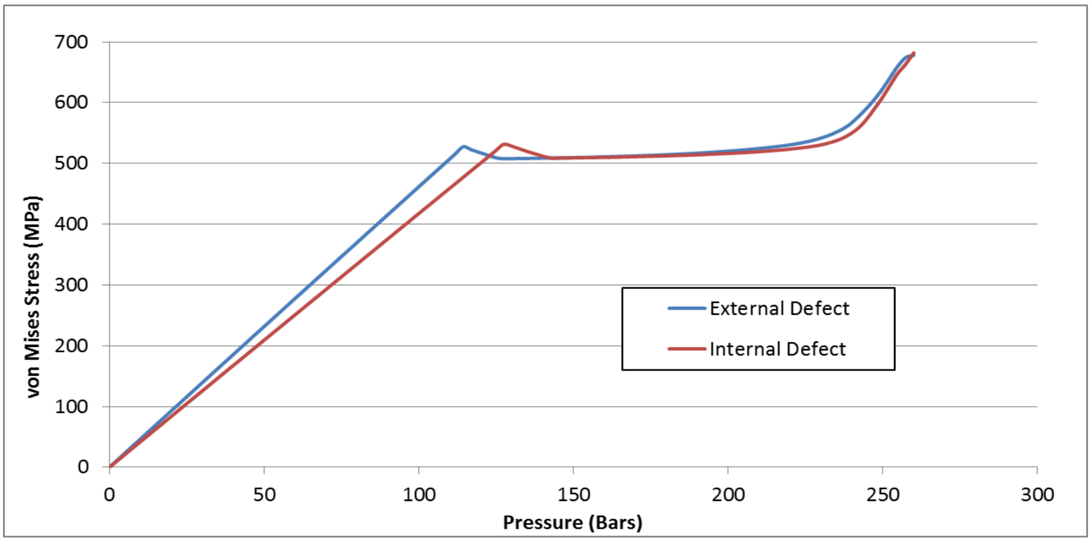

Figure 7-16: von Mises vs pressure for both internal and external single defects (values taken at centre of defect)

As shown in Table 7.8, for the defects spaced by 1t, the failure pressure differed by only 1%. The analysis performed on the failure pressure of both internal and external defects shows that both were having nearly the same failure pressure which indicates that modelling of the defects whether internal or external has negligible impact on the outcome.

7.9 Determination of Interaction Space for Diagonally Oriented Curved Boxed Defects

The experimental burst tests were carried out on circular defects oriented in the diagonal orientation without further testing of curved boxed defects, hence this parametric study. Table 7.9 below shows two pipe materials which were analysed to investigate the space where defects could potentially interact at. In order to produce comparable results, the type and both surface and through thickness elements were the same for the two numerical models as depicted in Figure 7-17 and Figure 7-18.

Table 7.9: Determination of interaction space for diagonally oriented curved boxed defects

No	Mat.	D (mm)	t (mm)	d (mm)	DL & DW (mm)	S_n	Defect type	P_f (MPa)	Defects interaction (Yes/No)
1	X52	508	9.5	4.75	35	1	CB	17.0	Yes
2	X52	508	9.5	4.75	35	2	CB	17.4	No
3	X60	508	9.5	4.75	35	1	CB	19.1	Yes
4	X60	508	9.5	4.75	35	2	CB	19.5	No

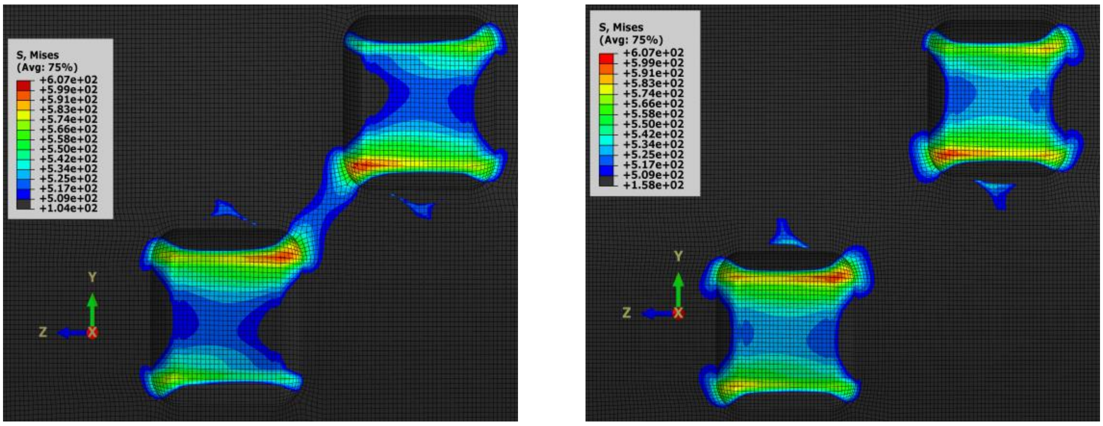

Figure 7-17: Stress contour for the X52 diagonal defects, spaced by 1t (left) and by 2t space (right)

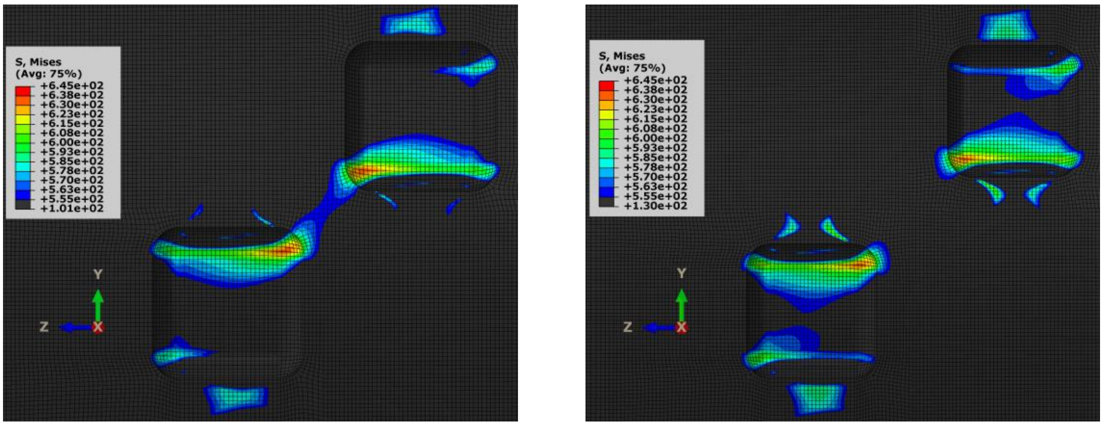

Figure 7-18: Stress contour for the X60 diagonal defects, spaced by 1t (left) and by 2t space (right)

The stress contours at the ligament between the two defects fall between the engineering UTS and the true UTS which gives a clear indication of defect interaction. The cases with 2t spacing are depicted in the right side of the figures above where it can be clearly seen that the stress contours were not merging, hence the stoppage of the defect interaction. It was seen from the experimental as well as the numerical cases for the circular defects that interaction in the diagonal oriental ceases to occur after 0.5t whereas it can be seen from this study, considering two materials, that interaction for the curved boxed defects is taking place up to and including 1t of spacing which could be attributed to the shape of defect where stress concentration builds up at the corner which allows the stress to increase more rapidly from one defect corner to the other.

7.10 Conclusion

The parametric study results presented in this chapter provide good evidence that FE analysis can be used when utilising the failure criteria presented in chapter 4 to give good prediction of the failure pressure of single and interacting defects. From this work, a generalised formula which takes into account the specific pipe parameters (wall thickness, diameter, material properties) to produce a predicted failure pressure with different defect dimensions can be developed. Although there is a distinct difference between the critical interaction spacing between defects in the variables studied, the difference in the predicted failure pressure for defects remains within less than 10%. Defects that are in contact (touching defects) tend to fail within the same failure pressure as a single lengthier defect. It can be stated that internal and external defects assessed under the same conditions will have similar failure pressures.

CHAPTER 8: CONCLUSIONS AND FUTURE WORK

8.1 General Brief

Carbon steel pipes remain the safest and most reliable means of transporting oil and gas throughout the world. Despite having such a good reputation and existence of maintenance programs to safeguard their integrity, these pipes tend to corrode either internally or externally. Once metal loss takes place, assessment of their magnitude and effect has to be carried out. Metal loss assessment has been done conservatively, with varying degrees of conservatism depending on the method and code used and FE analysis has been widely used to give more accurate results when compared to the experimental data. The main objective of this research work has been the analysis of metal loss defects in pipes with the aim of providing the safe working pressure, describing the defect interaction behaviour and addressing the conflicting defect spacing criteria currently in use. This objective has been accomplished by executing a comprehensive experimental program which has not only given means of comparing the existing analytical methods but also paves the way for better prediction of defects interaction (spacing) criteria.

It is generally concluded from this research work that there are various parameters which influence the critical spacing between defects including the pipe materials, pipe outside dimeter, wall thickness as well as the defect's shape, length, depth and orientation. The values of spacing obtained when considering these parameters were very different from the spacing values provided by ASME B31G, POF as well as DNV RP F101. The failure criteria proposed in this study also differ from previous works which was based on a single node reaching the maximum true UTS as the one proposed in this work takes into account the full ligament through thickness and between defects, which is considered much less sensitive to the local FE mesh refinement around the defect region. A general process described in this research work, starting from defining the failure criteria and ending with a parametric study can provide an accurate assessment of the spacing criterion. However, a fixed rule for all defects cannot be made due to the fact that there are infinite possibilities of defect dimensions and various pipe geometries and properties.

8.2 Experimental Work Concluding Remarks

In an effort to fill the gap due to insufficient experimental data that can be used to benchmark thin-wall pipe defect interaction criteria, the author has embarked on an extensive testing program to enhance the knowledge base of test results for reference to future studies and provide further knowledge in the development of predictive capabilities of the burst pressure of interacting defects in thin-wall pipes. In total, there were 31 pipes used in the experimental work. All the pipes were sourced from pipe stocks representing actual operational pipes used in the oil and gas industry and of material grades which are commonly used. The experimental programme was conducted using two types of ductile carbon steel; API 5L X52 and X60 with various wall thicknesses. The tests were conducted using different shapes of defects as well as in different orientations. The experimental test programme showed negligible effects of interaction in the hoop and diagonal orientations and with variable interaction spacings for the longitudinally oriented defects.

The burst pipe failure results were compared using both analytical and numerical methods. The percentage differences seen when using ASME B31G for single defects and when using the modified B31G were 21% and 15% respectively. While the percentage differences seen for DNV RP F101 single and interacting defects were 10% and 16% respectively. Using FE analysis gave the most accurate results with a difference of only 2% from the experimental results.

8.3 Parametric Study Concluding Remarks

One of the objectives set for the research work presented in this thesis is to create additional results through validated FE numerical models after careful calibration with the experimental data. The numerical modelling was performed to set up the basis for a parametric study so that more parameters can be investigated. The initial work started at an early stage of the research where literature data was used to test and validate the numerical models built for this work achieving results within 5% of those published in literature. Mesh sensitivity studies, looking at different element types and distributions across the wall thickness, were conducted to arrive at accurate results. Continuum 3D hexahedron 20 node quadratic reduced integration elements were chosen for the FE analyses with 3 or more elements across the wall thickness.

As stated in the previous section, the validation of the burst pipe failure pressures using the FE models used in this work gave the most accurate results. Good agreement was obtained between the strain gauge data from the experimental work and those obtained from the FE analysis. A case with and without axial load was also tested where the outcome shows that there is a negligible difference between the results obtained. This has given a good confidence level in the FE failure criterion developed in this study, and also the parametric study which was performed at a later stage in the research project.

A generalised formula was developed from the failure criteria and the FE models to produce a failure pressure associated with different defect spacings. It was concluded from the parametric study that defects which are in contact with each other (touching defects) tend to fail with the same failure pressure as of that of single lengthier defect in the axial direction. Analysis of internal and external defects assessed under the same conditions revealed that they tend to have similar failure pressures.

8.4 Research Study Contributions and Recommendations

The experimental, numerical and parametric studies conducted in this research project have yielded important findings that aid in the understanding and further development of pipe defect assessments methodology.

The following are key contributions and recommendations:

- For the first time, failure criteria that take into account both single and interacting defects based on experimental and numerical validated cases has been developed in this research work and recommended to be used in future studies and practical applications.
- It is recommended for industry to follow the parametric work presented in Chapter 7 by creating critical spacing and failure pressure maps for each of the pipes they operate. Such effort will reduce the work on the subsequent actions such as pressure de-rating, repair and replacement once defects are found and quantified. Additionally, the identification of critical spacing can be logged into the inspection tools and subsequent failure pressures can be deduced from similar equations presented in Chapter 7.
- FE Analysis has provided a good tool in the study of defect assessments and in particular for deducing the critical spacing between defects to be considered interacting.

- Critical operated pipes where repair actions have high economic consequences should be evaluated using numerical methods when it comes to the case of defect interaction.
- Analytical methods can be still used for defect assessments recognizing that these will always give a quick and conservative prediction.

8.5 Future Work

The following studies are suggested for future work:-

- Residual stress effects on the failure pressure of interacting defects need to be investigated in both seamless and seamed pipes. Carrying out such investigations will reveal the differences in failure pressure as well as the critical spacing in these two types of pipes.
- Experimental and numerical validations similar to those presented in this research work need to be repeated for higher strength steels, such as API 5L X100.
- Defect interaction of various complex shapes should be studied in order to gain further understanding of the failure behaviour as well as the spacing criterion. Complex shaped defects include defects that have varying depths within each single defect.
- Fracture mechanics and crack propagation studies are needed to look at the influence of interacting defect spacing on crack growth. Remaining life assessment studies are also required for the combined effects of corrosion and crack growth.
- Integrity assessments, similar to the research work presented in this study, are required to focus on interacting defects at the pipe weld regions.

REFERENCES

1. Pipeline-Operator-Forum, *Specifications and requirements for intelligent pig inspection of pipelines*. 2009.
2. NTSB, *Integrity Management of Gas Transmission Pipelines in High Consequence Areas*. 2015, National Transportation Safety Board: Washingon, DC, USA.
3. Kiefner, J., Maxey, W., Eiber, R., and Duffy, A., *Failure Stress Levels of Flaws in Pressurized Cylinders*. 1973, ASTM: USA. p. 461-481.
4. Shannon, R.W.E., *The failure behaviour of line pipe defects.* International Journal of Pressure Vessels and Piping, 1974. **2**(4): p. 243-255.
5. Kiefner, J. and Vieth, P., *New method corrects criterion for evaluating corroded pipe.* Oil and Gas Journal, 1990. **8**.
6. ASME, A.S.o.M.E., *Manual for Determining the Remaining Strength of Corroded Pipelines*. 2009, ASME: USA.
7. Kirkwood, M., Fu, B., Vu, D., and Batte, A. *Assessing the Integrity of Corroded Linepipe-An Industry Initiative*. in *Aspect'96: Advances in Subsea Pipeline Engineering and Technology*. 1996. Society of Underwater Technology.
8. Chouchaoui, B.A. and Pick, R.J., *Behaviour of longitudinally aligned corrosion pits.* International Journal of Pressure Vessels and Piping, 1996. **67**(1): p. 18.
9. Bjornoy, O.H., Sigurdsson, G., and Marley, M.J. *Background and Development of DNV-RP-F101 "Corroded Pipelines"*. in *Proceedings of the Eleventh (2001) International Offshore and Polar Engineering Conference*. 2001. Stavanger, Norway.
10. Cosham, A. and Hopkins, P. *Pipeline Defect Assessment Manual PDAM*. in *International Pipeline Conference*. 2002. Calgary, Alberta, Canada.
11. Benjamin, A.C. and Andrade, E.Q.d. *Predicting the failure pressure of pipelines containing nonuniform depth of corrosion defects using FEA*. in *Proceedings of OMAE’03: 22nd International Conference on Offshore Mechanics and Arctic Engineering*. 2003. Cancun, Mexico.
12. Netto, T.A., Ferraz, U.S., and Botto, A., *On the effect of corrosion defects on the collapse pressure of pipelines.* International Journal of Solids and Structures, 2007. **44**(22-23): p. 7597-7614.
13. Kim, J.W., Park, C.Y., and Lee, S.H., *Local Failure Criteria for Wall-Thinning Defect in Piping Components based on Simulated Specimen and Real-Scale Pipe*

Tests, in *20th International Conference on Structural Mechanics in Reactor Technology (SMiRT 20)* 2009: Espoo, Finland.

14. Belachew, C.T., Ismail, M.C., and Karuppanan, S., *Burst Strength Analysis of Corroded Pipelines by Finite Element Method.* J. Applied Sci., 2011. **11**: p. 1845-1850.
15. Hosseini, A., Cronin, D.S., and Plumtree, A., *Crack in Corrosion Defect Assessment in Transmission Pipelines.* Journal of Pressure Vessel Technology, 2013. **135**: p. 8.
16. Abdalla Filho, J.E., Machado, R.D., Bertin, R.J., and Valentini, M.D., *On the failure pressure of pipelines containing wall reduction and isolated pit corrosion defects.* Computers & Structures, 2014. **132**(0): p. 22-33.
17. ASME, A.S.o.M.E., *Manual for Determining the Remaining Strength of Corroded Pipelines*. 2012, ASME: USA.
18. DNV, *DNV-RP-F101: Corroded Pipeline* 2010: Norway.
19. Xu, L.Y. and Cheng, Y.F., *Development of a finite element model for simulation and prediction of mechanoelectrochemical effect of pipeline corrosion.* Corrosion Science, 2013. **73**: p. 150-160.
20. Fekete, G. and Varga, L., *The effect of the width to length ratios of corrosion defects on the burst pressures of transmission pipelines.* Engineering Failure Analysis, 2012. **21**: p. 21-30.
21. Chauhan, V., Swankie, T.D., Espiner, R., and Wood, I. *Developments in Methods for Assessing the Remaining Strength of corroded pipelines*. in *NACE CORROSION 2009*. 2009. Atlanta, GA: NACE International.
22. Cosham, A. and Hopkins, P., *The Assessment of Corrosion in Pipelines guidance in the Pipeline Defect Assessment Manual*, in *Pipeline Pigging and Integrity Management Conference*. 2004: Amsterdam, The Netherlands.
23. Ma, B., Shuai, J., Liu, D., and Xu, K., *Assessment on failure pressure of high strength pipeline with corrosion defects.* Engineering Failure Analysis, 2013. **32**: p. 209-219.
24. Hosseini, S.A., *Crack in Corrsion Flaw Assessment in Thin-Walled Pipe*, in *Mechanical Engineering*. 2014, University of Waterloo: Waterloo, Canada.
25. Mok, D.R.B., Pick, R.J., and Glover, A.G., *Behavior of Line Pipe With Long External Corrosion.* Material Performance, 1990. **29**(5): p. 75-79.

26. Freire José, L.F., Vieira Ronaldo, D., Fontes Pablo, M., Benjamin Adilson, C., Murillo Luis, S., and Miranda Antonio, C., *The Critical Path Method for Assessment of Pipelines With Metal Loss Defects.* Journal of Pipeline Engineering, 2013. **12**(2): p. 14.
27. JFE, *JFE Speciality Pipe and Tube for Boiler and Petrochemical Plant*. 2008: Japan.
28. TATA-Steel, *High Frequency Induction (HFI) Welded Pipe*, Steel, T., Editor. 2012: UK.
29. Tsuru, E., Nagata, Y., Shinohara, Y., Agata, J., and Shirakami, S., *Forming and Buckling Simulation on High-strength UOE Pipe with Plastic Anisotropy*. 2013, Nippon Plate, Pipe, Tube & Shape Research Lab., Steel Research Laboratories.: Japan.
30. TATA-Steel, *TATA UOE Douple Submerged Arc Welded (DSAW) Pipe*. 2012: UK.
31. NPV, *Nippon Steel HSAW pipe* LTD, N.S.a.S.P.V.C., Editor. 2014.
32. Al-Anezi, M. and Rao, S., *Failures by SOHIC in Sour Hydrocarbon Service.* Journal of Failure Analysis and Prevention, 2011. **11**(4): p. 8.
33. Baker, M. and Fessler, R.R., *Pipeline Corrsion - Final Report*, Transportation, U.S.D.o., Administration, P.a.H.M.S., and Safety, O.o.P., Editors. 2008: USA.
34. Ilman, M.N. and Kusmono, *Analysis of internal corrosion in subsea oil pipeline.* Case Studies in Engineering Failure Analysis, 2014. **2**(1): p. 1-8.
35. (ASME), T.A.S.O.M.E., *ASME B31.8S - Managing System Integrity of Gas Pipelines*. 2010: USA.
36. Findley, K.O., O'Brien, M.K., and Nako, H., *Critical assessment 19: mechanisms of hydrogen induced cracking in pipeline steels.* Materials Science and Technology, 2016. **32**(1): p. 1-8.
37. Cameron, N.B., *Recommended practice for magnetic flux leakage inspection of atmospheric storage tank floors*, Executives, H., Editor. 2006, HSE executives: UK.
38. Barbian, A., M. Beller, M., Niese, F., Thielager, N., and Willems, H. *New Multi-Technology In-Line Inspection Tool For the Quantitative Wall Thickness Measurement of Gas Pipelines*. in *Pipeline Technology Conference*. 2008. Hannover, Germany.
39. Beller, M., *Pipeline Inspection Utilizing Ultransound Technology-On The Issue of Resolution*. 2007.

40. Motta, R.d.S., Afonso, S.M.B., Willmersdorf, R.B., Paulo R. M. Lyra, and Andrade, E.Q.d., *Automatic Modeling And Analysis Of Pipelines With Colonies Of Corrosion Defects.* Mecánica Computacional, 2010. **XXIX**: p. 7871-7890.

41. ASME, *ASME B31G: Manual for Determining the Remaining Strength of Corroded Pipelines*. 2009: USA.

42. Chiodo, M.S.G. and Ruggieri, C., *Failure assessments of corroded pipelines with axial defects using stress-based criteria: Numerical studies and verification analyses.* International Journal of Pressure Vessels and Piping, 2009. **86**(2-3): p. 164-176.

43. Lamontagne, M. *Interaction rules - An integral factor*. in *Corrosion 2002*. 2002. USA: NACE.

44. Chauhan, V. and Brister, J., *A Review of Methods for Assessing the Remaining Strength of Corroded Pipelines*, Transportation, U.D.o., Editor. 2009: USA.

45. Cronin, D., *Assessment of Corrosion Defects in Pipelines*, in *Mechanical Engineering*. 2000, The University of Waterloo: Waterloo, Ontario, Canada. p. 309.

46. Tomasz, S., *The Finite Element Method Analysis for Assessing the Remaining Strength of Corroded Oil Field Casing and Tubing*, in *Faculty of earth sciences geotechnical and mining*. 2006, The Technical University of Freiberg: Germany.

47. Cronin, D. and Pick, R., *Prediction of the failure pressure for complex corrosion defects.* International Journal of Pressure Vessels and Piping, 2002. **79**(4): p. 8.

48. Kim, J.W., Park, C.Y., and Lee, S.H. *Local failure criteria for defects in piping based on simulated specimen and real scale pipe tests*. in *20th International Conference on Structural Mechanics in Reactor Technology*. 2009. Espoo, Finland.

49. Su, C.-l., Li, X., and Zhou, J., *Failure pressure analysis of corroded moderate-to-high strength pipelines.* China Ocean Engineering, 2016. **30**(1): p. 69-82.

50. Bedairi, B., Cronin, D., Hosseini, A., and Plumtree, A., *Failure prediction for Crack-in-Corrosion defects in natural gas transmission pipelines.* International Journal of Pressure Vessels and Piping, 2012. **96-97**: p. 90-99.

51. Abaqus(V.6.14), *Abaqus Documentation*. 2015, Dassault Systèmes: Providence, RI, USA.

52. Chauhan, V. and Sloterdijk, W. *Advances in interaction rules for corrosion defects in pipelines*. in *Proceedings of the International Gas Research Conference* 2004. Vancouver, Canada.

53. Cronin, D.S. and Pick, R.J. *Experimental Database for Corroded Pipe: Evaluation of RSTRENG and B31G*. in *PROCEEDINGS OF THE INTERNATIONAL PIPELINE CONFERENCE*. 2000.

54. Ma, B., Shuai, J., Wang, J., and Han, K., *Analysis on the Latest Assessment Criteria of ASME B31G-2009 for the Remaining Strength of Corroded Pipelines.* Journal of Failure Analysis and Prevention, 2011. **11**(6): p. 666-671.

55. Withers, P.J., *Residual stress and its role in failure.* Reports on Progress in Physics, 2007. **70**(12): p. 2211-2264.

56. ECRS. *9th European conference on residual stresses*. 2014; Available from: http://ecrs9.utt.fr/.

57. Law, M., Prask, H., Luzin, V., and Gnaeupel-Herold, T., *Residual stress measurements in coil, linepipe and girth welded pipe.* Materials Science and Engineering: A, 2006. **437**(1): p. 60-63.

58. Chelette, K., Moore, P., Long, X., Scheel, J., Hornbach, D., and Prevey, P. *Management of Residual Stress: An Emerging Technology for Oil Industry Tubular Products*. in *Offshore Technology Conference*. 2011. Rio de Janeiro, Brazil.

59. Kandil, F.A., Lord, D.J., Fry, A.T., and Laboratory, N.P., *A Review of Residual Stress Measurement Methods: A Guide to Technique Selection*. 2001: National Physical Laboratory.

60. Lu, J., *Prestress Engineering of Structural Material: A Global Design Approach to the Residual Stress Problem*, in *Handbook of Residual Stress and Deformation of Steel*, Totten, G., Howes, M., and Inoue, T., Editors. 2002. p. 16-31.

61. Been, J., King, F., and Sutherby, R., *Environmentally assisted cracking of pipeline steels in near-neutral pH environments*, in *Environment-Induced Cracking of Materials*, Shipilov, S.J., Russell Olive, Jean-Marc Rebak, Raúl Editor. 2008.

62. Liu, J., Zhang, Z.L., and Nyhus, B., *Residual stress induced crack tip constraint.* Engineering Fracture Mechanics, 2008. **75**(14): p. 4151-4166.

63. Sekar, C., Sivagnanam, M., and Preethi, M., *Effect of heat treatment method in minimizing the residual stress level in Cold Drawn Welded Tubes*.

64. Aleshin, V., Kobyakov, V., and Seleznev, V., *A Simulation Technology for a Full Cycle of Steel Line Pipe Manufacturing Operations.* Advances in Mechanical Engineering, 2011. **2011**.

65. ASME, *ASME B31.4: Pipeline Transportation Systems for Liquid Hydrocarbons and Other Liquids*. 2009: New York, USA.

66. Creo-2.0, *Creo 2.0 Academic Edition* 2013, PTC: USA.
67. ISO, *ISO 3183: Petroleum and natural gas industries - Steel pipe for pipeline transportation systems* 2012.
68. Kiefner, J. and Trench, C., *Oil Pipeline Characteristics and Risk Factors: Illustrations from the Decade of Construction*. 2001, American Petroleum Institute.
69. Davis, J., *Tensile Testing, 2nd Edition*. 2004: ASM International.
70. Becker, A.A., *An Introductory Guide to Finite Element Analysis*. 2003, London: Wiley.
71. Hellen, T.K. and Becker, A.A., *Finite Element Analysis for Engineers-A Primer*. 2013, Glasgow: NAFEMS.
72. Zhang, J., Liang, Z., and Han, C.J., *Effects of Ellipsoidal Corrosion Defects on Failure Pressure of Corroded Pipelines Based on Finite Element Analysis.* International Journal of Electrochem Science, 2015. **10**: p. 5036 - 5047.
73. Karuppanan, S., Wahab, A.A., Patel, S., and Zahari, M.A., *Estimation of Burst Pressure of Corroded Pipeline Using Finite Element Analysis (FEA).* Advanced Materials Research, 2014. **879**: p. 191-198.
74. Netto, T.A., Ferraz, U.S., and Estefen, S.F., *The effect of corrosion defects on the burst pressure of pipelines.* Journal of Constructional Steel Reserach, 2005. **61**: p. 1185-1204.
75. Dick, I. and Inegiyemiema, M., *Predicting the Structural Response of a Corroded Pipeline Using Finite Element (FE) Analysis.* International Journal of Scientific & Engineering Research, 2014. **5**(11).
76. Al-Owaisi, S.S., Becker, A.A., and Sun, W., *Analysis of shape and location effects of closely spaced metal loss defects in pressurised pipes.* Engineering Failure Analysis, 2016. **68**: p. 172-186.
77. Fu, B. and Kirkwood, M., *Predicting failure pressure of internally corroded linepipe using the finite element method*, in *International conference on offshore mechanics and arctic engineering*. 1995, American Society of Mechanical Engineers, New York, NY (United States): Copenhagen, Denmark.
78. Becker, A.A., *Practical Guidelines For Finite Element Applications*. 2013: The University of Nottingham, Nottingham, UK.
79. Chen, Y., Zhang, H., Zhang, J., Liu, X., Li, X., and Zhou, J., *Failure assessment of X80 pipeline with interacting corrosion defects.* Engineering Failure Analysis 2014.

80. ASME, *ASME B31.8: Gas Transmission and Distribution Piping Systems*. 2012: New York, USA.

81. Kim, J.H., Kim, M.H., and Choi, D.H., *Analysis and Depth Estimation of Complex Defects on the Underground Gas Pipelines.* Journal of Magnetics, 2013. **18**(2): p. 202-206.

82. Medjo, B., Rakin, M., Arsić, M., Šarkoćević, Z., Zrilić, M., and Putić, S., *Determination of the Load Carrying Capacity of Damaged Pipes Using Local Approach to Fracture.* MATERIALS TRANSACTIONS, 2012. **53**(1): p. 185-190.

83. Bedairi, B., *Numerical Failure Pressure Prediction of Crack-in-Corrosion Defects in Natural Gas Transmission Pipelines*, in *Mechanical Engineering*. 2010, University of Waterloo: Waterloo, Canada.

84. Diniz, J.L.C., Vieira, R.D., Castro, J.T., Benjamin, A.C., and Freire, J.L.F., *Stress and Strain Analysis of Pipelines with Localized Metal Loss.* Experimental Mechanics, 2006. **46**(6): p. 765-775.

Appendix A: Experimental Burst Test Photos & Details

1. Table of Experimental tests

Test Case No.	Pipe Details (All with OD of 508 mm)			Defect Type and Orientation CB = Curve Boxed CR = Circular		Actual. Defect Dimensions (mm)			Defect Spacing Xt(mm)	Failure Pressure (Bar)	Defects interaction (Yes/No/NA)
	Grade	Nom t (mm)	Actual t (mm)	Type	Orientation	Length (mm)	Width (mm)	Depth (mm)		Exp	Exp
1	X60	8.9	8.88	CB	Single	35	35	4.44	Single	195.40	NA
2	X60	8.9	8.88	CR	Single	34.1	34.1	4.44	Single	199.70	NA
3	X60	9.5	9.65	CR	Longitudinal	35.5	35.5	4.82	1t (9.65)	190.50	Yes
4	X60	9.5	9.61	CR	Longitudinal	35.4	35.4	4.8	2t (19.2)	193.50	Yes
5	X60	9.5	9.54	CB	Longitudinal	35	35	4.77	1t (9.54)	190.30	Yes
6	X60	9.5	9.54	CB	Longitudinal	35	35	4.77	2t (19.1)	196.10	Yes
7	X60	9.5	9.44	CB	Hoop	35	35	4.72	1t (9.44)	193.20	No
8	X60	9.5	9.58	CB	Hoop	35	35	4.79	2t (19.4)	195.00	No
9	X60	9.5	9.55	CR	Diagonal	35.3	35.3	4.77	1t (9.55)	196.20	No
10	X60	9.5	9.52	CR	Diagonal	35.2	35.2	4.76	2t (19.0)	193.80	No
11	X60	10.5	10.6	CR	Single	37.1	35.1	5.3	Single	246.70	NA
12	X60	10.5	10.7	CR	Longitudinal	37.2	37.2	5.39	3t (32.1)	241.70	Yes
13	X60	10.5	10.7	CR	Longitudinal	37.2	37.2	5.37	4t (42.6)	250.00	Yes
14	X60	10.5	10.65	CR	Longitudinal	37.2	37.2	5.44	5t (53.7)	243.20	No
15	X60	10.5	10.6	CB	Longitudinal	35	35	5.41	3t (32.1)	239.40	Yes
16	X60	10.5	10.7	CB	Longitudinal	35	35	5.39	4t (42.8)	238.40	Yes
17	X60	10.5	10.7	CB	Longitudinal	35.1	35.1	5.54	5t (53.5)	241.00	No
18	X52	9.5	9.7	CR	Single	35.5	33.9	4.87	Single	195.50	NA
19	X52	9.5	9.85	CR	Longitudinal	35	35	4.84	1t (9.90)	191.10	Yes
20	X52	9.5	9.7	CR	Longitudinal	35.5	33.5	4.88	4t (38.7)	195.90	No
21	X52	9.5	9.7	CR	Longitudinal	35.5	33.6	4.84	5t (48.7)	196.50	Yes
22	X52	9.5	9.75	CR	Longitudinal	35.8	33.6	4.9	6t (58.2)	200.80	Yes
23	X52	9.5	9.8	CR	Longitudinal	35.4	33.6	4.84	7t (67.9)	202.70	Yes
24	X52	9.5	9.86	CB	Longitudinal	35	35	4.92	1t (9.70)	184.20	No
25	X52	9.5	9.7	CB	Longitudinal	35	34.9	4.9	4t (39.0)	187.70	Yes
26	X52	9.5	9.7	CB	Longitudinal	35	35	4.86	5t (48.6)	192.80	Yes
27	X52	9.5	9.7	CB	Longitudinal	35	35	4.85	6t (58.2)	199.10	Yes
28	X52	9.5	9.7	CB	Longitudinal	35	35	4.87	7t (68.0)	197.30	Yes
29	X52	9.5	9.8	CB	Hoop	35	35	4.93	1t (9.75)	195.50	No
30	X52	9.5	9.7	CR	Hoop	35.5	33.7	4.8	0.5t (4.80)	206.80	No
31	X52	9.5	9.7	CR	Diagonal	35.5	33.8	4.8	0.5t (4.80)	196.70	Yes

2. Burst Test 1

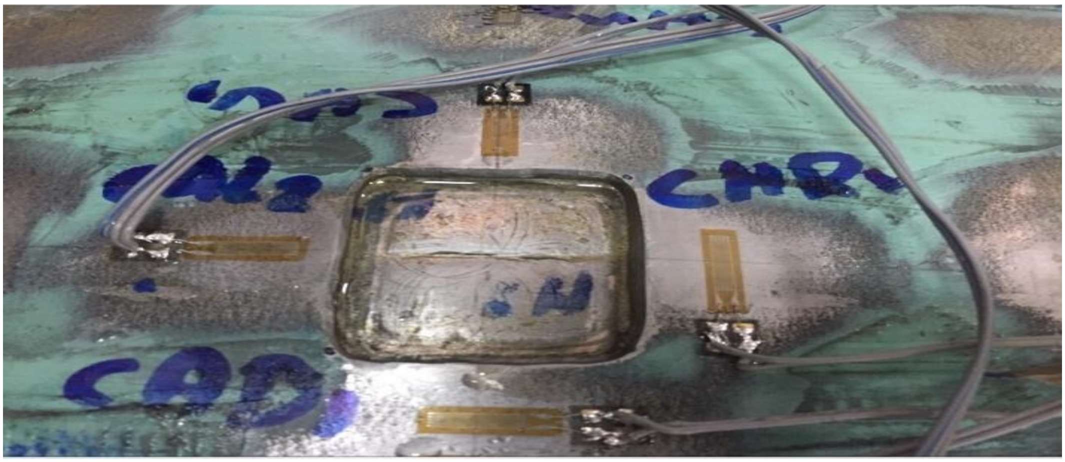

Figure 1: Burst Test 1

3. Burst Test 2

Figure 2: Burst Test 2

4. Burst Test 3

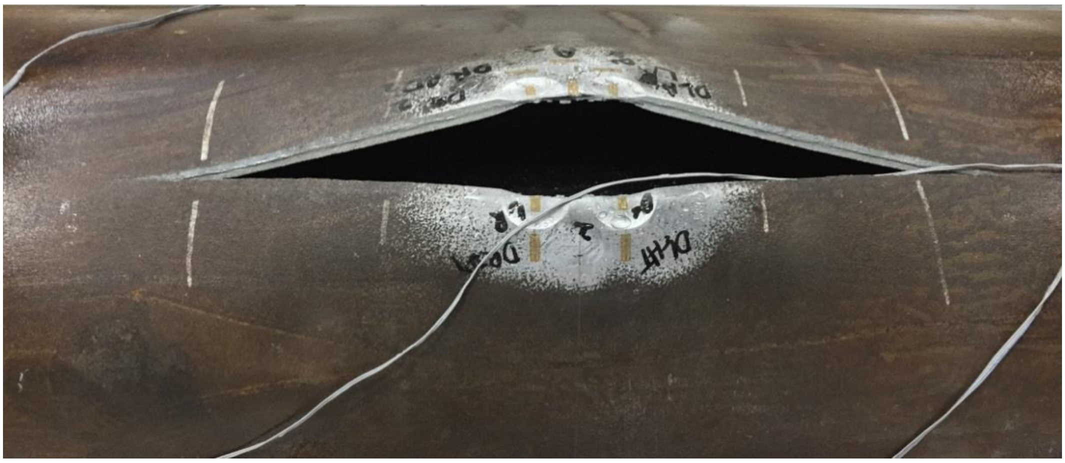

Figure 3: Burst Test 3

5. Burst Test 4

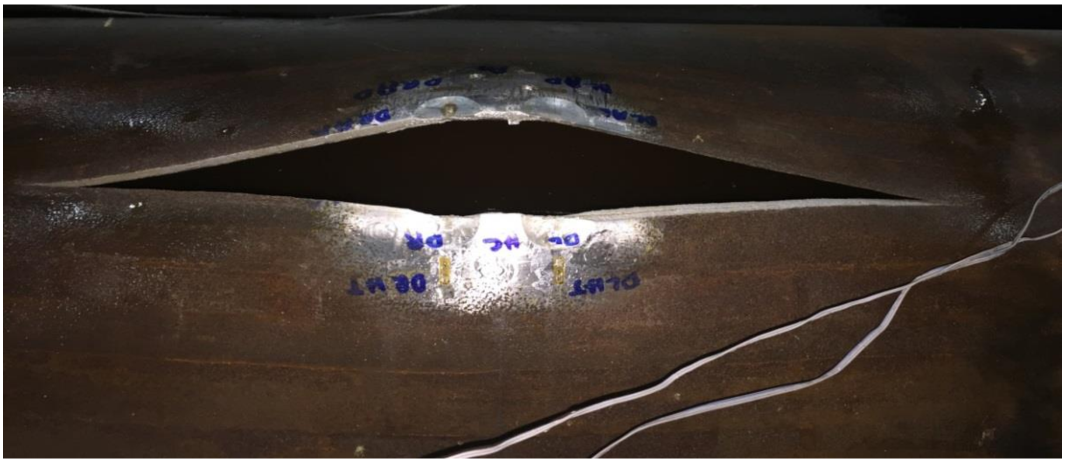

Figure 4: Burst Test 4

6. Burst Test 5

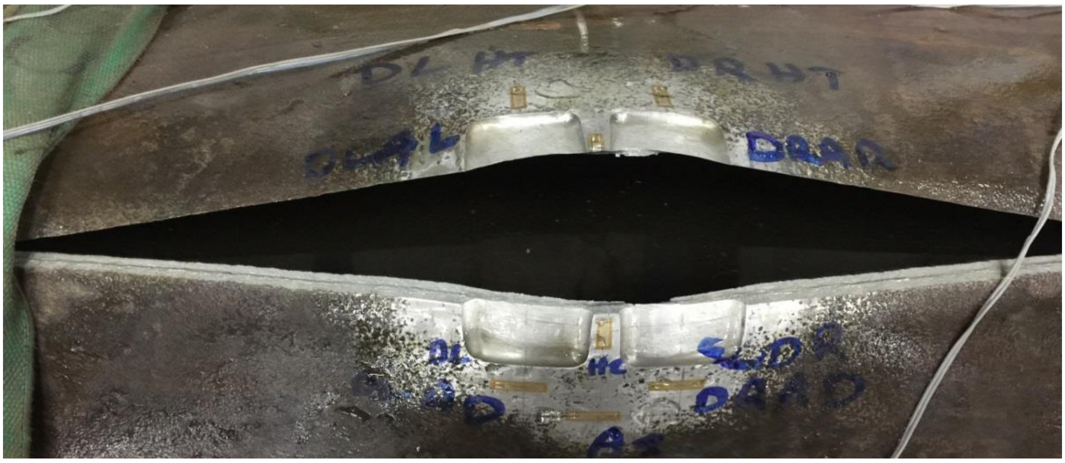

Figure 5: Burst Test 5

7. Burst Test 6

Figure 6: Burst Test 6

8. Burst Test 7

Figure 7: Burst Test 7

9. Burst Test 8

Figure 8: Burst Test 8

10. Burst Test 9

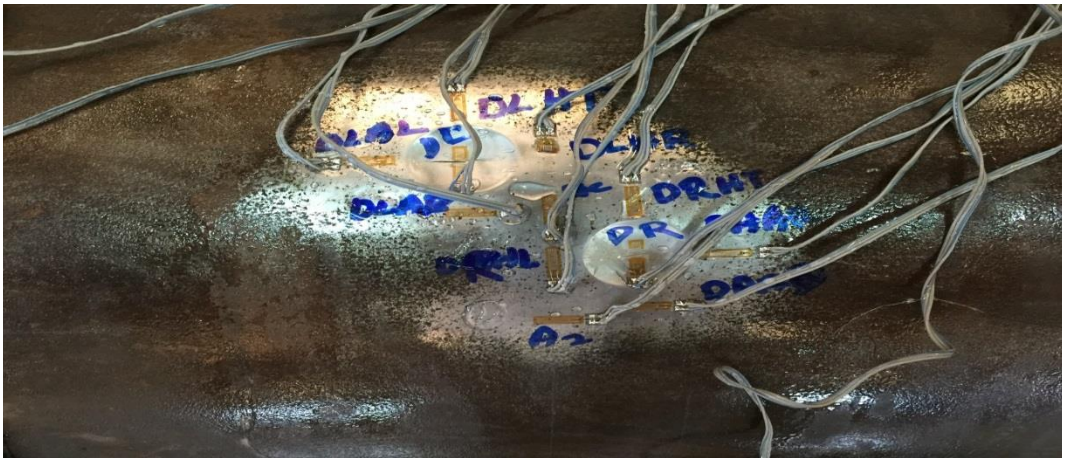

Figure 9: Burst Test 9

11. Burst Test 10

Figure 10: Burst Test 10

12. Burst Test 11

Figure 11: Burst Test 11

13. Burst Test 12

Figure 12: Burst Test 12

14. Burst Test 13

Figure 13: Burst Test 13

15. Burst Test 14

Figure 14: Burst Test 14

16. Burst Test 15

Figure 14: Burst Test 14

17. Burst Test 16

Figure 16: Burst Test 16

18. Burst Test 17

Figure 17: Burst Test 17

19. Burst Test 18

Figure 18: Burst Test 18

20. Burst Test 19

Figure 19: Burst Test 19

21. Burst Test 20

Figure 20: Burst Test 20

22. Burst Test 21

Figure 21: Burst Test 21

23. Burst Test 22

Figure 22: Burst Test 22

24. Burst Test 23

Figure 23: Burst Test 23

25. Burst Test 24

Figure 24: Burst Test 24

26. Burst Test 25

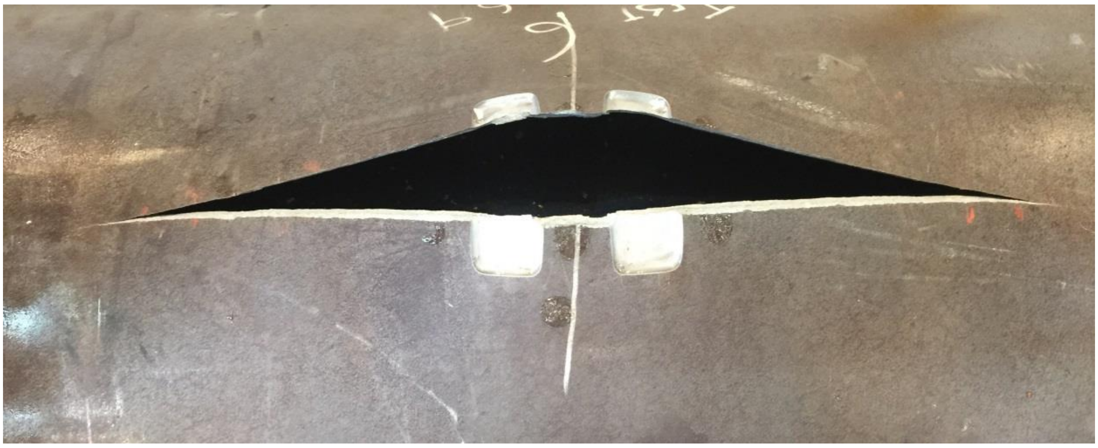

Figure 25: Burst Test 25

27. Burst Test 26

Figure 26: Burst Test 26

28. Burst Test 27

Figure 27: Burst Test 27

29. Burst Test 28

Figure 28: Burst Test 28

30. Burst Test 29

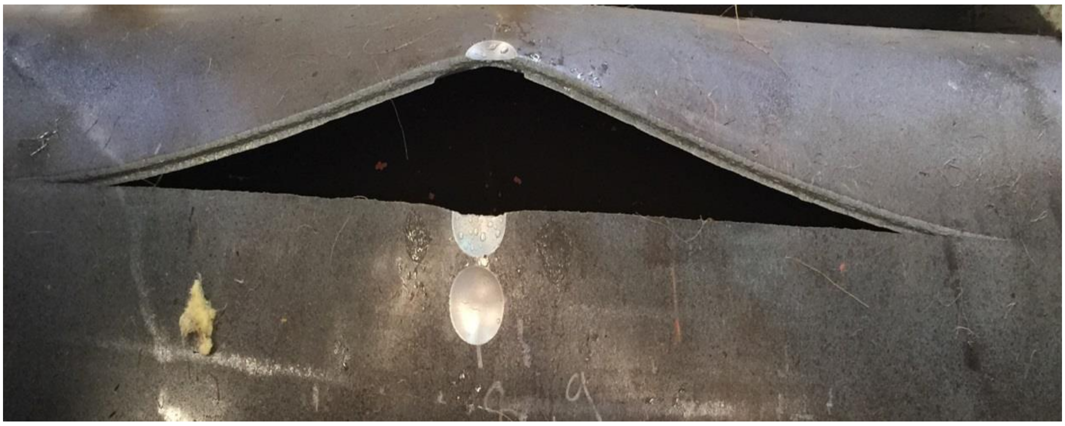

Figure 29: Burst Test 29

31. Burst Test 30

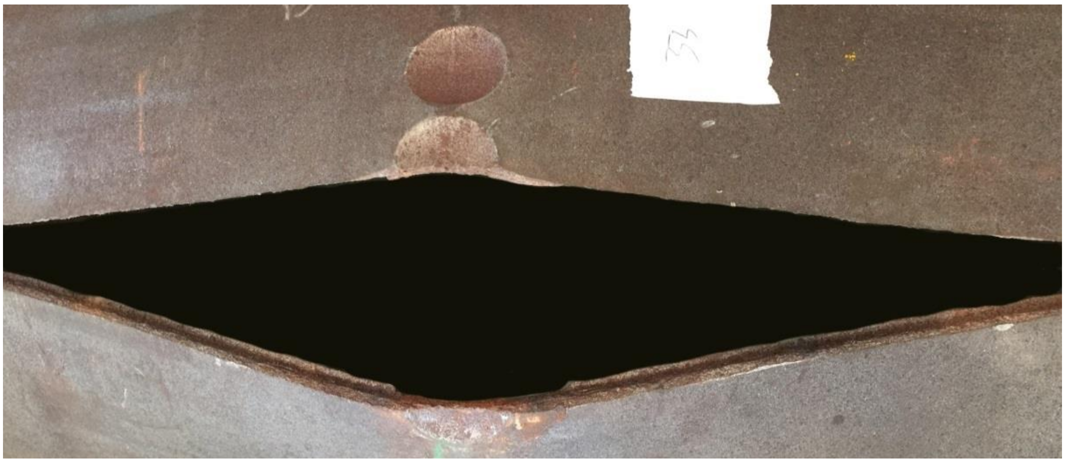

Figure 30: Burst Test 30

32. Burst Test 31

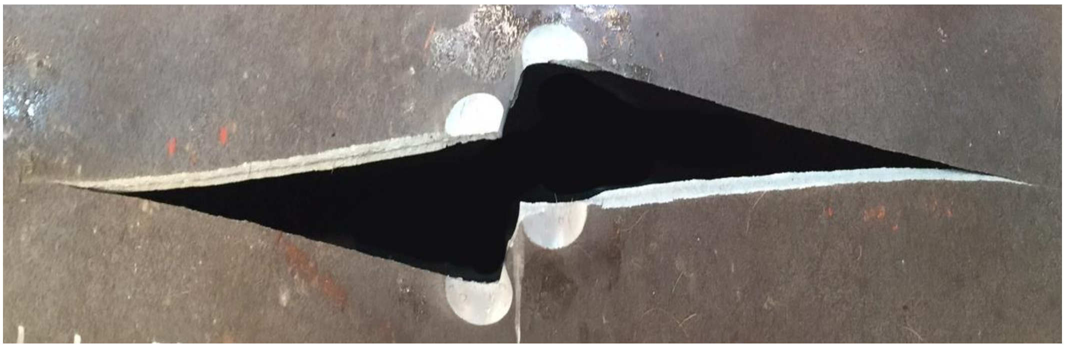

Figure 31: Burst Test 31

Appendix B: Parametric Study Cases Details

1.   Case Study 1P-a

Case No.	Test No	Test Name	Defect Details and Orientation			Defect Spacing Xt	Defect length / t	FEA Predicted Failure Pressure (Bars)	Nomralised Pressure (Pf/Pbarlow)	Defects interaction (Yes/No)
			Wall Loss (%)	Length	Type					
1P-a	1	PMTC-DL-17.5MM-X60-CircL-Single	50	17.5	Circular	0	1.7	247.0	0.8813	N/A
	2	PMTC-DL-17.5MM-X60-CircL-1t	50	17.5	Circular	1	1.7	240.0	0.8563	Yes
	3	PMTC-DL-17.5MM-X60-CircL-2t	50	17.5	Circular	2	1.7	243.0	0.8670	Yes
	4	PMTC-DL-17.5MM-X60-CircL-3t	50	17.5	Circular	3	1.7	243.0	0.8670	Yes
	5	PMTC-DL-17.5MM-X60-CircL-4t	50	17.5	Circular	4	1.7	246.0	0.8777	Yes
	6	PMTC-DL-17.5MMMM-X60-CircL-5t	50	17.5	circular	5	1.7	246.0	0.8777	No
	7	PMTC-DL-35MM-X60-CircL-Single	50	35	Circular	0	3.3	245.0	0.8741	NA
	8	PMTC-DL-35MM-X60-CircL-1t	50	35	Circular	1	3.3	236.6	0.8442	Yes
	9	PMTC-DL-35MM-X60-CircL-2t	50	35	Circular	2	3.3	236.6	0.8442	Yes
	10	PMTC-DL-35MM-X60-CircL-3t	50	35	Circular	3	3.3	239.2	0.8534	Yes
	11	PMTC-DL-35MM-X60-CircL-4t	50	35	Circular	4	3.3	239.2	0.8534	Yes
	12	PMTC-DL-35MM-X60-CircL-5t	50	35	Circular	5	3.3	239.2	0.8534	No
	13	PMTC-DL-70MM-X60-CircL-Single	50	70	Circular	0	6.7	241.0	0.8599	N/A
	14	PMTC-DL-70MM-X60-CircL-1t	50	70	Circular	1	6.7	225.0	0.8028	Yes
	15	PMTC-DL-70MM-X60-CircL-2t	50	70	Circular	2	6.7	228.0	0.8135	Yes
	16	PMTC-DL-70MM-X60-CircL-3t	50	70	Circular	3	6.7	228.0	0.8135	Yes
	17	PMTC-DL-70MM-X60-CircL-4t	50	70	Circular	4	6.7	228.0	0.8135	Yes
	18	PMTC-DL-70MM-X60-CircL-5t	50	70	Circular	5	6.7	230.0	0.8206	Yes
	19	PMTC-DL-70MM-X60-CircL-6t	50	70	Circular	6	6.7	233.0	0.8313	Yes
	20	PMTC-DL-70MM-X60-CircL-7t	50	70	circular	7	6.7	233.0	0.8313	Yes
	21	PMTC-DL-70MM-X60-CircL-8t	50	70	circular	8	6.7	233.0	0.8313	No
	22	PMTC-DL-17.5MM-X60-CBL-4t	50	17.5	Curved Boxed	0	1.7	246.0	0.8777	NA
	23	PMTC-DL-17.5MM-X60-CBL-1t	50	17.5	Curved Boxed	1	1.7	240.0	0.8563	Yes
	24	PMTC-DL-17.5MM-X60-CBL-2t	50	17.5	Curved Boxed	2	1.7	240.0	0.8563	Yes
	25	PMTC-DL-17.5MM-X60-CBL-3t	50	17.5	Curved Boxed	3	1.7	243.0	0.8670	Yes
	26	PMTC-DL-17.5MM-X60-CBL-4t	50	17.5	Curved Boxed	4	1.7	243.0	0.8670	No
	27	PMTC-DL-35MM-X60-CBL-Single	50	35	Curved Boxed	0	3.3	243.0	0.8670	NA
	28	PMTC-DL-35MM-X60-CBL-1t	50	35	Curved Boxed	1	3.3	231.4	0.8256	Yes
	29	PMTC-DL-35MM-X60-CBL-2t	50	35	Curved Boxed	2	3.3	231.4	0.8256	Yes
	30	PMTC-DL-35MM-X60-CBL-3t	50	35	Curved Boxed	3	3.3	231.4	0.8256	Yes
	31	PMTC-DL-35MM-X60-CBL-4t	50	35	Curved Boxed	4	3.3	231.4	0.8256	Yes
	32	PMTC-DL-35MM-X60-CBL-5t	50	35	Curved Boxed	5	3.3	231.4	0.8256	No
	33	PMTC-DL-70MM-X60-CBL-Single	50	70	Curved Boxed	0	6.7	225.0	0.8028	N/A
	34	PMTC-DL-70MM-X60-CBL-1t	50	70	Curved Boxed	1	6.7	207.0	0.7386	Yes
	35	PMTC-DL-70MM-X60-CBL-2t	50	70	Curved Boxed	2	6.7	210.0	0.7493	Yes
	36	PMTC-DL-70MM-X60-CBL-3t	50	70	Curved Boxed	3	6.7	213.0	0.7600	Yes
	37	PMTC-DL-70MM-X60-CBL-4t	50	70	Curved Boxed	4	6.7	216.0	0.7707	Yes
	38	PMTC-DL-70MM-X60-CBL-5t	50	70	Curved Boxed	5	6.7	216.0	0.7707	Yes
	39	PMTC-DL-70MM-X60-CBL-6t	50	70	Curved Boxed	6	6.7	216.0	0.7707	Yes
	40	PMTC-DL-70MM-X60-CBL-7t	50	70	Curved Boxed	7	6.7	216.0	0.7707	Yes
	41	PMTC-DL-70MM-X60-CBL-8t	50	70	Curved Boxed	8	6.7	216.0	0.7707	No

2. Case Study 1P-b

Case No.	Test No	Test Name	Defect Details and Orientation			Defect Spacing Xt	Defect length / t	FEA Predicted Failure Pressure (Bars)	Nomralised Pressure (Pf/Pbarlow)	Defects interaction (Yes/No)
			Wall Loss (%)	Length	Type					
1P-b	1	PMTC-DL-17.5MM-X52-CircL-Single	50	17.5	Circular	0	1.7	210.0	0.8369	N/A
	2	PMTC-DL-17.5MM-X52-CircL-1t	50	17.5	Circular	1	1.7	200.0	0.7971	Yes
	3	PMTC-DL-17.5MM-X52-CircL-2t	50	17.5	Circular	2	1.7	205.0	0.8170	Yes
	4	PMTC-DL-17.5MM-X52-CircL-3t	50	17.5	Circular	3	1.7	208.0	0.8289	Yes
	5	PMTC-DL-17.5MM-X52-CircL-4t	50	17.5	Circular	4	1.7	208.0	0.8289	No
	6	PMTC-DL-35MM-X52-CircL-Single	50	35	Circular	0	3.3	208.0	0.8289	NA
	7	PMTC-DL-35MM-X52-CircL-1t	50	35	Circular	1	3.3	195.0	0.7771	Yes
	8	PMTC-DL-35MM-X52-CircL-2t	50	35	Circular	2	3.3	200.0	0.7971	Yes
	9	PMTC-DL-35MM-X52-CircL-3t	50	35	Circular	3	3.3	203.0	0.8090	Yes
	10	PMTC-DL-35MM-X52-CircL-4t	50	35	Circular	4	3.3	203.0	0.8090	Yes
	11	PMTC-DL-35MM-X52-CircL-5t	50	35	Circular	5	3.3	205.0	0.8170	Yes
	12	PMTC-DL-35MM-X52-CircL-6t	50	35	Circular	6	3.3	205.0	0.8170	No
	13	PMTC-DL-70MM-X52-CircL-Single	50	70	Circular	0	6.7	198.0	0.7891	N/A
	14	PMTC-DL-70MM-X52-CircL-1t	50	70	Circular	1	6.7	185.0	0.7373	Yes
	15	PMTC-DL-70MM-X52-CircL-2t	50	70	Circular	2	6.7	188.0	0.7492	Yes
	16	PMTC-DL-70MM-X52-CircL-3t	50	70	Circular	3	6.7	190.0	0.7572	Yes
	17	PMTC-DL-70MM-X52-CircL-4t	50	70	Circular	4	6.7	190.0	0.7572	Yes
	18	PMTC-DL-70MM-X52-CircL-5t	50	70	Circular	5	6.7	193.0	0.7692	Yes
	19	PMTC-DL-70MM-X52-CircL-6t	50	70	Circular	6	6.7	195.0	0.7771	Yes
	20	PMTC-DL-70MM-X52-CircL-7t	50	70	circular	7	6.7	195.0	0.7771	No
	21	PMTC-DL-17.5MM-X52-CBL-4t	50	17.5	Curved Box	0	1.7	210.0	0.8369	NA
	22	PMTC-DL-17.5MM-X52-CBL-1t	50	17.5	Curved Box	1	1.7	200.0	0.7971	Yes
	23	PMTC-DL-17.5MM-X52-CBL-2t	50	17.5	Curved Box	2	1.7	205.0	0.8170	Yes
	24	PMTC-DL-17.5MM-X52-CBL-3t	50	17.5	Curved Box	3	1.7	208.0	0.8289	Yes
	25	PMTC-DL-17.5MM-X52-CBL-4t	50	17.5	Curved Box	4	1.7	208.0	0.8289	No
	26	PMTC-DL-35MM-X52-CBL-Single	50	35	Curved Box	0	3.3	200.0	0.7971	NA
	27	PMTC-DL-35MM-X52-CBL-1t	50	35	Curved Box	1	3.3	190.0	0.7572	Yes
	28	PMTC-DL-35MM-X52-CBL-2t	50	35	Curved Box	2	3.3	193.0	0.7692	Yes
	29	PMTC-DL-35MM-X52-CBL-3t	50	35	Curved Box	3	3.3	195.0	0.7771	Yes
	30	PMTC-DL-35MM-X52-CBL-4t	50	35	Curved Box	4	3.3	195.0	0.7771	Yes
	31	PMTC-DL-35MM-X52-CBL-5t	50	35	Curved Box	5	3.3	198.0	0.7891	Yes
	32	PMTC-DL-35MM-X52-CBL-6t	50	35	Curved Box	6	3.3	198.0	0.7891	No
	33	PMTC-DL-70MM-X52-CBL-Single	50	70	Curved Box	0	6.7	185.0	0.7373	N/A
	34	PMTC-DL-70MM-X52-CBL-1t	50	70	Curved Box	1	6.7	175.0	0.6974	Yes
	35	PMTC-DL-70MM-X52-CBL-2t	50	70	Curved Box	2	6.7	178.0	0.7094	Yes
	36	PMTC-DL-70MM-X52-CBL-3t	50	70	Curved Box	3	6.7	180.0	0.7173	Yes
	37	PMTC-DL-70MM-X52-CBL-4t	50	70	Curved Box	4	6.7	180.0	0.7173	Yes
	38	PMTC-DL-70MM-X52-CBL-5t	50	70	Curved Box	5	6.7	180.0	0.7173	Yes
	39	PMTC-DL-70MM-X52-CBL-6t	50	70	Curved Box	6	6.7	180.0	0.7173	Yes
	40	PMTC-DL-70MM-X52-CBL-7t	50	70	Curved Box	7	6.7	183.0	0.7293	Yes
	41	PMTC-DL-70MM-X52-CBL-8t	50	70	Curved Box	8	6.7	183.0	0.7293	No

3. Case Study 2P

Case No.	Test No	Test Name	Defect Details and Orientation			Defect Spacing Xt	Normalised Defect depth	FEA Predicted Failure Pressure (Bars)	Nomralised Pressure (Pf/Pbarlow)	Defects interaction (Yes/No)
			Wall Loss (%)	Length	Type					
2P	1	PMTC-DD25%-X60-CircL-Single	25	35	Circular	0	2.6	257.0	0.9170	N/A
	2	PMTC-DD25%-X60-CircL-1t	25	35	Circular	1	2.6	250.0	0.8920	Yes
	3	PMTC-DD25%-X60-CircL-2t	25	35	Circular	2	2.6	252.0	0.8991	Yes
	4	PMTC-DD25%-X60-CircL-3t	25	35	Circular	3	2.6	252.0	0.8991	Yes
	5	PMTC-DD25%-X60-CircL-4t	25	35	Circular	4	2.6	252.0	0.8991	Yes
	6	PMTC-DD25%-X60-CircL-5t	25	35	Circular	5	2.6	252.0	0.8991	Yes
	7	PMTC-DD25%-X60-CircL-6t	25	35	Circular	6	2.6	252.0	0.8991	Yes
	8	PMTC-DD25%-X60-CircL-7t	25	35	Circular	7	2.6	252.0	0.8991	Yes
	9	PMTC-DD25%-X60-CircL-8t	25	35	Circular	8	2.6	252.0	0.8991	No
	10	PMTC-DD50%-X60-CircL-Single	50	35	Circular	0	5.3	245.0	0.8741	NA
	11	PMTC-DD50%-X60-CircL-1t	50	35	Circular	1	5.3	236.6	0.8442	Yes
	12	PMTC-DD50%-X60-CircL-2t	50	35	Circular	2	5.3	236.6	0.8442	Yes
	13	PMTC-DD50%-X60-CircL-3t	50	35	Circular	3	5.3	239.2	0.8534	Yes
	14	PMTC-DD50%-X60-CircL-4t	50	35	Circular	4	5.3	239.2	0.8534	Yes
	15	PMTC-DD50%-X60-CircL-5t	50	35	Circular	5	5.3	239.2	0.8534	No
	16	PMTC-DD75%-X60-CircL-Single	75	35	Circular	0	7.9	233.0	0.8313	N/A
	17	PMTC-DD75%-X60-CircL-1t	75	35	Circular	1	7.9	215.0	0.7671	Yes
	18	PMTC-DD75%-X60-CircL-2t	75	35	Circular	2	7.9	215.0	0.7671	Yes
	19	PMTC-DD75%-X60-CircL-3t	75	35	Circular	3	7.9	220.0	0.7849	Yes
	20	PMTC-DD75%-X60-CircL-4t	75	35	Circular	4	7.9	220.0	0.7849	No
	21	PMTC-DD25%-X60-CBL-Single	25	35	Curved Boxed	0	2.6	247.0	0.8813	NA
	22	PMTC-DD25%-X60-CBL-4t	25	35	Curved Boxed	1	2.6	242.0	0.8634	Yes
	23	PMTC-DD25%-X60-CBL-4t	25	35	Curved Boxed	2	2.6	244.0	0.8706	Yes
	24	PMTC-DD25%-X60-CBL-4t	25	35	Curved Boxed	3	2.6	244.0	0.8706	Yes
	25	PMTC-DD25%-X60-CBL-4t	25	35	Curved Boxed	4	2.6	244.0	0.8706	Yes
	26	PMTC-DD25%-X60-CBL-5t	25	35	Curved Boxed	5	2.6	244.0	0.8706	No
	27	PMTC-DD50%-X60-CBL-Single	50	35	Curved Boxed	0	5.3	243.0	0.8670	NA
	28	PMTC-DD50%-X60-CBL-4t	50	35	Curved Boxed	1	5.3	231.4	0.8256	Yes
	29	PMTC-DD50%-X60-CBL-4t	50	35	Curved Boxed	2	5.3	231.4	0.8256	Yes
	30	PMTC-DD50%-X60-CBL-4t	50	35	Curved Boxed	3	5.3	231.4	0.8256	Yes
	31	PMTC-DD50%-X60-CBL-4t	50	35	Curved Boxed	4	5.3	231.4	0.8256	Yes
	32	PMTC-DD50%-X60-CBL-5t	50	35	Curved Boxed	5	5.3	231.4	0.8256	No
	33	PMTC-DD75%-X60-CBL-Single	75	35	Curved Boxed	0	7.9	215.0	0.7671	N/A
	34	PMTC-DD75%-X60-CBL-1t	75	35	Curved Boxed	1	7.9	189.0	0.6743	Yes
	35	PMTC-DD75%-X60-CBL-2t	75	35	Curved Boxed	2	7.9	190.0	0.6779	No

4. Case Study 3P

Case No.	Test No.	Test Name	Defect Details and Orientation			Defect Spacing Xt	OD/t	FEA Predicted Failure Pressure (Bars)	Nomralised Pressure (Pf/Pbarlow)	Defects interaction (Yes/No)
			Wall Loss (%)	Length	Type					
3P	1	PMTC-X60-OD10-50%-Circle-Single	50	35	Circular	0	24.2	495.0	0.8831	NA
	2	PMTC-X60-OD10-50%-Circle-1t	50	35	Circular	1	24.2	470.0	0.8385	Yes
	3	PMTC-X60-OD10-50%-Circle-2t	50	35	Circular	2	24.2	475.0	0.8474	Yes
	4	PMTC-X60-OD10-50%-Circle-3t	50	35	Circular	3	24.2	475.0	0.8474	Yes
	5	PMTC-X60-OD10-50%-Circle-4t	50	35	Circular	4	24.2	480.0	0.8563	Yes
	6	PMTC-X60-OD10-50%-Circle-5t	50	35	Circular	5	24.2	480.0	0.8563	No
	7	PMTC-X60-OD20-50%-Circle-Single	50	35	Circular	0	48.4	248.0	0.8848	NA
	8	PMTC-X60-OD20-50%-Circle-1t	50	35	Circular	1	48.4	236.6	0.8442	Yes
	9	PMTC-X60-OD20-50%-Circle-2t	50	35	Circular	2	48.4	236.6	0.8442	Yes
	10	PMTC-X60-OD20-50%-Circle-3t	50	35	Circular	3	48.4	239.2	0.8534	Yes
	11	PMTC-X60-OD20-50%-Circle-4t	50	35	Circular	4	48.4	239.2	0.8534	Yes
	12	PMTC-X60-OD20-50%-Circle-5t	50	35	Circular	5	48.4	239.2	0.8534	No
	13	PMTC-X60-OD30-50%-Circle-Single	50	35	Circular	0	72.6	162.0	0.8670	NA
	14	PMTC-X60-OD30-50%-Circle-1t	50	35	Circular	1	72.6	159.0	0.8509	Yes
	15	PMTC-X60-OD30-50%-Circle-2t	50	35	Circular	2	72.6	159.0	0.8509	Yes
	16	PMTC-X60-OD30-50%-Circle-3t	50	35	Circular	3	72.6	160.0	0.8563	Yes
	17	PMTC-X60-OD30-50%-Circle-4t	50	35	Circular	4	72.6	160.0	0.8563	Yes
	18	PMTC-X60-OD30-50%-Circle-5t	50	35	Circular	5	72.6	160.0	0.8563	Yes
	19	PMTC-X60-OD30-50%-Circle-6t	50	35	Circular	6	72.6	160.0	0.8563	No
	20	PMTC-X60-OD10-50%-CBL-Single	50	35	Curved Boxed	0	24.2	465.0	0.8295	NA
	21	PMTC-X60-OD10-50%-CBL-1t	50	35	Curved Boxed	1	24.2	437.0	0.7796	Yes
	22	PMTC-X60-OD10-50%-CBL-2t	50	35	Curved Boxed	2	24.2	437.0	0.7796	Yes
	23	PMTC-X60-OD10-50%-CBL-3t	50	35	Curved Boxed	3	24.2	437.0	0.7796	Yes
	24	PMTC-X60-OD10-50%-CBL-4t	50	35	Curved Boxed	4	24.2	442.0	0.7885	No
	25	PMTC-X60-OD20-50%-CBL-Single	50	35	Curved Boxed	0	48.4	243.0	0.8670	NA
	26	PMTC-X60-OD20-50%-CBL-1t	50	35	Curved Boxed	1	48.4	231.4	0.8256	Yes
	27	PMTC-X60-OD20-50%-CBL-2t	50	35	Curved Boxed	2	48.4	231.4	0.8256	Yes
	28	PMTC-X60-OD20-50%-CBL-3t	50	35	Curved Boxed	3	48.4	231.4	0.8256	Yes
	29	PMTC-X60-OD20-50%-CBL-4t	50	35	Curved Boxed	4	48.4	231.4	0.8256	Yes
	30	PMTC-X60-OD20-50%-CBL-5t	50	35	Curved Boxed	5	48.4	231.4	0.8256	No
	31	PMTC-X60-OD30-50%-CBL-Single	50	35	Curved Boxed	0	72.6	158.0	0.8456	NA
	32	PMTC-X60-OD30-50%-CBL-1t	50	35	Curved Boxed	1	72.6	155.0	0.8295	Yes
	33	PMTC-X60-OD30-50%-CBL-2t	50	35	Curved Boxed	2	72.6	155.0	0.8295	Yes
	34	PMTC-X60-OD30-50%-CBL-3t	50	35	Curved Boxed	3	72.6	155.0	0.8295	Yes
	35	PMTC-X60-OD30-50%-CBL-4t	50	35	Curved Boxed	4	72.6	155.0	0.8295	Yes
	36	PMTC-X60-OD30-50%-CBL-5t	50	35	Curved Boxed	5	72.6	155.0	0.8295	No

5. Case Study 4P

Case No.	Test No.	Test Name	Defect Details and Orientation			Defect Spacing Xt	OD/t	FEA Predicted Failure Pressure (Bars)	Nomralised Pressure (Pf/Pbarlow)	Defects interaction (Yes/No)
			Wall Loss (%)	Length	Type					
4P	1	PMTC-t-6-4MM-X60-CircL-Single	50	35	Circular	0	80.0	147.0	0.8673	N/A
	2	PMTC-t-6-4MM-X60-CircL-1t	50	35	Circular	1	80.0	142.0	0.8378	Yes
	3	PMTC-t-6-4MM-X60-CircL-2t	50	35	Circular	2	80.0	143.0	0.8437	Yes
	4	PMTC-t-6-4MM-X60-CircL-3t	50	35	Circular	3	80.0	143.0	0.8437	Yes
	5	PMTC-t-6-4MM-X60-CircL-4t	50	35	Circular	4	80.0	143.0	0.8437	Yes
	6	PMTC-t-6-4MM-X60-CircL-5t	50	35	Circular	5	80.0	143.0	0.8437	Yes
	7	PMTC-t-6-4MM-X60-CircL-6t	50	35	Circular	6	80.0	144.0	0.8496	Yes
	8	PMTC-t-6-4MM-X60-CircL-7t	50	35	Circular	7	80.0	144.0	0.8496	Yes
	9	PMTC-t-6-4MM-X60-CircL-8t	50	35	Circular	8	80.0	144.0	0.8496	Yes
	10	PMTC-t-6-4MM-X60-CircL-9t	50	35	Circular	9	80.0	144.0	0.8496	No
	11	PMTC-t- 10.5 MM-X60-CircL-Single	50	35	Circular	0	48.4	248.0	0.8848	NA
	12	PMTC-t- 10.5 MM-X60-CircL-1t	50	35	Circular	1	48.4	236.6	0.8442	Yes
	13	PMTC-t- 10.5 MM-X60-CircL-2t	50	35	Circular	2	48.4	236.6	0.8442	Yes
	14	PMTC-t- 10.5 MM-X60-CircL-3t	50	35	Circular	3	48.4	239.2	0.8534	Yes
	15	PMTC-t- 10.5 MM-X60-CircL-4t	50	35	Circular	4	48.4	239.2	0.8534	Yes
	16	PMTC-t- 10.5 MM-X60-CircL-5t	50	35	Circular	5	48.4	239.2	0.8534	No
	17	PMTC-t-15MM-X60-CircL-Single	50	35	Circular	0	33.9	356.0	0.8891	N/A
	18	PMTC-t-15MM-X60-CircL-1t	50	35	Circular	1	33.9	344.0	0.8592	Yes
	19	PMTC-t-15MM-X60-CircL-2t	50	35	Circular	2	33.9	344.0	0.8592	Yes
	20	PMTC-t-15MM-X60-CircL-3t	50	35	Circular	3	33.9	348.0	0.8691	Yes
	21	PMTC-t-15MM-X60-CircL-4t	50	35	Circular	4	33.9	352.0	0.8791	Yes
	22	PMTC-t-15MM-X60-CircL-5t	50	35	circular	5	33.9	352.0	0.8791	No
	23	PMTC-t-6-4MM-X60-CBL-Single	50	35	Curved Boxed	0	80.0	144.0	0.8496	N/A
	24	PMTC-t-6-4MM-X60-CBL-1t	50	35	Curved Boxed	1	80.0	135.0	0.7965	Yes
	25	PMTC-t-6-4MM-X60-CBL-2t	50	35	Curved Boxed	2	80.0	135.0	0.7965	Yes
	26	PMTC-t-6-4MM-X60-CBL-3t	50	35	Curved Boxed	3	80.0	137.0	0.8083	Yes
	27	PMTC-t-6-4MM-X60-CBL-4t	50	35	Curved Boxed	4	80.0	137.0	0.8083	Yes
	28	PMTC-t-6-4MM-X60-CBL-5t	50	35	Curved Boxed	5	80.0	137.0	0.8083	Yes
	29	PMTC-t-6-4MM-X60-CBL-6t	50	35	Curved Boxed	6	80.0	137.0	0.8083	Yes
	30	PMTC-t-6-4MM-X60-CBL-7t	50	35	Curved Boxed	7	80.0	137.0	0.8083	Yes
	31	PMTC-t-6-4MM-X60-CBL-8t	50	35	Curved Boxed	8	80.0	137.0	0.8083	No
	32	PMTC-t-10.5 MM-X60-CBL-Single	50	35	Curved Boxed	0	48.4	243.0	0.8670	NA
	33	PMTC-t-10.5 MM-X60-CBL-1t	50	35	Curved Boxed	1	48.4	231.4	0.8256	Yes
	34	PMTC-t-10.5 MM-X60-CBL-2t	50	35	Curved Boxed	2	48.4	231.4	0.8256	Yes
	35	PMTC-t-10.5 MM-X60-CBL-3t	50	35	Curved Boxed	3	48.4	231.4	0.8256	Yes
	36	PMTC-t-10.5 MM-X60-CBL-4t	50	35	Curved Boxed	4	48.4	231.4	0.8256	Yes
	37	PMTC-t-10.5 MM-X60-CBL-5t	50	35	Curved Boxed	5	48.4	231.4	0.8256	No
	38	PMTC-t-15MM-X60-CBL-Single	50	35	Curved Boxed	0	33.9	348.0	0.8691	N/A
	39	PMTC-t-15MM-X60-CBL-1t	50	35	Curved Boxed	1	33.9	336.0	0.8392	Yes
	40	PMTC-t-15MM-X60-CBL-2t	50	35	Curved Boxed	2	33.9	336.0	0.8392	Yes
	41	PMTC-t-15MM-X60-CBL-3t	50	35	Curved Boxed	3	33.9	336.0	0.8392	Yes
	42	PMTC-t-15MM-X60-CBL-4t	50	35	Curved Boxed	4	33.9	340.0	0.8492	Yes
	43	PMTC-t-15MM-X60-CBL-5t	50	35	Curved Boxed	5	33.9	340.0	0.8492	No